UNIVERSITY OF OKLAHOMA

GRADUATE COLLEGE

ENZYMATIC AND NON-ENZYMATIC BIOANODES: NOVEL MATERIALS FOR GLUCOSE OXIDASE AND POLYVIOLOGEN BIOSENSORS AND BIOFUEL CELLS

A DISSERTATION

SUBMITTED TO THE GRADUATE FACULTY

in partial fulfillment of the requirements for the

Degree of

DOCTOR OF PHILOSOPHY

By

STEPHEN J. WILSON

Norman, Oklahoma

2023

Enzymatic and Non-enzymatic Bioanodes: Novel Materials for Glucose Oxidase and Polyviologen Biosensors and Biofuel Cells

A DISSERTATION APPROVED FOR THE

DEPARTMENT OF CHEMISTRY AND BIOCHEMISTRY

BY THE COMMITTEE CONSISTING OF

Dr. Daniel T. Glatzhofer, Chair

Dr. Indrajeet Sharma

Dr. Charles V. Rice

Dr. Wai Tak Yip

Dr. Edgar A. O'Rear

Acknowledgements

Most great accomplishments are not a lone effort but the efforts of many people supporting a single goal. I would like to take this opportunity to thank all those who have supported me during my time at the University of Oklahoma. First, I would like to thank Dr Glatzhofer for his patient, gentle and wise guidance. Through his mentorship I have learned much about chemistry, life and leadership. I would like to thank my lab mates, (particularly Matthew Houck, Christopher Thrutchley, Pingmei Wang, and Theo Russmore) and fellow grad students for their time and efforts helping me in the lab and in the classroom and providing a positive environment for growth and learning to occur. I would like to thank my committee for their guidance and patience through this process. I also thank my wife for her constant and unwavering support and encouragement through late nights and tired mornings. Last, I would like to thank God for giving me this opportunity and placing all of these people around me at the University of Oklahoma.

Table of Contents

List of Figures

List of Schemes

List of Tables

Abstract

A fundamental study of the interaction of iodide and glucose oxidase (GOx) was carried out, showing that the iodide acts as a direct mediator with GOx in enzymatic glucose biosensors. This direct mediation may be happening in parallel with the known electron transport chain through hydrogen peroxide. The aqueous $I^-/I_3^-/I_2$ redox reactions are discussed and studied through the use of cyclic voltammetry and chronoamperometry in conjunction with glucose and GOx. These results are compared with water soluble ferrocenyl salts known to mediate GOx biosensors. This study shows that iodide can mediate GOx in the presence and absence of oxygen, making this the first work, to our knowledge, to show iodide can act as a direct mediator, rather than an indirect mediator for GOx.

Layer-by-layer (LBL) modification of gold electrodes with GOx has been an effective way to make enzymatic electrochemical glucose bioanodes for biofuel cells and biosensors. The use of a cystamine attachment layer is usually used to establish a functionalizable initial layer upon which to build up more material for these systems. While this is an easy and fast way to functionalize gold, it was unknown how this attachment layer affects access to the electrode surface. This work explores the use of carbon disulfide (CS_2) substituted linear- and branched-polyethylenimine (LPEI and BPEI respectively) as the first layer of these LBL bioanodes. The dithiocarbamate groups attached to the polymer allows it to react with the gold surface and establish a polymeric-first layer. This work shows that the polymeric first layer immobilizes ~2.5 times more material than the first three layers of the cystamine-modified electrodes. The inclusion of ferrocenyl groups in the first-layer PEI also wires the upper layers to the electrode resulting in

a ~6 fold increase in current density in the 3-layer system. The Fc-CS_2-LPEI- and Fc-CS_2-BPEI-based electrodes are also more stable than the cystamine-first layer electrodes. The 9L Fc-CS_2-LPEI anode was found to produce 978 $\mu A/cm^2$ current density, and 271 $\mu W/cm^2$ peak power at saturating glucose conditions as a biofuel cell while the 19L Fc-CS_2-BPEI anode was found to produce 2.1 mA/cm^2 current density, and 677 $\mu W/cm^2$ peak power. Under physiological glucose concentrations the Fc-CS_2-LPEI had a sensitivity of 47 $\mu A/cm^2$ mM while the Fc-CS_2-BPEI anode had a sensitivity of 64 $\mu A/cm^2$ mM, making these some of the most sensitive enzymatic glucose bio-anodes made to date.

This work also explores electropolymerization techniques for the fabrication cucurbit[7]uril (CB7)/Polyviologen-based bioanodes. This non-enzymatic electrode was fabricated using cyclic voltammetry, constant potential and pulsed potentials. It was found that the cyclic voltametric method was the best technique to fabricate functional glucose anodes. This method was used to functionalize the high surface-area material carbon felt, and highly stable glucose electrodes were made that produced ~20 $\mu W/cm^2$ peak power and were able to also utilize sucrose as a fuel source.

1. Introduction

1.1 Background

1.1.1 Need for Glucose Sensors

According to the CDC's 2020 diabetes report 32 million, or around 12 percent, of US citizens suffer from diabetes, and the numbers are getting worse as indicated by their statistics[1]. People who have diabetes either do not produce insulin (type 1) or have problems utilizing insulin

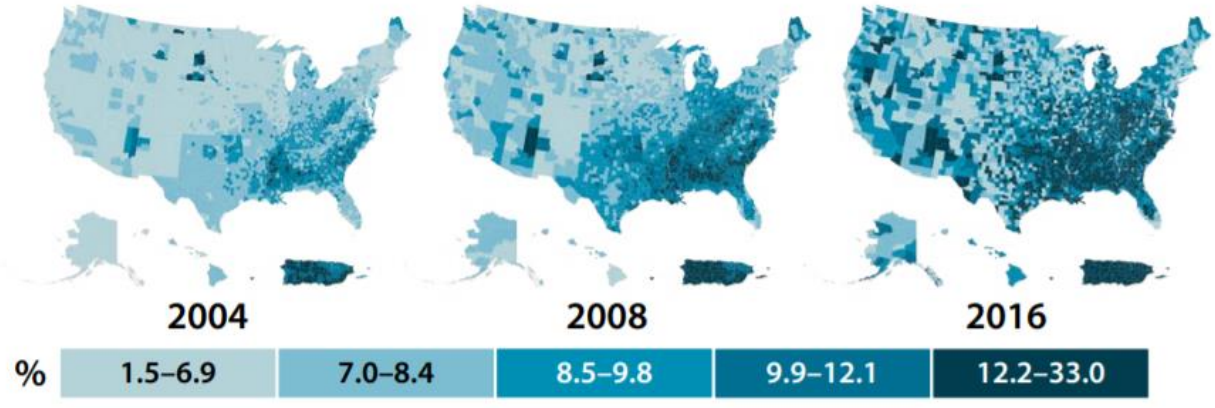

Note: Data were unavailable for some US territories.
Data sources: US Diabetes Surveillance System; Behavioral Risk Factor Surveillance System.

Figure 1.1 Age adjusted county level prevalence of diabetes among adults 20 and older in the United States from the USA.[1]

properly (type 2). Insulin is a hormone that helps regulate blood glucose levels; therefore, people who have diabetes will have unregulated spikes and drops in blood glucose levels depending on what and when they eat. Unregulated blood glucose levels can lead to many complications including peripheral arterial disease, a narrowing of the arteries in the extremities, which can lead to the morbidity and loss of the limbs. Current treatment of diabetes generally consists of frequent, self-administered, blood-glucose monitoring, usually collected by pin pricks, and treatment with sugary snacks if the glucose levels are too low, and with insulin injections if the glucose levels are

too high[2]. While these treatments are effective, there is still a significant risk of glucose spikes and drops with any testing/treatment inconsistencies. The ideal diabetes treatment would involve a continuously running glucose monitor (CGM) that could last for a long period of time without any apparatus needing to be replaced. While some CGMs have been produced, they only last ~2 weeks before needing to be replaced and most are currently sold as a monthly subscription service for ~$400 a month, making them impractical for most of the world to use. CGMs, along with appropriate treatment with insulin or sugar, can diminish the negative long term effects diabetes has on the human body.

Glucose sensors developed thus far have primarily detected products of enzymatic processes amperometrically. While some effort has been put into developing colorimetric sensors, most efforts have been made in developing electrochemical sensors that can sense glucose concentrations instantaneously *in vivo*[3-4]. Enzymes have inherent selectivity advantages over other non-enzymatic approaches that are susceptible to electroactive interferants like ascorbic acid, acetaminophen and dopamine. The focus of the work presented here is primarily the development and testing of cheap and long-lasting novel enzymatic glucose bioanodes, with a secondary focus on power generation from these anodes, as well as from novel non-enzymatic polyviologen anodes.

1.1.2 Principals of Enzymatic Glucose Sensors

Because of their selectivity, enzymes are ideal for carrying out one reaction repeatedly without reacting with other molecules or producing extraneous side products. Sensors using these enzymes are usually designed using low toxicity materials to maintain biocompatibility. Because the enzyme Glucose Oxidase (GOx) is non-toxic[5] and can be used in biological systems, it has been the main enzyme used in the development of *in vivo* enzymatic sensors.

GOx in nature uses oxygen to oxidize glucose to gluconolactone as shown in Scheme 1.1. Since this redox process utilizes oxygen and produces hydrogen peroxide, concentration measurements of these two species on treated aliquot samples were the first assays/sensors to be made that determined glucose concentrations. With time, redox mediators that interact directly with $FADH_2$ (dihydroflavine-adenine dinucleotide), GOx's redox active site, were developed, allowing for real time electrochemical sensing of the concentration of glucose based on the enzyme's reaction (see Scheme 1.1). These catalytic redox mediators are molecules that can be reduced by the $FADH_2$ active site of GOx and oxidized at an electrode to enable a constant flow of electrons through a circuit. This flow can be measured, and the amperometric response can be

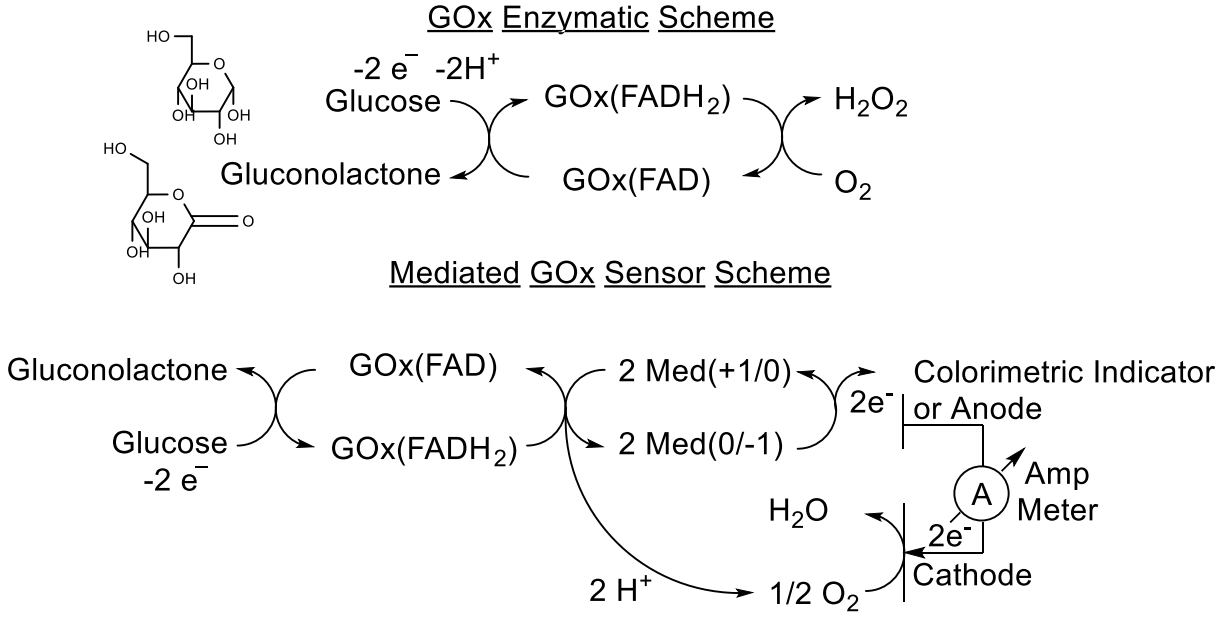

Scheme 1.1 The enzymatic scheme in nature shown on top and the scheme for an enzymatic mediated electrochemical glucose biosensor on bottom.

correlated to the concentration of glucose in the sample. The electrons can also be passed to a colorimetric indicator that changes colors upon reduction, indicating the solution's gross glucose concentration[6].

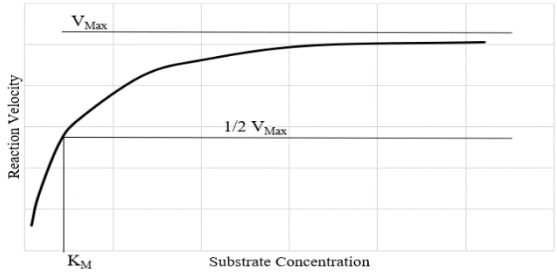

Figure 1.2 An enzyme reaction rate plotted vs substrate concentration, aka a Michaelis-Menten curve, with graphical aids for Vmax and K_M produced using data from one of the sensors made in Chapter 3.

In order to better understand these sensors, it is important to understand how the enzyme itself functions. The kinetics of enzymes have been extensively studied and the principals of their reaction rate with varying substrate concentration has been well defined[7-9]. Using these kinetic principles, it is possible to calculate the concentration of glucose in a sample if the rate of the GOx reaction is below the V_{Max} of the enzyme. Enzyme reaction curves are plotted with substrate

Equation 1.1 $$v = \frac{dP}{dt} = V_{Max}\frac{[S]}{K_M+[S]}$$ Michaelis-Menten Equation

Equation 1.2 $$\frac{1}{v} = \frac{K_M+[S]}{v_{Max}[S]} = \frac{K_M}{v_{Max}}\frac{1}{[S]} + \frac{1}{v_{Max}}$$ Lineweaver-Burk Equation

concentration on the X axis and reaction velocity (turnover rate) on the Y axis (see Figure 1.2). Using this type of plot Michaelis and Menten derived a general equation for the kinetics of enzymatic reactions. Electrochemistry can be used to monitor the enzymatic reaction using the amperometric output to follow the reaction velocity and glucose concentration. This can is done using Equation 1.1[10], where ν is the reaction velocity (or current), P is the product, t is time, S is the substrate concentration, V_{Max} is the maximum theoretical reaction velocity, and K_M is the Michaelis constant which is equal to the concentration at which v is half of V_{Max}. While V_{Max} will depend on the enzyme concentration, K_M is independent of enzyme concentration and will be

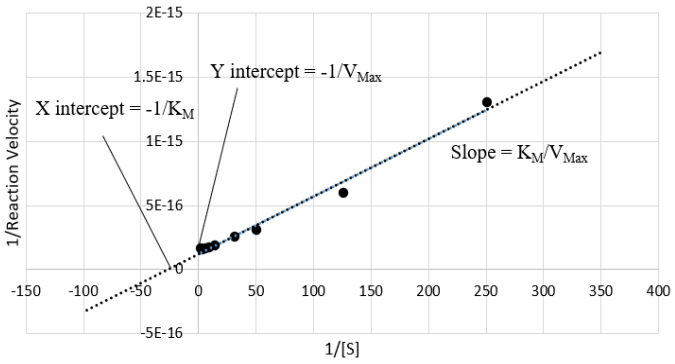

Figure 1.3 A Lineweaver-Burk plot made using the data from Figure 1.2 showing the relationship between the equation/graphical elements and the KM and VMax.

unique to each enzyme. By taking the double reciprocal of the Michaelis-Menten equation (Lineweaver-Burk Equation 1.2)[11], a linear plot can be generated (Figure 1.3) where the slope is K_M/V_{Max} and the y intercept is $1/V_{Max}$. If the enzyme process produces a current in an electrochemical sensor, the reaction rate for a given system will be proportional to the current output if the enzymatic reaction is the rate limiting step in the electron transport chain, and Equations 1.1 and 1.2 can be used to determine these constants and evaluate how well an enzyme is performing in a given system. A Michaelis-Menten plot (Figure 1.2) has different concentration regions for enzyme kinetics behavior[10]. At low substrate concentrations, the rate is roughly first order (linear) with respect to the substrate concentration, since the rate of reaction is such that every time a substrate molecule meets an enzyme, the site will probably be available. The reaction rate can be approximated with a linear plot with respect to substrate concentration in this zone. Due to the limitations of hardware and software in the early days of biosensors, linearity was essential for a sensor since only very simple calculations could be done without a large computer or much time. Since the biological concentration of glucose in humans lies in the first order domain of its Michaelis-Menten curve, GOx is an ideal catalyst for a glucose biosensor. The enzyme kinetics move from first order with low substrate concentration to zero order (independent of substrate concentration) at high substrate concentrations, where each enzyme is nearly always

occupied by a substrate molecule (saturating conditions). The development of amperometric glucose biosensors used these principles to produce three generations of enzymatic glucose sensors, each with its own characteristic features discussed below.

1.2 Generations of Enzymatic Glucose Sensors

The first continuous electrochemical enzymatic glucose bio-sensor was discussed in 1962 by Clark and Lyons[12]. They described a pH sensitive glass electrode (B in Figure 1.4) in an electrolyte solution (D) with glucose oxidase (GOx) in a thin layer (F) between an inner ion-conduction membrane (E) and an outer size exclusion membrane (G). A glucose solution can be pumped by the outer layer (G), the glucose can diffuse into the enzyme layer and react with the GOx to form gluconolactone, which quickly hydrolyzes to gluconic acid. This gluconic acid will diffuse through the ion-conductive membrane into solution D, changing its pH, which is then detected by the pH sensor. The sensitivity of this electrode could be tuned by adjusting the GOx concentration and flow rate of the glucose-solution.

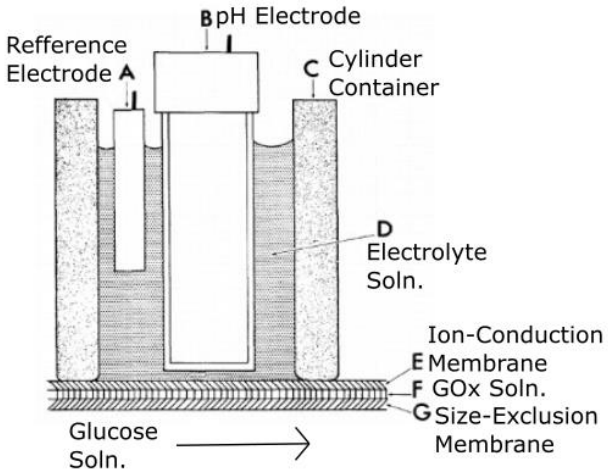

Figure 1.4 Clark and Lyon's glucose sensing system[12] in which A is a reference electrode, B is a pH sensing electrode, C is a cylinder, D is an electrolyte solution, E is an ion-conducting membrane, F is a pocket containing a GOx solution, G is a size-exclusion membrane to keep the GOx in the F region and the glucose solution (or blood) is continuously flowing by outside of G.

While Clark and Lyon's glucose sensor was conceived as a part of a larger instrument that was impractical for mobile use, this concept was significantly improved upon by Updike and Hicks in 1967 when they immobilized GOx in a polyacrylamide gel column and ran glucose solutions through the column. The concentration of oxygen in the eluent was determined by an oxygen electrode to measure the oxygen content of the eluent[13] (Figure 1.5). Because GOx uses oxygen to oxidize glucose to gluconolactone, the measured changes in oxygen concentration before and after exposure to the enzyme gel can be correlated to the glucose concentration of a sample. This method was used on whole blood and plasma samples to determine the blood-glucose concentrations. The sensitivity of this sensor could be adjusted by changing the time on the column, or achieved through changing the amount of enzyme or the length of the enzyme-gel column. A modified form of this method was made by Updike and Hicks with an enzyme gel covered electrode coupled to a gel-less electrode that could be implanted into a live subject for continuous glucose concentration measurement[14].

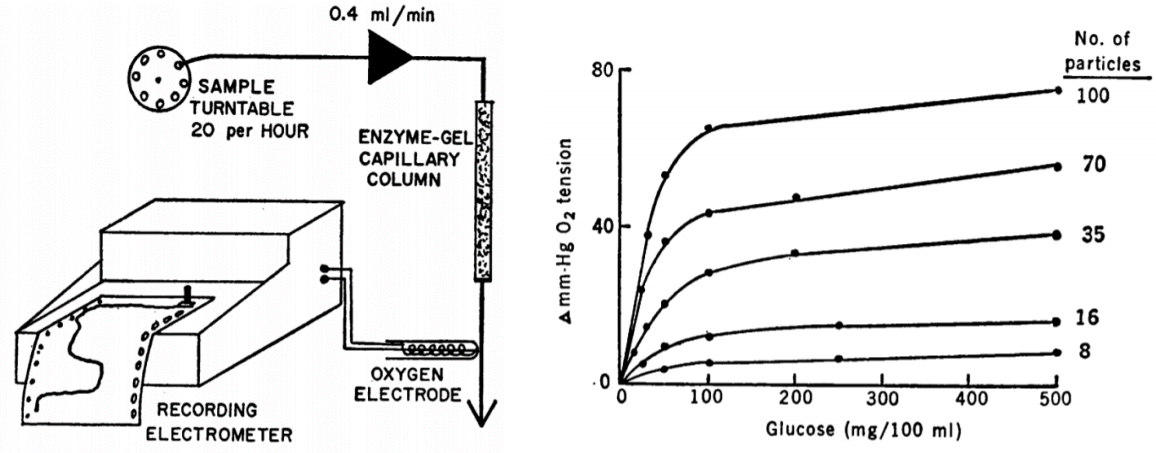

Figure 1.5 Updike and Hick's glucose sensor as illustrated in their 1967 paper[13] as well as its performance.

In 1973 the first sensor was made that relied on the reduction of hydrogen peroxide produced in the oxidation of glucose by GOx[15]. These developments led to the production of the first commercial glucose biosensor, the model 23 YSI analyzer in 1975 (see Figure 1.6). This

system also utilized two size exclusion membranes (much like Clark and Lyon's initial oxygen sensing electrode), an outer polycarbonate membrane and an inner cellulose acetate membrane with glucose oxidase gel sandwiched between. This simplified setup allowed for the miniaturization of the sensor since no pH electrode or columns were needed. However, the high operating voltage of (+ 0.7 V vs Ag/AgCl) required for the hydrogen peroxide sensors necessitated new developments for long term and *in vivo* testing, since many interferants in biological samples would oxidize at this voltage.

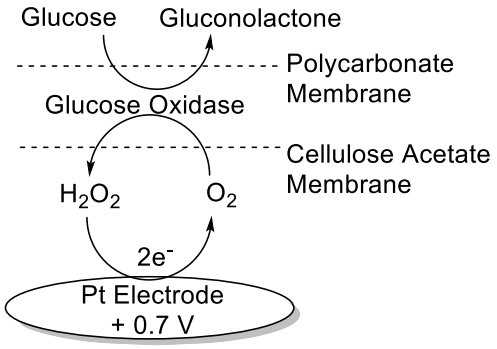

Figure 1.6 A graphical representation of the model 23 YSI glucose biosensor.

It is now common to classify these electrochemical sensors in different "generations", of which the electrochemical sensors described above are 1st generation glucose sensors; meaning that they rely directly on the sensing of oxygen concentrations before and after use, or on the oxidation/reduction of the products of the GOx/Glucose reaction directly (Scheme 1.2)[3]. These

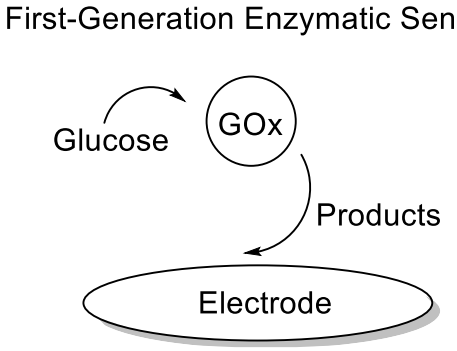

Scheme 1.2 How first-generation enzyme based electrochemical glucose sensors pass electrons to an electrode surface.

electrodes work great in theory, however the physiological concentration fluxuates causing errors in the glucose determination due to oxygen deficits. Given that these products can also oxidize at high voltages these 1st-generation sensors are prone to interference by many biological molecules. These difficulties spurred the development of a new approach to enzymatic glucose sensing.

Second-generation glucose sensors replaced the oxygen/hydrogen peroxide redox couple with a catalytic redox mediator that interacts directly with the active site of the enzyme (Scheme 1.3). These mediators outcompete the oxygen in their ability to bind to the active site and reversibly switch between two states, making them catalytic. The mediator is needed to pass the electrons to the electrode because the $FADH_2$ site is buried in the middle of the enzyme, and the mediator can diffuse into and react directly with the $FADH_2$ site that is protected from the electrode surface. The use of these mediators allowed for lower operating potentials and fewer endogenous electroactive interferents like ascorbic acid, some drugs, and uric acid. Many effective mediators

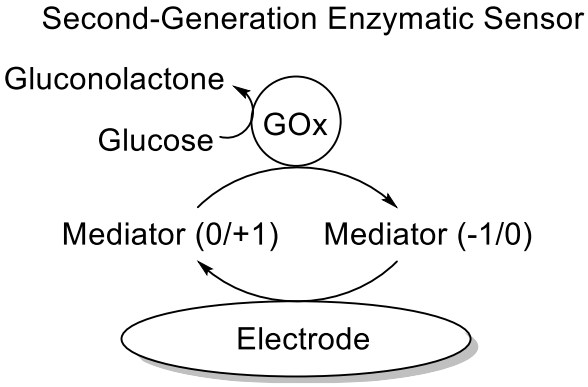

Scheme 1.3 A representation of how second-generation enzyme-based electrochemical glucose sensors pass electrons to an electrode surface.

have been found including ferrocyanide, ferrocene derivatives, methyl viologen, tetracyanoquinodimethane, tetrathiafulvalene and methylene blue[16-18]. While the first of these, ferrocyanide, was found in 1970, mediators were not rapidly included into commercial devices. The second generation mediators were put into a commercial sensor for the first time with a screen

printed electrode using glucose dehydrogenase and a ferrocene derivative as a mediator to produce the first "on-the-go, pen-sized" glucose sensor[19], dramatically changing the lives of millions of diabetics.

Because of the highly efficient electron transport from the GOx to the electrode, second-generation type electrodes have historically been among the most sensitive enzymatic sensors developed. To allow this, many different strategies for enzyme and mediator immobilization on electrode surfaces have been developed to produce second-generation enzymatic glucose sensors. The immobilization matrices used are usually hydrophilic in order to allow for the diffusion of dissolved molecules through the gel. However, in our group's experience this causes them to be susceptible to delamination from material swelling forces. Second-generation sensors also rely on the passing of electrons through an electron mediator, requiring a step down in voltage between the enzyme and the mediator and the mediator and the anode, lowering the voltage generated by this system each step of the way. These problems necessitated research into a new approach to enzymatic sensor development, and more recently more research has been focused on a third generation of enzymatic and non-enzymatic glucose sensors[4].

In the 1990's, third-generation biosensors were developed that rely on the direct transfer of electrons from the enzyme to the electrode surface (see Scheme 1.4). While often referred to as mediatorless sensors, they have relied on the use of a layer of conducting organic salts such as

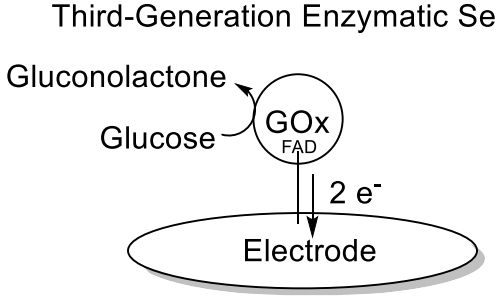

Scheme 1.4 How third-generation enzyme-based electrochemical glucose sensors pass electrons to an electrode surface.

tetrathiafulvalene-tetracyanoquinodimethane (TTF-TTCNQ)[20] that has long thin crystals to conduct electrons from the enzyme to the electrode surface. These have been shown to work with pyrrole-quinolinequinone-based enzymes such as glucose dehydrogenase. Electrodes have also been assembled with carbon nanotubes and other nanoparticles functionalized with FAD and treated with the apo-enzyme to wire the active site of the enzyme directly to the electrode[21]. While these electrodes have good selectivity, they have lower sensitivity and accuracy than second-generation glucose sensors. However, the direct electron transport from the enzyme to the electrode eliminates the need for a hydrogel immobilization material, alleviating the matrix swelling and disintegration problem and allowing for the production of more robust sensors. While the direct electron transfer from the enzyme to the electrode surface generates a larger voltage than second-generation sensors, the monolayer nature of these electrodes leads to small current outputs from these sensors, yielding a lower sensitivity to glucose concentration.

Nonetheless, these more stable third-generation sensors have led to the production of needle electrodes incorporated into the first "continuous glucose monitor" (CGM) made by Medtronic MiniMed, which was approved by the FDA in June 1999[22]. While these devices offer a dramatic increase in quality of life and patient health, they are not truly continuous but take measurements of the sub-cutaneous glucose levels every few minutes. These measurements of the interstitial glucose levels (as opposed to blood-glucose concentrations) correlates to blood glucose levels[23], however, they require a prompted pin prick test with a second-generation glucose sensor to confirm out-of-range glucose readings. These third-generation monitors have also been used in tandem with wearable insulin pumps for immediate and efficient treatment of glucose irregularities. While these subcutaneous glucose monitors are a dramatic improvement over pin prick only testing, they are costly, and only currently last 12-14 days before needing to be replaced.

Since blood glucose monitoring is still needed with these CGM devices, the holy grail of CGM would be to produce an electrode with high stability, selectivity, sensitivity, and blood biocompatibility, all of which have been displayed in the second-generation glucose sensors except for stability. In addition to this, the second-generation glucose sensors have much higher amperometric output, giving them some potential utility as anodes in electrochemical biofuel cells which could also power an insulin pump. This combination of sensor and fuel cell could be used as a stand-alone artificial pancreas device.

While it is generally clear which generation a particular sensor belongs to, there are some that are still not well understood. For example, in 1964 a potentiometric glucose sensor was made[24] that was assumed to be a first generation sensor, as it was found a mere 2 years after the first amperometric glucose sensor was outlined by Lyons and Clark in 1962[12]. This sensor relied on a redox reaction between iodide and the H_2O_2 produced in the oxidation of glucose by GOx as seen outlined in Figure 1.6. This redox chain was thought to be the means of the production of iodine in this system and the resulting catalytic current. In fact, since this sensor was first developed there have been iterations of sensors and biofuel cells relying on the production of iodine from this reaction with hydrogen peroxide in order to function. These typically are colorimetric sensors that rely on the iodine oxidizing an indicator/electrode or complexing with starch to show the glucose

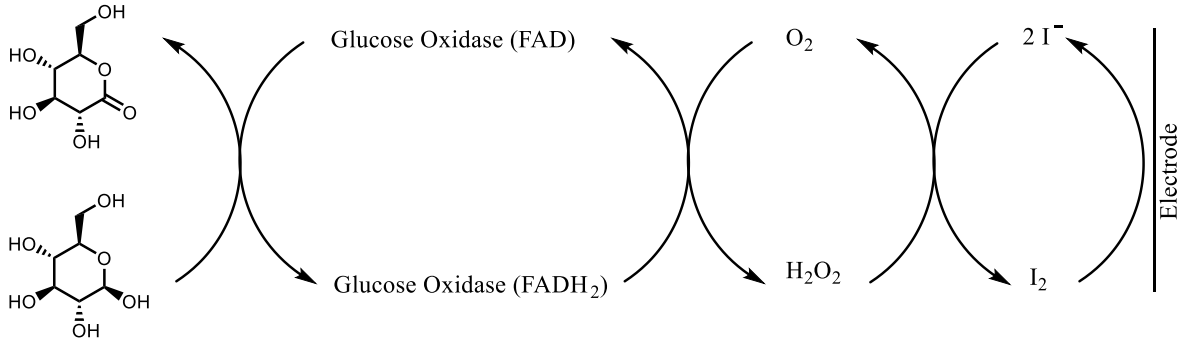

Figure 1.6 Postulated electron transport chain from glucose to an electrode through GOx, oxygen/hydrogen peroxide and iodide/iodine redox couples.

concentration of the solution[6, 25-26]. While this reaction between the iodide and hydrogen peroxide certainly takes place, the possibility that the iodine was being reduced directly by the GOx was not considered as a way that the electrons could move from the enzyme to the electrode surface since there were no known second-generation sensors at the time. Even today the question remains; could the iodide be acting like a second-generation redox mediator and directly oxidizing the $FADH_2$ active site?

1.3 Second-Generation Stabilization Strategies

1.3.1 Bulk Material Crosslinking

In order to be considered for real time *in vivo* testing, a glucose powered bio-electrode must have both the enzyme and the mediator immobilized on the surface of the electrode to prevent inactivity from either the GOx or mediator diffusing away from the electrode, as well as to prevent the leaching of potentially toxic redox mediators into the blood stream. The first fully immobilized enzyme and mediator electrode was made by Heller's group with a poly(vinylpyridine)-osmium bipyridine copolymer (see Figure 1.7)[27]. This material was deposited on an electrode surface by dipping in a highly saturated solution of the polymer, and the GOx was deposited on the electrode by its inherent adsorption onto the redox polymer surface. Given this, it can be assumed that this material would eventually dissolve in whatever aqueous media it was measuring, severely limiting

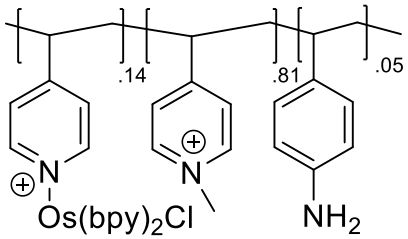

Figure 1.7: The first redox polymer used to immobilize GOx on an electrode surface in a second-generation glucose sensor.

the lifetime of this type of sensor. In order to overcome this problem, crosslinking of the polymer on the electrode surface could be carried out.

To keep all of the components (the polymer matrix, redox mediator and GOx) on the electrode, the immobilization of GOx with the matrix without the loss of its function is necessary. This keeps the GOx in proximity of the electrode, minimizing the amount of material needed for the construction of these electrodes. Heller and Guilbault demonstrated the covalent attachment of a ferrocenyl group to the protein shell of the GOx, and showed that GOx could be functionalized and covalently crosslinked into a polymer matrix without loss of enzyme function[15,27]. It is also important to identify the best materials from the long list of potential mediators, enzymes, and polymer matrices for the construction of these electrodes.

As previously stated, the immobilized material must be durable, biologically inert, and water permeable to allow for the diffusion of glucose through the material. Further, the mediator must be electrochemically stable over many cycles, non-toxic, and able to interact with the GOx reactive center and transfer electrons to the electrode surface. Initially the materials used in these sensors were lacking in water solubility, which has led to their replacement with other materials such as chitosan and polyethylenimine (PEI). These materials have been functionalized with many mediators including osmium complexes, manganese and chromium sandwich complexes, naphthoquinone, and a few different functionalized ferrocene mediators[28,29,30]. Some of these electrodes even included the use of an assortment of gold nanoparticles and carbon nanotubes to wire the enzymes to the electrode surface[18, 31-33].

The Glatzhofer group has used ferrocene-functionalized PEI to study the basics of enzymatic glucose biofuel cells[33-39]. Originally the Glatzhofer group used the cheaper and widely used branched-PEI (BPEI) functionalized by reductive amination with ferrocenecarboxaldehyde[40]. The amines in this material, when mixed with ethylene glycol diglycidyl ether (EGDGE) and GOx, will react with the epoxides of the EDGDE and crosslink the PEI around the GOx and entrap it within the electrode material (see Figure 1.8**)**. These work well until the BPEI, upon absorbing water under use, will swell and eventually delaminate from the electrode, deactivating the electrode. The crosslinked BPEI molecules can be described as "fuzzy caterpillars" that have more hydrophilic primary amine domains on the outside surrounding tertiary amines in its core, leading to inhomogeneous swelling and high stress points on the crosslinks between polymer molecules. It was then shown that linear-PEI (LPEI) outperforms the BPEI in these electrodes, producing a current density of ~480 μA/cm^2 at saturating glucose concentrations[41].

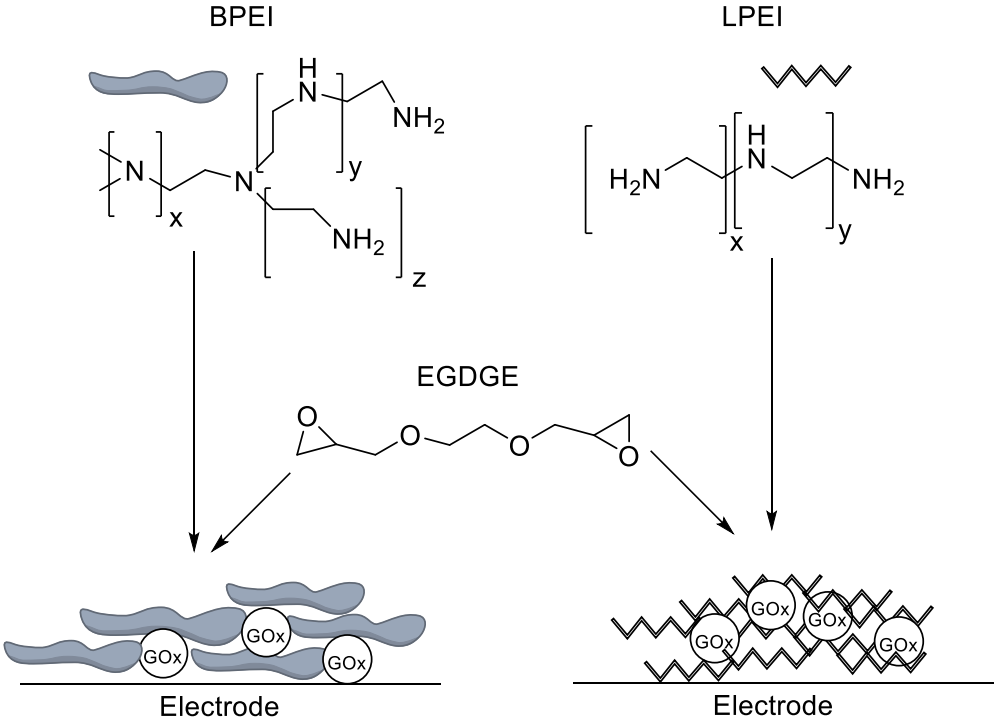

Figure 1.8 Crosslinked electrodes entrapping GOx, constructed using EGDGE and PEI.

The use of ferrocene carboxaldehyde to functionalize the PEI (LPEI and BPEI) in these electrodes resulted in a one-carbon linker between the ferrocene and the polymer matrix, giving them a short diffusion range from the polymer backbone (first structure in Figure 1.9). As mentioned earlier, the mediator needs to penetrate the enzyme and interact with the $FADH_2$ active site inside the enzyme. Therefore to improve performance further, ferrocene mediators with three- and six-carbon linkers to the LPEI (see Figure 1.9) were developed and incorporated into the biosensor[35] and compared to the one-carbon linker. The three-carbon link from the ferrocene to the LPEI performed the best, producing ~1 mA/cm^2 compared to ~800 and ~600 μA/cm^2 at saturating glucose concentrations for the one- and six-carbon links, respectively. The 3-carbon linker was also shown to be more stable to continuous cyclic voltammetry than the other two mediators. While this improvement was a step in the right direction, more stability was needed for these electrodes to be commercially viable.

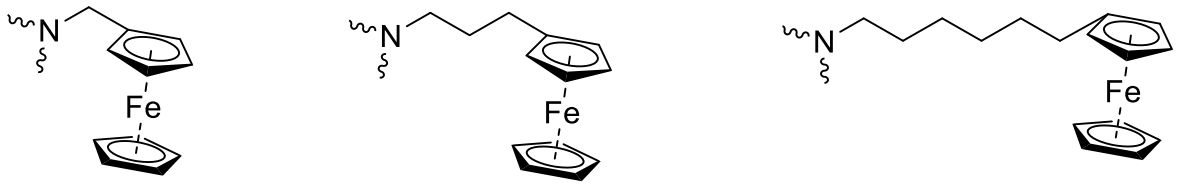

Figure 1.9 comparison of one- (Fc-C_1-LPEI), three- (Fc-C_3-LPEI), and six-carbon (Fc-C_6-LPEI) linker between ferrocene and the PEI polymer.

In order to improve this sensor, single walled carbon nanotubes (SWCNTs) were incorporated to effectively wire the enzyme to the electrode surface electrically. While the nanotubes had a dramatic effect on the current density (increasing it to 3 mA/cm^2) they did not dramatically change the stability of the films, which retained 67% of their original current after 24 hours of operation as a sensor at 0.4 V compared to 55% without any SWCNTs added[42]. Given these materials' lack of stability our group decided to look for a more stable electrode construction technique to produce enzymatic GOx biosensors.

These surface crosslinked electrodes still would swell and as a result, delaminate from the surface of the electrode, causing a large decrease in activity after a day of CV cycling. The time and material needed to make these electrodes was also somewhat high. The negative attributes of these crosslinked electrodes were sidestepped by the Glatzhofer group when they produced their first layer-by-layer (LBL)[37, 39] constructed bioanodes using Fc-LPEI and GOx materials.

1.3.2: Second-Generation Stabilization Strategies, Layer-By-Layer Construction

Several groups have investigated using LBL techniques to construct electrodes[43-44]. The Glatzhofer group did this using cystamine to attach the material covalently and electrostatically to gold surfaces (see Figure 1.10). This cystamine provides amines that are mostly positively charged and can electrostatically attract the negatively charged surface of the GOx. The GOx in these electrodes was modified using sodium meta-periodate to oxidize residual sugars on the GOx surface, introducing aldehyde functional groups (p-GOx)[45]. The nitrogens of the ferrocene-modified LPEI provide another layer of positively charged material and can also react with the aldehydes on the surface of the p-GOx, making a crosslinked network built up by successive dipping in solutions of each material (see Figure 1.10). With this system it has been easy to test a number of basic properties related to these ferrocene-mediated GOx glucose sensors. These electrodes produced ~1.4 mA/cm^2 at saturating glucose concentrations and 59 μA/mM cm^2 at 5 mM glucose concentrations (physiological range)[39]. However, these electrodes still had a large decrease in activity after a few hours of use. This was largely attributed again to the delamination of the electrode material as much of the ferrocene was not present on the electrode, as measured

by cyclic voltammetry after use. Therefore, more development of covalent attachment methods for the electrode surface is needed to optimize the stability of these enzymatic glucose sensors.

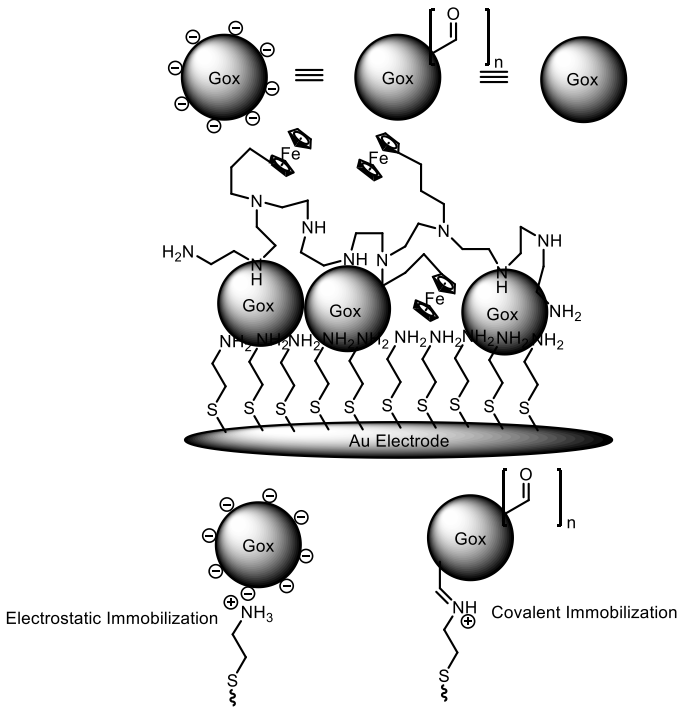

Figure 1.10 The cystamine first layer electrode of a LBL-fabricated glucose-sensing gold electrode.

1.4 Electrochemical Biofuel Cells

1.4.1 How Electrochemical Biofuel Cells Work

Because the sensors discussed above generate a potential that can drive an electric current, they can be utilized as anodes in biofuel cells. These fuel cells and sensors can be understood from a few basic principles. In order to outline the basics of a fuel cell better it is useful to illustrate this with a simple hydrogen/oxygen fuel cell as shown in Figure 1.11. This is the diagram of a fuel cell that oxidizes hydrogen to protons at the anode and reduces oxygen to water at the cathode while passing electrons through a circuit between the electrodes. These electrons traveling through

the circuit can be used to do work, thus transforming the energy contained in the chemical bonds into useful electrochemical energy. The amount of energy this circuit produces can be calculated using the Gibb's free energy relationship for electrochemical processes, (expressed in Equation 1.4) shown below where ΔG_{Cell} is the amount of energy available in the cell to do work in kJ/mol, n is the number of electrons transferred from the anode to the cathode through the circuit, F (Faraday's constant) is the magnitude of charge of one mole of electrons, and E_{cell} is the potential of the cell. This E_{cell} can be found (Equation 1.5) by taking the voltage of the half reaction occurring at the cathode ($E_{cathode}$) and subtracting the potential of the half reaction at the anode (E_{anode}). For a hydrogen/oxygen fuel cell that has an E_{cell} of +1.23V, the Gibbs free energy is -237

Equation 1.4 $\Delta G_{Cell} = -nFE_{Cell}$ Gibb's Free Energy

Equation 1.5 $E_{Cell} = E_{Cathode} - E_{Anode} = +1.23V - 0V = 1.23V$

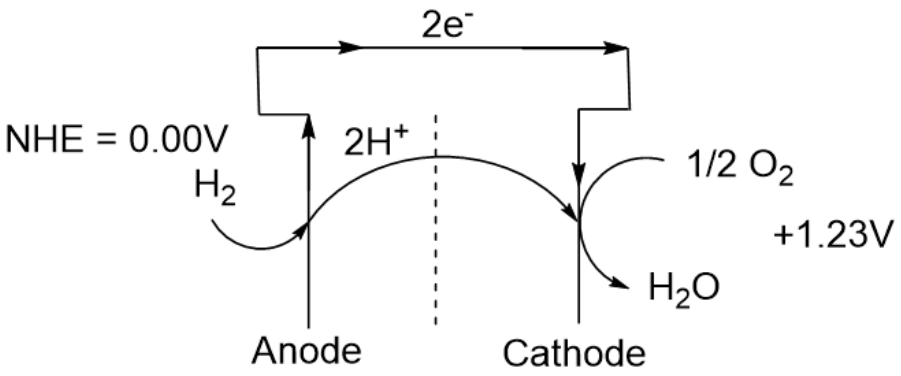

Figure 1.11 A basic hydrogen/oxygen fuel cell.

kJ/mol.

The experimental voltages (V, in volts) obtained can be multiplied by the current produced (I, in amperes) to obtain the power (P, in Watts) output of the fuel cell. Fuel cells can be scanned from the open circuit potential (the potential with infinite resistance and no current flowing) to the limiting current (no resistance) by changing the resistance (R) of the circuit, and the resulting plot

generated is called a polarization curve. These polarization curves can be multiplied by the voltage to generate a power curve (Figure 1.12). The power curves are important in fuel cell characterization since they indicate the amount of power that can be obtained from the fuel cell at

Equations for Power Curves

$$V = IR$$
$$P = IV$$

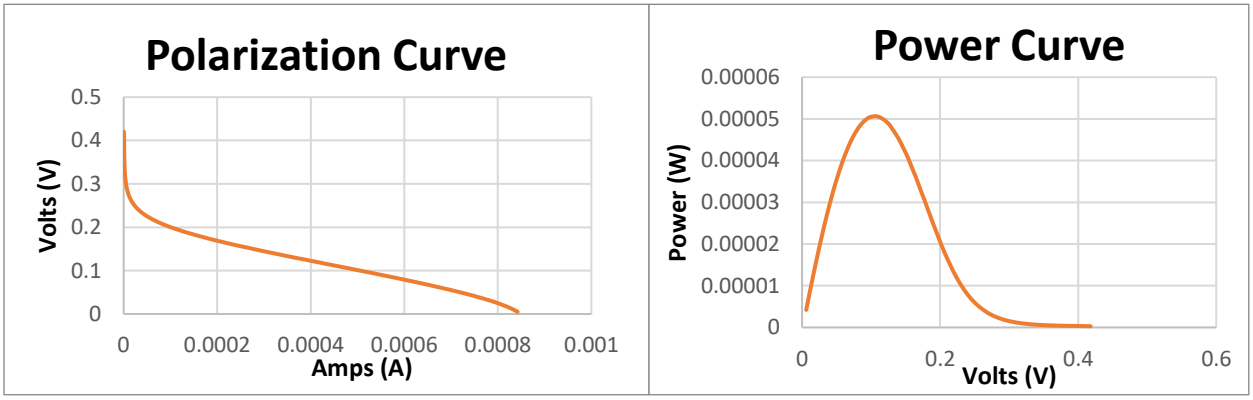

Figure 1.12 An example of a polarization curve of a fuel cell and its corresponding power curve obtained from electrodes made in Chapter 3.

a given potential, and what that potential is.

Electrochemical fuel cells work on the same principals as any chemical or combustion fuel cell; the transformation of molecules from high energy starting materials to lower energy products while extracting the energy from the changes in chemical bonds to do work. Fuel cells rely on energetic molecules interacting with metal electrode surfaces, building up charge (voltage) and transferring their electrons and energy from one electrode to the other through the wire connecting them. The molecules interacting with the electrodes must be close to or touching the electrode surface, which is why the buried GOx active site is usually coupled to the electrode surface with a mediator that can diffuse between the inaccessible active site and the electrode surface. There must be a drop in potential from the GOx active site[46] (see Figure 1.13[39]) to the mediator for the electrons to move to the mediator, and then to the electrode. It is desirable to match the mediator

redox potential with the $FADH_2$ potential in order to produce higher voltages between the cathode and the anode and produce more energy.

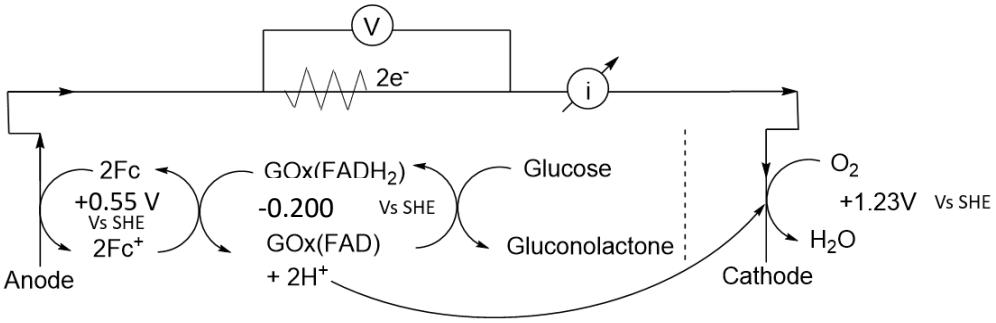

Figure 1.13 A ferrocene (Fc) mediated glucose biofuel cell with a bioanode poised against an oxygen breathing cathode. All voltages are shown vs SHE.

There are many types of fuel cells with all kinds of advantages and disadvantages. The advantage of using a glucose powered fuel cell is that the fuel is abundant, renewable, the product of the fuel consumption is completely non-toxic, and there is the potential for implantable electronic devices with no battery that would need replacing. It also has an advantage over the hydrogen/oxygen fuel cell in the sense that there is no need for the storage of explosive gases since the anode is powered by a water-soluble fuel, and the cathode from oxygen in the air. This glucose biofuel cell concept is pictured in (Figure 1.13) as a second-generation GOx bioanode poised against a platinum air breathing cathode. While the theoretical E_{cell} of the glucose/oxygen fuel cell would be a staggering 1.43 V, the passing of electrons stepwise through the GOx and ferrocene mediator results in a potential loss between the two electrodes to 0.68 V which comes out to 66 kJ/mol. This potential drops further given the fact that the oxygen cathode is pH dependent, and the observed potential will be significantly lower than the theoretically 1.23 V due to neutral pH of this particular GOx system (the platinum electrode works best at low pH). Implanted biofuel cells must use dissolved oxygen and operate at a pH of 7.35-7.45, since this is the pH of the human body.

Biofuel cells with biofueled anodes and cathodes have been constructed, removing all need for any gas electrodes. These biofuels could potentially contain a large amount of energy; however, the fact that they must be dissolved in water significantly lowers the energy density of these fuels. For example, GOx typically reaches its V_{Max} around 0.1 M glucose in our group's electrodes, leading to a large decrease in energy density of these fuels when compared with pure liquids and gases. While this doesn't matter in implanted fuel cells since the blood-glucose concentration is roughly 4-15 mM, it is a real problem in all other enzymatic fuel cell applications where fuel concentration is not limited by biological constraints. For fuel cells that are not in living organisms, selectivity and pH can largely be ignored, therefore non-enzymatic glucose biofuel cells are more popularly explored as an alternative to enzymatic glucose biofuel cells when glucose sensing is not in consideration.

1.4.2 Non-Enzymatic Glucose Sensors and Fuel Cells

While non-enzymatic glucose biosensors can be highly sensitive to glucose, they generally lack the substrate specificity of an enzyme. This makes them a bad choice specifically for sensing glucose in the human body or any other biological sample where many different oxidizable molecules can be present. However, the non-enzymatic electrodes have many advantages over enzymatic electrodes in fuel cells. For example, GOx has a relatively low substrate saturation concentration, limiting the output current that can be achieved in these systems, while non-enzymatic systems have greater promise in accommodating larger concentrations of glucose without their current plateauing. This is due to the need for the substrate to diffuse into the enzyme active site, whereas a non-enzymatic reaction site is often a surface or redox-active molecule. GOx can also only oxidize glucose to gluconolactone (extracting 2 electrons) and needs an enzyme cascade to completely oxidize gluconolactone to CO_2 and produce 24 electrons[47]. Enzymes are

also susceptible to denaturing under unfavorable pH conditions, high heat, or after long use. These disadvantages can be sidestepped in fuel cells by removing the enzyme from the cycle all together.

Some non-enzymatic systems have been reported to oxidize glucose (see Scheme 1.5), extracting all 24 electrons and producing only water and carbon dioxide. The theoretical energy output of these electrodes 4430 W hr/kg[48]. While the energy density (assuming working near the solubility limit of 909 g/L) is about 1/3 that of gasoline (9700 W hr/L) this would be an ideal cheap energy source for many applications. With current technologies it would also take a very large surface area electrode, as well as many fuel cells in series and parallel, to extract this energy quickly enough to compete with the power of an internal combustion engine. However, such glucose fuel cells could be looked at as a renewable cheap energy source for many other stationary applications.

$$C_6H_{12}O_6 + 24\ OH^- \longrightarrow 6\ CO_2 + 18\ H_2O + 24\ e^-$$ Anode

$$6\ O_2 + 12\ H_2O + 24\ e^- \longrightarrow 24\ OH^-$$ Cathode

$$C_6H_{12}O_6 + 6\ O_2 \longrightarrow 6\ CO_2 + 6\ H_2O$$ Overall

Scheme 1.5 Electrochemical equations for the non-enzymatic polyviologen fuel cell and the overall reaction of the cell.

Non-enzymatic glucose biofuel cells have been made using many different materials, from nanoparticles to surfaces to organic redox mediators[3-4, 49-50]. Many of these fuel cells use cobalt, copper, nickel or gold nanoparticles, complexes, nanowires and more. While these electrodes are not generally as selective as enzymatic electrodes, some of them have very linear amperometric plots with respect to glucose concentration and are extremely stable, some being reported stable after two months of use. While nanoparticles are great for use in fuel cells, they often are difficult

to fabricate, expensive, and are reported to be extremely toxic[51], so any long-term use of these *in vivo* would need to be tested extensively before use due to their biological accumulation over time. In 2013[52] it was reported that methyl viologen, a common 2nd generation GOx mediator[53] (see Figure 1.14), containing solutions were able to oxidize glucose without GOx present at elevated pH. While it is not practical for use in a biological system since the methyl viologen is toxic and not selective for glucose, and the cell was held at a high pH, these results are promising for the production of extremely cheap organic glucose fuel cells that could potentially run with high glucose concentrations.

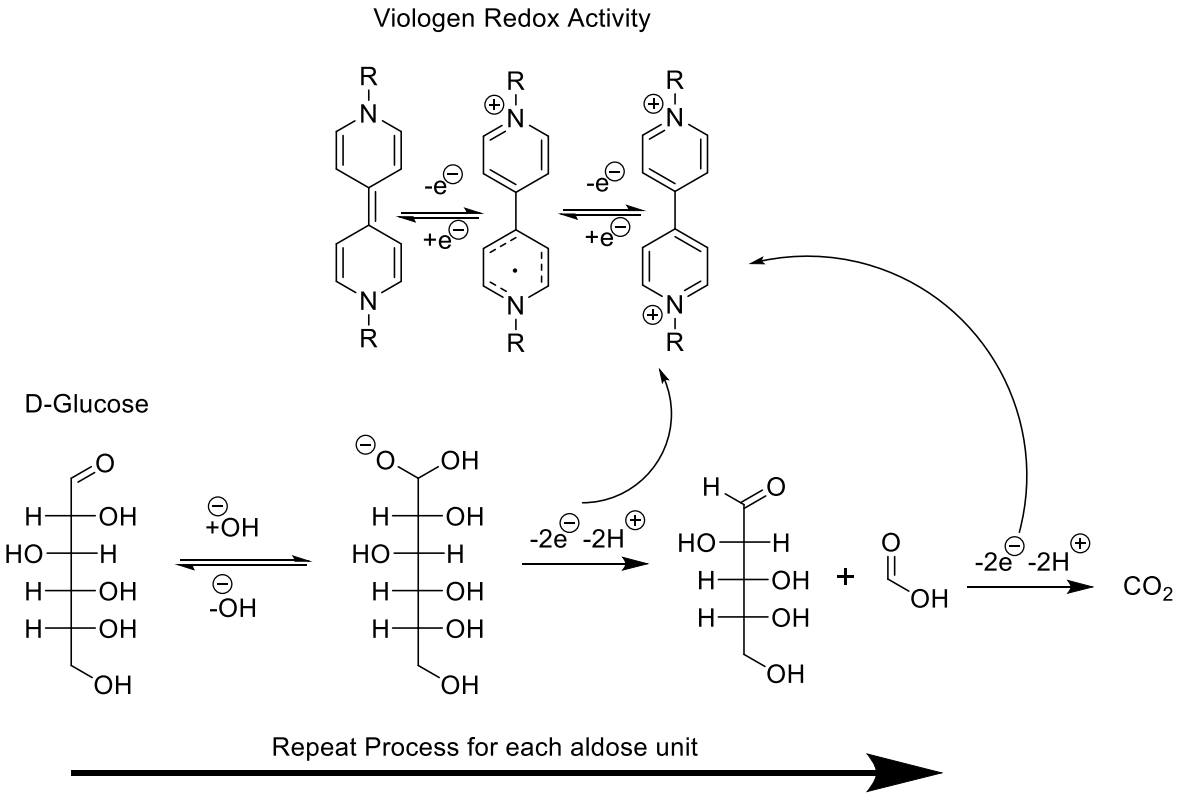

Figure 1.14 Electrochemical reduction of a viologen unit shown with its oxidation of D-glucose to show how 4 electrons are taken from each aldose unit.

1.4.3 Polyviologen Glucose Biofuel Cells

Since methyl viologen (paraquat) is an environmental toxin, it is important to control the material and to use as little of it as possible. The simplest way to do this with viologen electrodes is to polymerize the viologen on the electrode surface (Figure 1.15). Because of their electrical conductivity and ease of fabrication, our group has used polyviologens as an organic catalyst to oxidize glucose, potentially all the way to carbon dioxide and water[54]. Polyviologens can be made by reductive electropolymerization of poly(4-cyanopyridinium) compounds using a cyanide leaving group to clip two pyridinium rings together and form polyviologens. The viologen glucose fuel cell works most efficiently under high pH conditions due to a dependency of the process on the concentration of hydroxide ions. This abundance of hydroxide anions can lead to the oxidation of the viologen moieties, degrading the electrode's ability to oxidize glucose. The viologen moieties also have a strong tendency to dimerize due to the strong interaction between pi orbitals, also deactivating their catalytic capabilities. This has led to the need to develop and use other

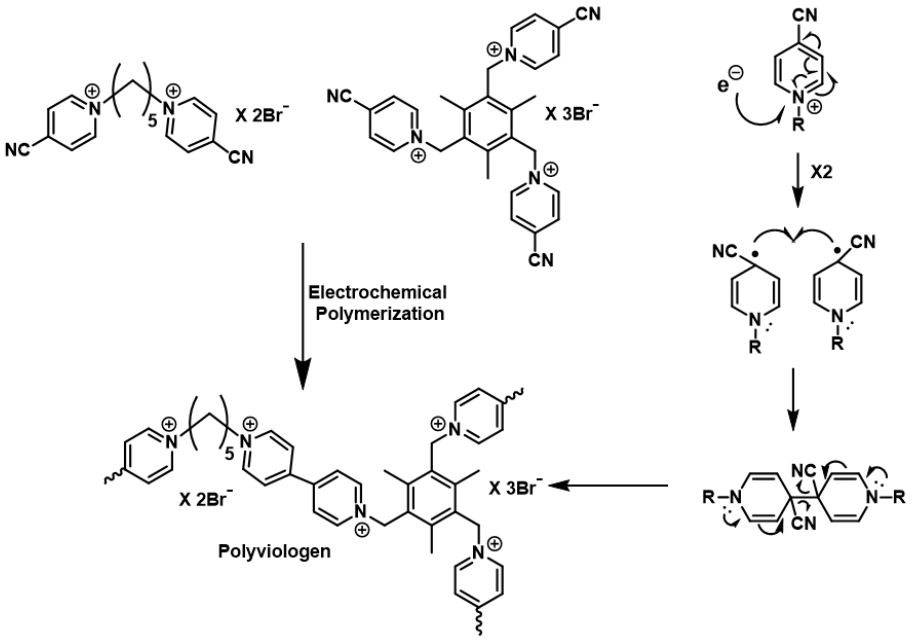

Figure 1.15 The molecules used, and the polymer produced for the polyviologen non-enzymatic glucose-fueled anode.

mediators, or to find a way to protect the viologens from dimerization or oxidation by hydroxide while still allowing them to oxidize glucose.

1.5 Project Goals

1.5.1 Determination of Iodide's Mechanistic Interaction with Glucose Oxidase and Ferrocene

As discussed in Chapter 1.2, the accepted mechanism of mediation of GOx by iodide involves an indirect chain of reactions with glucose oxidase oxidizing glucose to gluconolactone, and then in turn passing those electrons on to oxygen reducing it to H_2O_2, and finally this H_2O_2 oxidizing iodide to iodine. In studying the interaction of glucose oxidase and ferrocene-based mediators, our group has produced water soluble ferrocene salts. Using these salts, the kinetics of the electron exchange between the glucose oxidase and the ferrocene mediator were studied and were found to be consistent with two ferrocenes bound by each glucose oxidase enzyme[55]. In the course of these studies, one of the mediators used was the ferrocenylmethyl-N,N,N-trimethylammonium iodide (FcTMAI) salt (see Figure 1.16) and it was found that the ferrocene and iodide redox potentials were within 0.15 V of one another using cyclic voltammetry. This means that the redox processes are close enough in potential that they can interfere with one another, and in practice the iodide appeared to amplify the catalytic current of the ferrocene in the

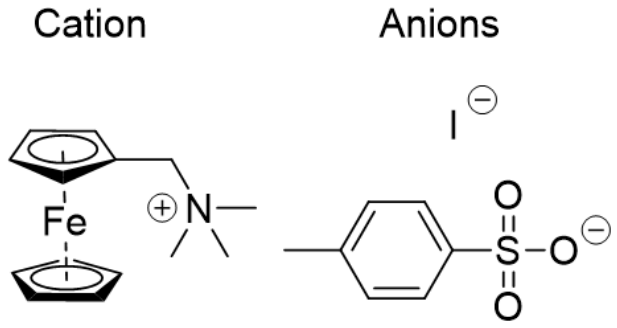

Figure 1.16 Water soluble ferrocene salts used to study ferrocene's interaction with GOx.

presence of GOx and glucose. Therefore, the iodide salts were replaced with chloride and tosylate salts for these studies. However, these findings led us to question the exact mechanism by which the iodide mediates electron transport from the enzyme to an electrode or to a colorimetric indicator.

In Chapter 2, the mechanism by which iodide mediates electron flow from GOx is examined. Experiments show that the function of a sensor with iodide as a mediator is not inhibited by the removal of oxygen from the system. Michaelis Menten curves using sodium iodide as the mediator after purging with N_2 and air, respectively, were made and statistical differences between the two were not found. These results indicate that the iodide mediates without the help of the O_2/H_2O_2 redox couple and is consistent with the idea that it may go through a process similar to the ferrocene mediators. Chapter 2 details these studies showing that iodide can mediate GOx on its own.

1.5.2 Carbon Disulfide Modified LPEI

Our group has constructed many efficient glucose biosensor and biofuel anodes using ferrocene modified PEI and GOx[30, 33-39, 41-42, 56-58]. Using methylated and chlorinated ferrocene, the tunability of the voltage output of these devices has been demonstrated. Improvements of current output by incorporating carbon nanotubes into the polymer matrix have also been shown. At the time of their publication, these anodes had among the highest power and current outputs of known biofuel cells and produced some of the most sensitive amperometric sensors based on the use of GOx oxidizing glucose. However, because of the drawbacks of crosslinked anodes, namely the long curing times, poor controllability of the crosslinking reaction, and most importantly, the material delamination issues these anodes experience, the use of layer-by-layer (LBL) electrode

fabrication techniques has been studied using ferrocene modified LPEI (Fc-LPEI) as a mediator/matrix.

The LBL assembly technique using materials pioneered by our group takes advantage of two structural properties. The first is the opposite polarity of our polymer backbone and enzyme GOx. The polymer LPEI has many amine units and when dissolved in water it becomes positively charged and is attracted to the GOx that naturally has a negatively charged surface at neutral pH's. The second factor is that the saccharide-coating of the GOx outer layer chemical is oxidized with sodium periodate. This oxidation produces many aldehyde functional groups that are then available for crosslinking with the nucleophilic amines of the polymer backbone. These factors lead to both the electrostatic attraction between the two materials and their subsequent covalent crosslinking and allows for the sequential addition of layers of material to the electrode surface as a covalently crosslinked gel made of PEI and GOx. These electrodes originally used cystamine dihydrochloride to produce an initial layer of positively charged amines on the surface of a gold electrode (see Figure 1.17) to build the rest of the electrode on. Since the production of these LBL

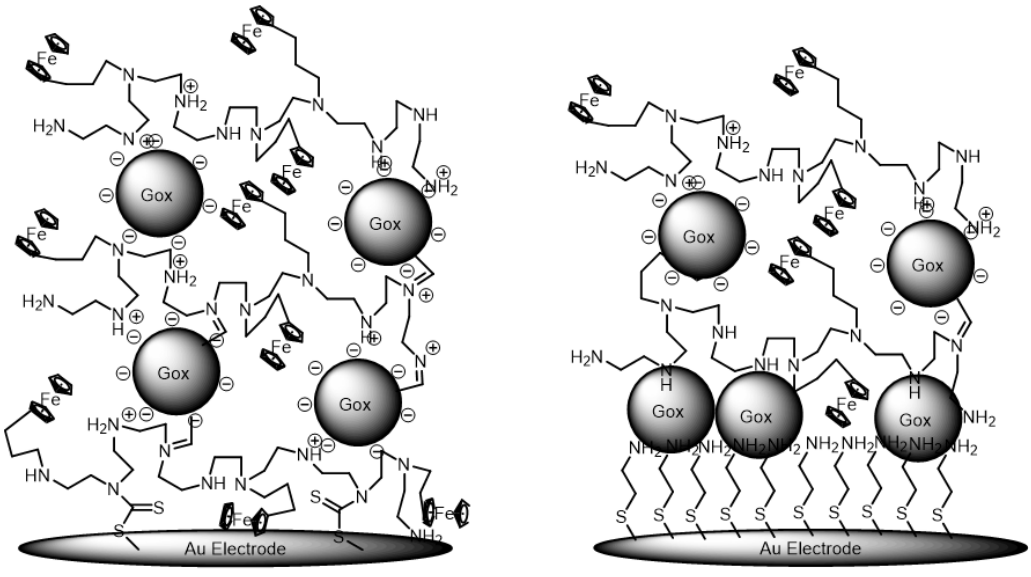

Figure 1.17 A multilayer Fc-LPEI based enzymatic electrode shown with Fc randomly dispersed in the material.

fabricated anodes, adjusting the tether length (from 1 to 6 and finally to 3 carbons) between the ferrocene groups and polymer backbone has led to high current density electrodes being fabricated extremely quickly and efficiently using LBL methods. Impressively, these electrodes, fabricated using a negligible amount of material, have roughly one half[39] (1.4 vs 3 mA/cm^2) of the current density when compared to the best bulk material crosslinked electrodes with CNT incorporation[42] produced by our group. However, these LBL constructed bioanodes still suffer from many of the lack of stability problems experienced by the bulk crosslinking method, likely from material delamination and enzyme deactivation through denaturization.

The first layer of these LBL constructed bioanodes utilizes cystamine dihydrochloride to produce a layer of cationic amines on the surface of a gold electrode and lay down the initial layer upon which the rest of the electrode is built. While sulfur makes a strong bond with the gold surface and the amine provides an anchoring point for the GOx, this does not contribute to the function of the bioanode. In fact, it adds a layer of insulating material between the electroactive components and the electrode surface. It is our hypothesis that by modifying this first layer of the electrode material to be electroactive, better and more stable glucose sensors could be made.

Amino groups are able to form strong bonds with CO_2 and PEI has been proposed as a cheap and efficient material to capture and sequester carbon dioxide from the atmosphere[59] (see Scheme 1.6). This reactivity of amines with carbon dioxide is mirrored by reaction with its cousin

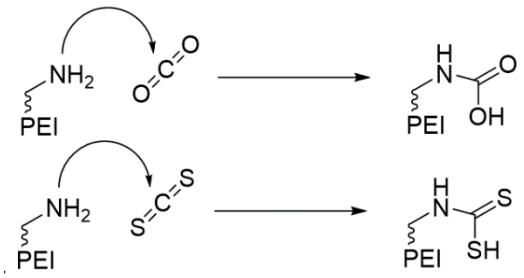

Scheme 1.6 A The reaction of PEI with CO_2 and CS_2.

carbon disulfide to form dithiocarbamate moieties. These dithiocarbamate groups have been used to immobilize DNA and lipid chains on gold surfaces[60-61]. In Chapter 3, the first LBL anodes using carbon disulfide substituted Fc-LPEI were constructed and studied with differing substitution amounts of both ferrocene and carbon disulfide substitution (see Figure 1.17). The effects of dipping pH and dipping time were also studied. The results show that these electrodes produce much higher current densities with lower numbers of layers and the same amount of current density at higher numbers of layers. These results indicate that the initial layer can greatly impact the overall performance of the sensor/fuel cell.

1.5.3 BPEI in LBL Glucose Biosensors

Because it is cheap, BPEI is widely available and was the first material used in our group's crosslinked glucose bioanodes. However, due to the non-homogeneous domain structure forming stress points between individual BPEI domains our group switched to using LPEI for a more cohesive and homogeneous polymer network with more crosslinks between different LPEI molecules. This difference can be thought of as the difference between gluing a bunch of footballs together *versus* gluing a network of string together. The LPEI forms a more cohesive network that resists breaking apart upon swelling when submerged in water while in use for long periods of time. For this reason, we initially used LPEI for our LBL constructed bio-anodes. However, BPEI contains about 25% primary amines on its outer periphery and it is our hypothesis that the way these "fuzzy caterpillar"-like molecules are deposited in a LBL construction leads to concentrated channels of ferrocene and GOx in the BPEI matrix efficiently wired to the electrode surface with very few inaccessible enzymes (Figure 1.18). In Chapter 4 the development of the first LBL constructed CS_2-Fc-BPEI/GOx/Fc-BPEI bioanodes is presented. These anodes were found to have

the highest current and power densities and sensitivity to glucose concentration of any of the LBL constructed bioanodes made by our group.

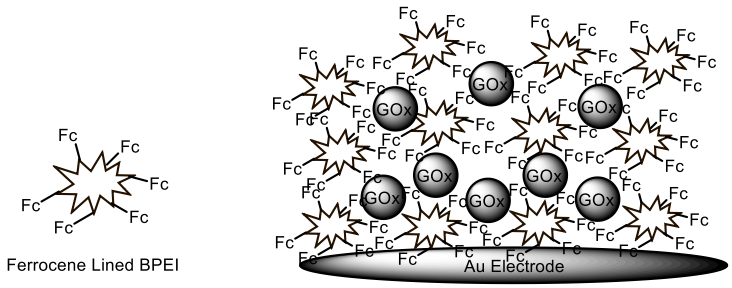

Figure 1.18 A multilayer Fc-BPEI based enzymatic electrode shown with ferrocene and GOx concentrated between the BPEI polymer cores.

1.5.4 Polyviologen Non-Enzymatic Glucose Biofuel Cells

Novel solution biofuel cells utilizing methyl viologen mediators have recently been developed that can oxidize glucose under basic conditions[52]. Theoretically, these fuel cells should extract 24 electrons per molecule of glucose in the system and up to 70% of these electrons have been extracted experimentally. This is extremely promising for the goal of producing high energy density biofuel cells. While methyl viologen interacts well with glucose under basic conditions, it can oxidize in the presence of hydroxide (Figure 1.19) and is also toxic, which presents a waste

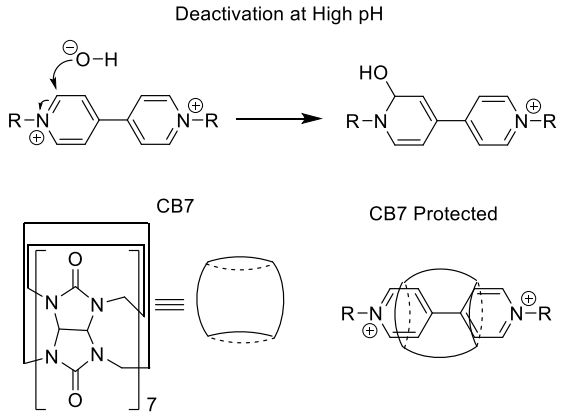

Figure 1.19 Encapsulation of viologen moieties protects them from oxidation under basic conditions.

problem. Since it would be difficult to separate the viologen from the glucose solution and regenerate the catalytic activity of the solution, using this mediator would cause a huge toxic waste problem and is not viable as a periodically replaced catalyst for the production of power from glucose in the long term.

While methyl viologen is a dangerous, water-soluble, environmental toxin, polyviologens that can be placed directly on an electrode surface to catalyze the oxidation of glucose avoids most of the problems involved in the environmental dangers of methyl viologen. This could also allow for the use of much less material than in solution biofuel cells where the methyl viologen to glucose ratio in the most efficient glucose fuel cells is 8:1. The concentration of viologen in a polymer on the electrode surface allows for a high local viologen to glucose ratio and high oxidation efficiency with minimal material. Our group has produced polyviologen fuel cells through the polymerization of para-cyanopyridinium salts on electrode surfaces[54]. The polymerization of the cyanopyridinium salts has been performed with a tris-pyridinium mesitylene salt to introduce branch points for a more porous polymer matrix to allow more surface area for the glucose to interact with the viologens (see Figure 1.15). The use of cucurbit[7]uril (CB7) as an encapsulation agent has also been shown by our group to insulate the vulnerable viologen units from the basic solution in these fuel cells (Figure 1.19). While the composition and concentrations of the monomers in the polymerization have been optimized, it is still unknown what the best method of polymerization in the production of these materials is.

In Chapter 5 the polymerization of these monomers is studied using constant potential, cyclic voltametric, and pulsed voltage techniques. These electrodes were tested for catalytic activity to determine the best method of polymerization. The stability of these electrodes was tested and the current and power densities were determined. The process was also repeated on

high surface area carbon felt electrodes. This polyviologen material represents an important development in the field of non-enzymatic organic glucose biofuel cells and presents a promising path forward to further this research.

1.6 Chapter 1 Bibliography

1. Centers; for Disease Control and Prevention, U. S. D. o. H. a. H. S., Centers for disease control and prevention. National diabetes statistics report, 2020. **2020**,

2. Warshauer, J. T.; Bluestone, J. A.; Anderson, M. S., New frontiers in the treatment of type 1 diabetes. *Cell metabolism* **2020,** *31* (1), 46-61

3. Hassan, M. H.; Vyas, C.; Grieve, B.; Bartolo, P., Recent advances in enzymatic and non-enzymatic electrochemical glucose sensing. *Sensors* **2021,** *21* (14), 4672

4. Du, Y.; Zhang, X.; Liu, P.; Yu, D. G.; Ge, R., Electrospun nanofiber-based glucose sensors for glucose detection. *Frontiers in chemistry* **2022,** *10*, 944428,10.3389/fchem.2022.944428.

5. Fu, L.-H.; Qi, C.; Lin, J.; Huang, P., Catalytic chemistry of glucose oxidase in cancer diagnosis and treatment. *Chemical Society Reviews* **2018,** *47* (17), 6454-6472,10.1039/C7CS00891K.

6. Zhong, Q.; Chen, Y.; Qin, X.; Wang, Y.; Yuan, C.; Xu, Y., Colorimetric enzymatic determination of glucose based on etching of gold nanorods by iodine and using carbon quantum dots as peroxidase mimics. *Microchimica Acta* **2019,** *186* (3), 161,10.1007/s00604-019-3291-2.

7. Tao, Z.; Raffel, R. A.; Souid, A. K.; Goodisman, J., Kinetic studies on enzyme-catalyzed reactions: Oxidation of glucose, decomposition of hydrogen peroxide and their combination. *Biophysical journal* **2009,** *96* (7), 2977-88,10.1016/j.bpj.2008.11.071.

8. Bright, H. J.; Appleby, M., The pH dependence of the individual steps in the glucose oxidase reaction. *Journal of Biological Chemistry* **1969,** *244* (13), 3625-3634,10.1016/S0021-9258(18)83415-9.

9. Castner, J. F.; Wingard, L. B., Jr., Mass transport and reaction kinetic parameters determined electrochemically for immobilized glucose oxidase. *Biochemistry* **1984,** *23* (10), 2203-2210,10.1021/bi00305a016.

10. Srinivasan, B., A guide to the michaelis–menten equation: Steady state and beyond. *The FEBS Journal n/a* (n/a),https://doi.org/10.1111/febs.16124.

11. Lineweaver, H.; Burk, D., The determination of enzyme dissociation constants. *Journal of the American Chemical Society* **1934,** *56* (3), 658-666,10.1021/ja01318a036.

12. Clark Jr., L. C.; Lyons, C., Electrode systems for continuous monitoring in cardiovascular surgery. *Annals of the New York Academy of Sciences* **1962,** *102* (1), 29-45,https://doi.org/10.1111/j.1749-6632.1962.tb13623.x.

13. Updike, S. J.; Hicks, G. P., Reagentless substrate analysis with immobilized enzymes. *Science* **1967,** *158* (3798), 270-272,10.1126/science.158.3798.270.

14. Updike, S. J.; Hicks, G. P., The enzyme electrode. *Nature* **1967,** *214* (5092), 986-988,10.1038/214986a0.

15. Guilbault, G. G.; Lubrano, G. J., An enzyme electrode for the amperometric determination of glucose. *Analytica Chimica Acta* **1973,** *64* (3), 439-455,https://doi.org/10.1016/S0003-2670(01)82476-4.

16. Fultz, M. L.; Durst, R. A., Mediator compounds for the electrochemical study of biological redox systems: A compilation. *Analytica Chimica Acta* **1982,** *140* (1), 1-18,https://doi.org/10.1016/S0003-2670(01)95447-9.

17. Torres, E.; Panetta, C. A.; Heimer, N. E.; Clark, B. J.; Hussey, C. L., Synthesis and properties of 6-(hydroxymethyl)-9,9,10,10-tetracyanonaphthoquinodimethane. *J. Org. Chem.* **1991,** *56* (11), 3737-9,10.1021/jo00011a061.

18. Mena, M. L.; Yáñez-Sedeño, P.; Pingarrón, J. M., A comparison of different strategies for the construction of amperometric enzyme biosensors using gold nanoparticle-modified electrodes. *Analytical Biochemistry* **2005,** *336* (1), 20-27,https://doi.org/10.1016/j.ab.2004.07.038.

19. Matthews, D. R.; Bown, E.; Watson, A.; Holman, R. R.; Steemson, J.; Hughes, S.; Scott, D., Pen-sized digital 30-second blood glucose meter. *The Lancet* **1987,** *329* (8536), 778-779,https://doi.org/10.1016/S0140-6736(87)92802-9.

20. Cano, M.; Avila, J.; Mayén, M.; Mena, M. L.; Pingarrón, J.; Rodríguez-Amaro, R., A new, third generation, pvc/ttf-tcnq composite amperometric biosensor for glucose determination. *Journal of Electroanalytical Chemistry* **2008,** *615*, 69-74,10.1016/j.jelechem.2007.11.032.

21. Mehmeti, E.; Stanković, D. M.; Chaiyo, S.; Zavasnik, J.; Žagar, K.; Kalcher, K., Wiring of glucose oxidase with graphene nanoribbons: An electrochemical third generation glucose biosensor. *Microchimica Acta* **2017,** *184* (4), 1127-1134,10.1007/s00604-017-2115-5.

22. Olczuk, D.; Priefer, R., A history of continuous glucose monitors (cgms) in self-monitoring of diabetes mellitus. *Diabetes & Metabolic Syndrome: Clinical Research & Reviews* **2018,** *12* (2), 181-187,https://doi.org/10.1016/j.dsx.2017.09.005.

23. Siegmund, T.; Heinemann, L.; Kolassa, R.; Thomas, A., Discrepancies between blood glucose and interstitial glucose—technological artifacts or physiology: Implications for selection of the appropriate therapeutic target. *J Diabetes Sci Technol* **2017,** *11* (4), 766-772,10.1177/1932296817699637.

24. Pardue, H. L.; Simon, R. K.; Malmstadt, H. V., An automatic potentiometric method for the determination of the absolute activity of glucose oxidase. *Analytical Chemistry* **1964,** *36* (4), 735-737,10.1021/ac60210a012.

25. Liu, Y.; Lei, L.; Zhang, Z., An ultrasensitive colorimetric immunoassay based on glucose oxidase catalyzed cascade formation of blue–black iodine–starch complex. *Sensors and Actuators B: Chemical* **2017,** *248*, 195-200,https://doi.org/10.1016/j.snb.2017.03.142.

26. Zhang, X.; Sucre-Rosales, E.; Byram, A.; Hernandez, F. E.; Chen, G., Ultrasensitive visual detection of glucose in urine based on the iodide-promoted etching of gold bipyramids. *ACS Applied Materials & Interfaces* **2020**,10.1021/acsami.0c16369.

27. Kenausis, G.; Taylor, C.; Katakis, I.; Heller, A., 'Wiring' of glucose oxidase and lactate oxidase within a hydrogel made with poly(vinyl pyridine) complexed with [os(4,4′-dimethoxy-2,2′-bipyridine)2cl]+/2+. *Journal of the Chemical Society, Faraday Transactions* **1996,** *92* (20), 4131-4136,10.1039/FT9969204131.

28. Forrow, N. J.; Walters, S. J., Transition metal half-sandwich complexes as redox mediators to glucose oxidase. *Biosensors & bioelectronics* **2004,** *19* (7), 763-70,10.1016/j.bios.2003.08.011.

29. El Atrash, S. S.; O'Neill, R. D., Characterisation in vitro of a naphthoquinone-mediated glucose oxidase-modified carbon paste electrode designed for neurochemical analysis in vivo. *Electrochimica Acta* **1995,** *40* (17), 2791-2797,https://doi.org/10.1016/0013-4686(95)00260-L.

30. Hickey, D. P.; Godman, N. P.; Schmidtke, D. W.; Glatzhofer, D. T., Chloroferrocene-mediated laccase bioelectrocatalyst for the rapid reduction of o_2. *Electrochimica Acta* **2021,** *383*, 138130,https://doi.org/10.1016/j.electacta.2021.138130.

31. Rafighi, P.; Tavahodi, M.; Haghighi, B., Fabrication of a third-generation glucose biosensor using graphene-polyethyleneimine-gold nanoparticles hybrid. *Sensors and Actuators B: Chemical* **2016,** *232*, 454-461,https://doi.org/10.1016/j.snb.2016.03.147.

32. Bollella, P.; Fusco, G.; Stevar, D.; Gorton, L.; Ludwig, R.; Ma, S.; Boer, H.; Koivula, A.; Tortolini, C.; Favero, G.; Antiochia, R.; Mazzei, F., A glucose/oxygen enzymatic fuel cell based on gold nanoparticles modified graphene screen-printed electrode. Proof-of-concept in human saliva. *Sensors and Actuators B: Chemical* **2018,** *256*, 921-930,https://doi.org/10.1016/j.snb.2017.10.025.

33. Chen, J.; Munje, R.; Godman, N. P.; Prasad, S.; Glatzhofer, D. T.; Schmidtke, D. W., Improved performance of glucose bioanodes using composites of (7,6) single-walled carbon nanotubes and a ferrocene-lpei redox polymer. *Langmuir : the ACS journal of surfaces and colloids* **2017,** *33* (31), 7591-7599,10.1021/acs.langmuir.7b00718.

34. Merchant, S. A.; Tran, T. O.; Meredith, M. T.; Cline, T. C.; Glatzhofer, D. T.; Schmidtke, D. W., High-sensitivity amperometric biosensors based on ferrocene-modified linear poly(ethylenimine). *Langmuir : the ACS journal of surfaces and colloids* **2009,** *25* (13), 7736-7742,10.1021/la9004938.

35. Merchant, S. A.; Meredith, M. T.; Tran, T. O.; Brunski, D. B.; Johnson, M. B.; Glatzhofer, D. T.; Schmidtke, D. W., Effect of mediator spacing on electrochemical and enzymatic response of ferrocene redox polymers. *The Journal of Physical Chemistry C* **2010,** *114* (26), 11627-11634,10.1021/jp911188r.

36. Meredith, M. T.; Hickey, D. P.; Redemann, J. P.; Schmidtke, D. W.; Glatzhofer, D. T., Effects of ferrocene methylation on ferrocene-modified linear poly(ethylenimine) bioanodes. *Electrochim. Acta* **2013,** *92*, 226-235,10.1016/j.electacta.2013.01.006.

37. DeLuca, J. L.; Hickey, D. P.; Bamper, D. A.; Glatzhofer, D. T.; Johnson, M. B.; Schmidtke, D. W., Layer-by-layer assembly of ferrocene-modified linear polyethylenimine redox polymer films. *Chemphyschem : a European journal of chemical physics and physical chemistry* **2013,** *14* (10), 2149-2158,10.1002/cphc.201300146.

38. Hickey, D. P.; Giroud, F.; Schmidtke, D. W.; Glatzhofer, D. T.; Minteer, S. D., Enzyme cascade for catalyzing sucrose oxidation in a biofuel cell. *ACS Catal.* **2013,** *3* (12), 2729-2737,10.1021/cs4003832.

39. Godman, N. P.; DeLuca, J. L.; McCollum, S. R.; Schmidtke, D. W.; Glatzhofer, D. T., Electrochemical characterization of layer-by-layer assembled ferrocene-modified linear poly(ethylenimine)/enzyme bioanodes for glucose sensor and biofuel cell applications. *Langmuir : the ACS journal of surfaces and colloids* **2016,** *32* (14), 3541-51,10.1021/acs.langmuir.5b04753.

40. Merchant, S.. 2007. The development of redox polymers based on linear poly(ethylenimine) for application in amperometric biosensors. Doctoral Dissertation, *University of Oklahoma,* ShareOK.org

41. Merchant, S. A.; Glatzhofer, D. T.; Schmidtke, D. W., Effects of electrolyte and ph on the behavior of cross-linked films of ferrocene-modified poly(ethylenimine). *Langmuir : the ACS journal of surfaces and colloids* **2007,** *23* (22), 11295-11302,10.1021/la701521s.

42. Tran, T. O.; Lammert, E. G.; Chen, J.; Merchant, S. A.; Brunski, D. B.; Keay, J. C.; Johnson, M. B.; Glatzhofer, D. T.; Schmidtke, D. W., Incorporation of single-walled carbon nanotubes into ferrocene-modified linear polyethylenimine redox polymer films. *Langmuir : the ACS journal of surfaces and colloids* **2011,** *27* (10), 6201-6210,10.1021/la104999f.

43. Rengaraj, S.; Mani, V.; Kavanagh, P.; Rusling, J.; Leech, D., A membrane-less enzymatic fuel cell with layer-by-layer assembly of redox polymer and enzyme over graphite electrodes. *Chemical communications (Cambridge, England)* **2011,** *47* (43), 11861-3,10.1039/c1cc15002b.

44. Tang, L.; Chang, S. J.; Chen, C. J.; Liu, J. T., Non-invasive blood glucose monitoring technology: A review. *Sensors (Basel)* **2020,** *20* (23),10.3390/s20236925.

45. Zhang, S.; Yang, W.; Niu, Y.; Sun, C., Multilayered construction of glucose oxidase on gold electrodes based on layer-by-layer covalent attachment. *Analytica Chimica Acta* **2004,** *523* (2), 209-217,https://doi.org/10.1016/j.aca.2004.07.053.

46. Stankovich, M. T.; Schopfer, L. M.; Massey, V., Determination of glucose oxidase oxidation-reduction potentials and the oxygen reactivity of fully reduced and semiquinoid forms. *Journal of Biological Chemistry* **1978,** *253* (14), 4971-4979,10.1016/S0021-9258(17)34643-4.

47. Xu, S.; Minteer, S. D., Enzymatic biofuel cell for oxidation of glucose to co2. *ACS Catalysis* **2012,** *2* (1), 91-94,10.1021/cs200523s.

48. Bahari, M.; Malmberg, M. A.; Brown, D. M.; Hadi Nazari, S.; Lewis, R. S.; Watt, G. D.; Harb, J. N., Oxidation efficiency of glucose using viologen mediators for glucose fuel cell

applications with non-precious anodes. *Applied Energy* **2020,** *261*, 114382,https://doi.org/10.1016/j.apenergy.2019.114382.

49. Hwang, D.-W.; Lee, S.; Seo, M.; Chung, T. D., Recent advances in electrochemical non-enzymatic glucose sensors – a review. *Analytica Chimica Acta* **2018,** *1033*, 1-34,https://doi.org/10.1016/j.aca.2018.05.051.

50. Thakur, N.; Mandal, D.; Nagaiah, T. C., Highly sensitive non-enzymatic electrochemical glucose sensor surpassing water oxidation interference. *Journal of Materials Chemistry B* **2021**,10.1039/D1TB01332G.

51. Buchman, J. T.; Hudson-Smith, N. V.; Landy, K. M.; Haynes, C. L., Understanding nanoparticle toxicity mechanisms to inform redesign strategies to reduce environmental impact. *Accounts of Chemical Research* **2019,** *52* (6), 1632-1642,10.1021/acs.accounts.9b00053.

52. Liu, X.; Hao, M.; Feng, M.; Zhang, L.; Zhao, Y.; Du, X.; Wang, G., A one-compartment direct glucose alkaline fuel cell with methyl viologen as electron mediator. *Applied Energy* **2013,** *106*, 176-183,https://doi.org/10.1016/j.apenergy.2013.01.073.

53. Zen, J.-M.; Lo, C.-W., A glucose sensor made of an enzymatic clay-modified electrode and methyl viologen mediator. *Analytical Chemistry* **1996,** *68* (15), 2635-2640,10.1021/ac960090j.

54. Wang, P..2021. Polyviologen-modified anodes for carbohydrate biofuel cells. Doctoral Dissertation, *University of Oklahoma*, ShareOK.org

55. Bamper, D. 2019. A binding isotherm between ferrocene mediators and glucose oxidase for use in bioanode development and intitial studies of an electrocatalytic deoxydehydration reaction. Doctoral Dissertation, University of Oklahoma, ShareOK.org

56. Minson, M.; Meredith, M. T.; Shrier, A.; Giroud, F.; Hickey, D.; Glatzhofer, D. T.; Minteer, S. D., High performance glucose/o2 biofuel cell: Effect of utilizing purified laccase with anthracene-modified multi-walled carbon nanotubes. *J. Electrochem. Soc.* **2012,** *159* (12), G166-G170,10.1149/2.062212jes.

57. Chen, J.; Tran, T. O.; Ray, M. T.; Brunski, D. B.; Keay, J. C.; Hickey, D.; Johnson, M. B.; Glatzhofer, D. T.; Schmidtke, D. W., Effect of surfactant type and redox polymer type on single-walled carbon nanotube modified electrodes. *Langmuir : the ACS journal of surfaces and colloids* **2013,** *29* (33), 10586-10595,10.1021/la401158y.

58. Hickey, D. P.; Halmes, A. J.; Schmidtke, D. W.; Glatzhofer, D. T., Electrochemical characterization of glucose bioanodes based on tetramethylferrocene-modified linear poly(ethylenimine). *Electrochim. Acta* **2014,** *149*, 252-257,10.1016/j.electacta.2014.10.077.

59. Chen, Z.; Deng, S.; Wei, H.; Wang, B.; Huang, J.; Yu, G., Polyethylenimine-impregnated resin for high co2 adsorption: An efficient adsorbent for co2 capture from simulated flue gas and ambient air. *ACS Applied Materials & Interfaces* **2013,** *5* (15), 6937-6945,10.1021/am400661b.

60. Almeida, I.; Cascalheira, A. C.; Viana, A. S., One step gold (bio)functionalisation based on cs2-amine reaction. *Electrochim. Acta* **2010,** *55* (28), 8686-8695,10.1016/j.electacta.2010.07.084.

61. Wang, L.; Wang, X.; Chen, X.; Liu, J.; Liu, S.; Zhao, C., Development of an electrochemical DNA biosensor with the DNA immobilization based on in situ generation of dithiocarbamate ligands. *Bioelectrochemistry* **2012,** *88*, 30-35,https://doi.org/10.1016/j.bioelechem.2012.04.003.

2. Mediation of Glucose Oxidase Oxidation of Glucose by Iodide

2.1 Introduction

Glucose oxidase (GOx)-based glucose sensors have developed in a variety of ways throughout their history[1], and the different types of sensor systems are often classified by reference to three glucose sensor "generations". First generation glucose sensors rely on the detection of oxygen or hydrogen peroxide (precursors or byproducts of the GOx/Glucose reaction), while second and third generation sensors rely on a mediator to replace or augment the oxygen/hydrogen peroxide redox couple[2]. The iodide/iodine redox couple has been used as an auxiliary mediator system for GOx in glucose sensors since the 1960's[3-7]. Current and past literature holds that the iodide is oxidized to iodine by the hydrogen peroxide produced by reduction of oxygen by GOx, which is reduced as it oxidizes glucose (see Figure 2.1)[8-9]. The iodine thus produced can be reduced back to iodide at a cathode of appropriate potential and functions as a key component in the catalytic redox cycle with glucose oxidase. The iodide is described as an auxiliary mediator since it interacts with the by-products of the reaction and not the GOx $FADH_2$ site itself. This

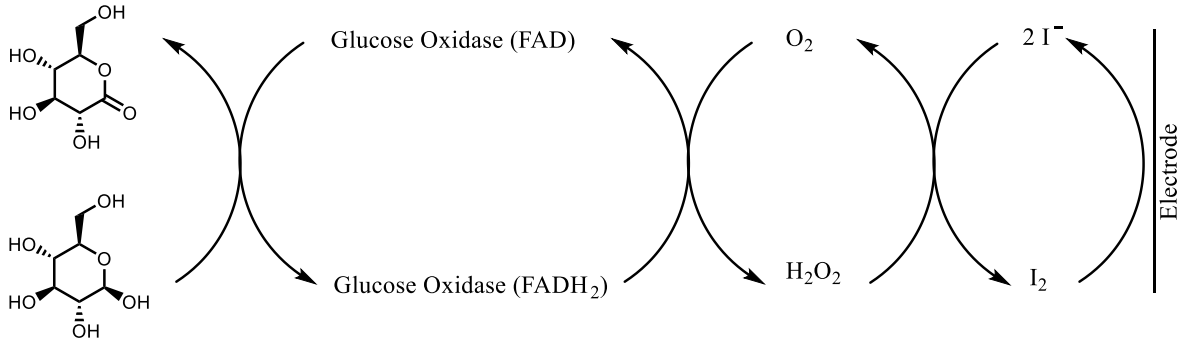

Figure 2.1 Postulated electron transport chain from glucose to an electrode through GOx, oxygen/Hydrogen peroxide and iodide/iodine

mechanism appears reasonable, and because second-generation sensors were not developed until the 1980's, it has just been generally accepted that iodide mediates indirectly through a redox reaction with H_2O_2[10]. Iodide has even been used to "trap" damaging hydrogen peroxide generated in a biofuel cell[11], based on the assumption that iodide functions only by reaction with the hydrogen peroxide.

Our group has used ferrocene-modified polymers to assemble a variety of 2nd generation glucose sensors[12-18]. During research on these materials, it became important to study how the ferrocene was binding to the enzyme through the use of small molecule ferrocene analogs[19]. For these studies, water soluble ferrocenylmethyl-trimethylammonium iodide and tosylate (FcTMAI and FcTMATos, respectively)[19-20] salts were synthesized using known synthetic routes (Figure 2.2). Ferrocene and its derivatives generally show single, one electron redox behavior. The

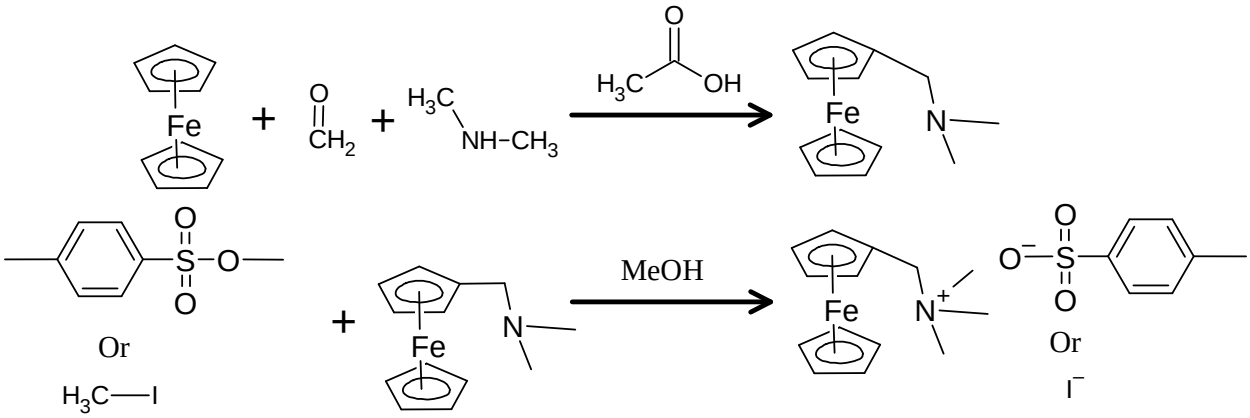

Figure 2.2 Aminomethylation of ferrocene followed by a methylation as carried out in our lab using a method established by Lindsay[19-20].

fundamental redox behavior of FcTMAI in a pH 7.0 aqueous phosphate buffer was studied using cyclic voltammetry (CV) versus a saturated calomel electrode (SCE) and it exhibited two redox waves at $E_{1/2}$ = ca. 0.43 and 0.59 V (Figure 2.3), suggesting that both ferrocene/ferrocenium and iodide/iodine redox processes are occurring. Because this behavior would potentially complicate interpretation of the results of GOx-FcTMAI interaction studies, and to elucidate the relative

contributions of the ferrocene moiety and the iodide to the overall redox behavior, FcTMATos was synthesized to replace the redox active iodide with redox inert (under these conditions) tosylate anions.

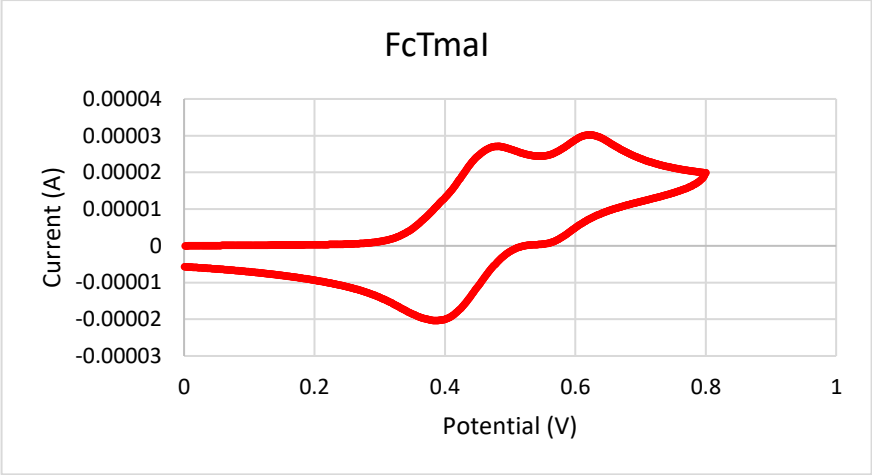

Figure 2.3 Cyclic voltammogram of 2.5 mM FcTMAI in 50 mM phosphate buffer pH 7.0 scanned at 50 mV/s using an SCE reference, a glassy carbon working electrode and a platinum wire counter electrode.

The redox behavior of FcTMATos was studied under the same conditions as for FcTMAI using CV and as expected, showed a single, reversible redox wave at $E_{1/2}$ = ca. 0.40 V (Figure 2.4) resulting solely from the redox behavior of the ferrocene moiety. In comparing the CV's for

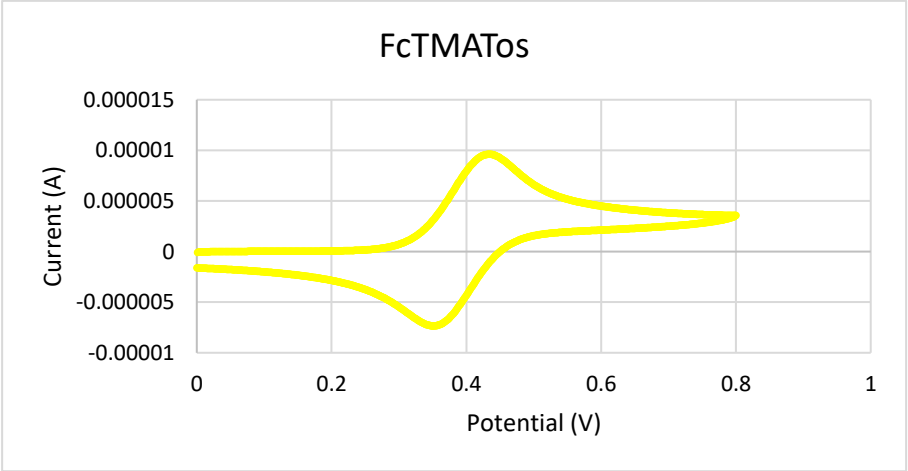

Figure 2.4 Cyclic voltammogram of 2.5 mM FcTMATos in 50 mM phosphate buffer pH 7.0 scanned at 50 mv/s using an SCE reference, a glassy carbon working electrode and a platinum wire counter electrode.

FcTMAI and FcTMATos (Figure 2.5), two features immediately stood out. The first was that the peak oxidation potential for the FcTMATos was ca. 30 mV lower that of the FcTMAI, and the second was that the current response of FcTMAI was significantly greater than that of the

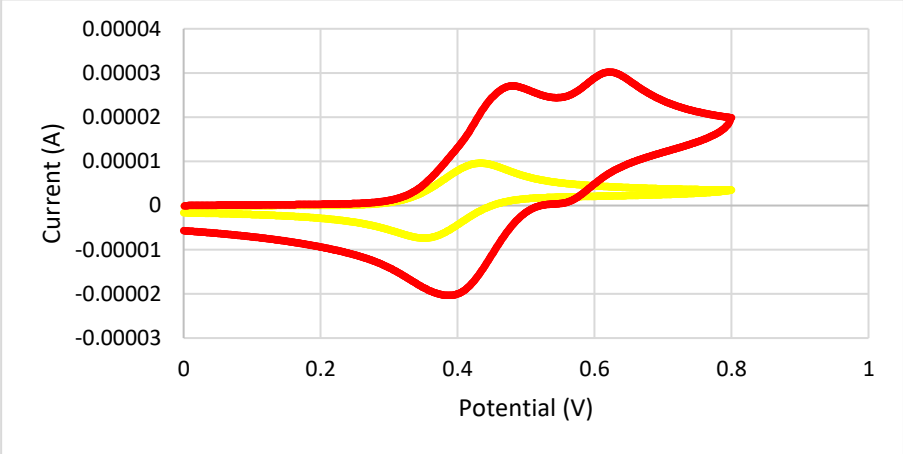

Figure 2.5 Cyclic voltammograms of 2.5 mM FcTMATos (yellow) and 1mM FcTMAI (Red) in 50mM phosphate buffer pH 7.0 scanned at 50 mv/s using an SCE reference, a glassy carbon working electrode and a platinum wire counter electrode.

FcTMATos at the same concentration. These observations suggested that the ferrocene/ferrocenium redox peaks overlap with iodide/iodine redox peaks under these conditions. On closer inspection, the ferrocene oxidation peak can be seen as a small shoulder on the first iodide oxidation peak (Figure 2.5) but is nearly completely obscured. To verify this, a CV was

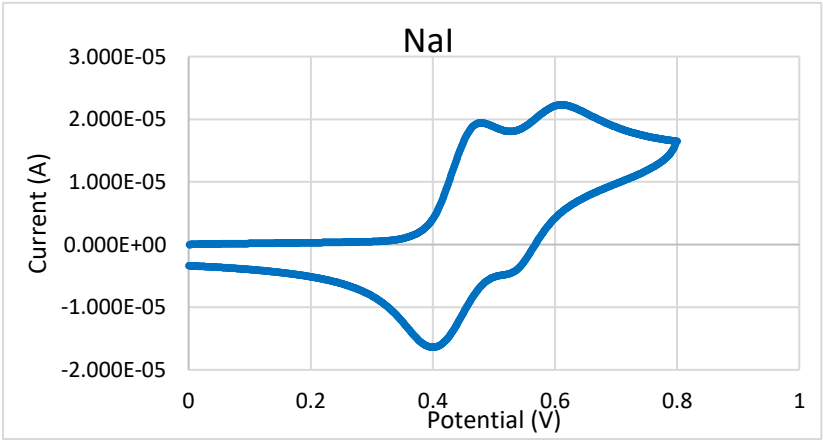

Figure 2.6 Cyclic voltammogram of 2.5 mM NaI in 50 mM phosphate buffer pH 7.0 scanned at 50 mV/s using an SCE reference, a glassy carbon working electrode and a platinum wire counter electrode.

obtained for sodium iodide under the same conditions and is shown in Figure 2.6. The sodium iodide exhibits two redox waves and is remarkably similar in appearance to that of FcTMAI. Indeed, since the CV's for FcTMAI, FcTMATos, and NaI were all taken at the same concentrations and under the same conditions, simple numerical addition of the responses for the FcTMATos (Fc redox only) and NaI (iodide redox only) results in a CV that is nearly identical to that of FcTMAI (Figure 2.7).

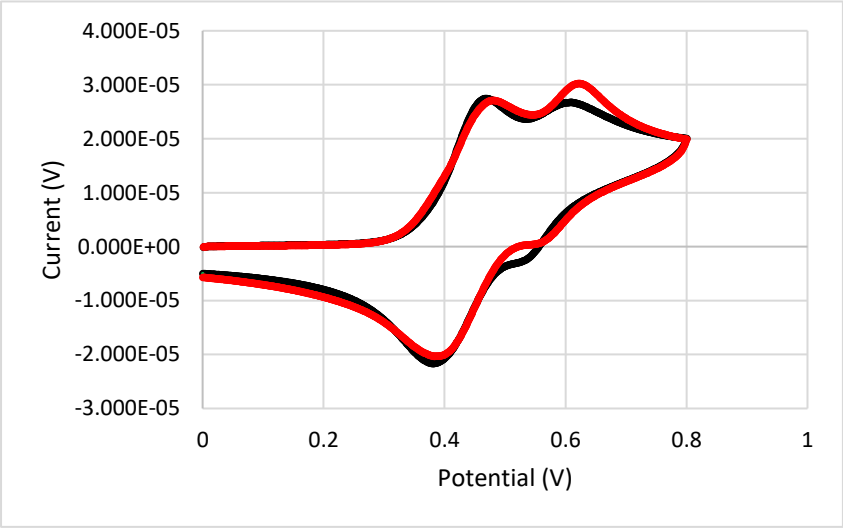

Figure 2.7 Cyclic voltammogram of 2.5 mM FcTMAI (Red) in 50 mM phosphate buffer pH 7.0 scanned at 50 mV/s using an SCE reference, a glassy carbon working electrode and a platinum wire counter electrode compared to the numerical addition of the NaI and FcTMATos voltammograms collected under the same conditions.

At first glance, the appearance of two redox waves for the iodide may seem unusual, but it has been observed before under specific conditions, resulting from electrochemical oxidation of iodide (I^-) to iodine (I_2), which further complexes with non-oxidized iodide to form triiodide $(I_3)^-$, which oxidizes to iodine at a higher potential[21-22]. The redox behavior of FcTMAI can therefore be understood as a combination of processes occurring in parallel. In Figure 2.4 the FcTMATos can be seen to have a very simple CV with the 1 electron ferrocene to ferrocenium oxidation peak (E_{pa}) at 0.433V (Equation 2.1) and the corresponding reduction peak (E_{pc}) at 0.355 V (see Equation

2.1). The difference in peak potentials (E_{pa}-E_{pc}) is 78 mV, and the ratio of peak currents (i_{pa}/i_{pc}) is 1.03, indicating good reversibility[23]. The NaI and FcTMAI exhibit a far more complicated ECE (electrochemical, chemical, electrochemical) redox behavior with 2 oxidation peaks for the I^-/I_2 and I_3^-/I_2 couples with $E_{1/2}$ values of 0.438 and 0.569 V respectively (see Equations 2.2 and 2.4) and a chemical step in between them where iodide and iodine combine to form triiodide (Equation 2.3), and possibly small amounts of polyiodide species. This is especially apparent in comparing Figures 2.3 and 2.6, the FcTMAI and NaI voltammograms. In the FcTMAI voltammogram (Figure 2.3) the ferrocene peaks can also be made out as shoulders on the first oxidation/reduction peaks, skewing the $E_{1/2}$ towards lower voltages; from 0.399 V for the NaI, to 0.383 V for the FcTMAI). As discussed earlier, the FcTMAI (Figure 2.3) is roughly equivalent to the algebraic addition of the FcTMATos (Figure 2.4) and NaI (Figure 2.6) voltammograms, but there are some small differences (see Figure 2.7). However, these differences are mainly manifested in the second peak, the shape of which varies with scan rate due to diffusion-controlled kinetics of the chemical reaction step to produce the redox active triiodide species.

$$FcTMA \rightarrow Fc^+ + e^- \qquad E_{1/2} = +0.394\ V \qquad \textbf{Equation 2.1}$$

$$2I^- \rightarrow I_2 + 2e^- \qquad E_{1/2} = +0.438\ V \qquad \textbf{Equation 2.2}$$

$$I^- + I_2 \rightarrow I_3^- \qquad \textbf{Equation 2.3}$$

$$2I_3^- \rightarrow 3I_2 + 2e^- \qquad E_{1/2} = +0.569\ V \qquad \textbf{Equation 2.4}$$

Because iodide and ferrocene have similar redox potentials, as seen in Figures 2.3, 2.4, 2.5 and 2.6, and any diffusion barrier to iodine species into and out of GOx would likely be small, the question arises of whether the iodide/iodine couple can act in a similar manner to the ferrocene/ferricenium couple in relation to the mediation of GOx (Figure 2.8). Our group has

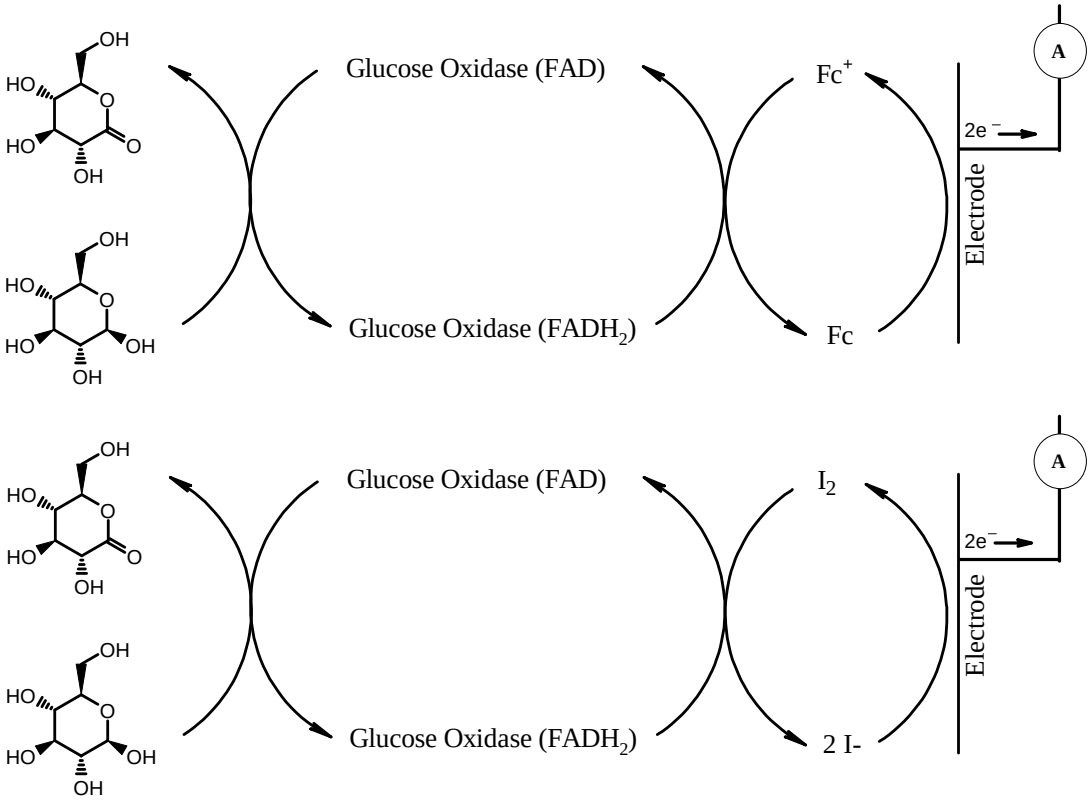

Figure 2.8 The commonly accepted transport chain from glucose to an electrode through GOx, and Fc to the electrode surface, compared to iodine mediated electron transport.

also observed anomalous results in the current density of Fc-based/Gox glucose sensors in the presence of iodide relative to controls. To the best of our knowledge, there has been no investigation in the literature probing whether iodide can directly interact with the glucose oxidase as a second-generation mediator. Since the ferrocene mediator used in our sensors should reduce or eliminate the presence of H_2O_2, this led us to test the hypothesis that the iodide/iodine couple is able to function as a primary, rather than auxiliary, mediator for the electrocatalytic oxidation of

glucose with GOx and act as a second-generation glucose sensor, not a first-generation sensor, as has been assumed in the literature.

In this work electrochemical mediation by iodide of the enzymatic oxidation of glucose using GOx was probed using cyclic voltammetry and coulombic amperometry, as well as being visualized using polarization curves. This iodide mediation was studied with and without the ferrocene moiety present, and in the absence and presence of oxygen by saturating the solutions with air or N_2. Nitrogen saturation should, in the case of a first-generation auxiliary mediation mechanism, completely impede the sensor by removing the oxygen electron-scavenger, while the presence of oxygen should either increase the performance of the sensor or have no effect. These studies shown for the first time that iodide can act as a direct (second-generation like) mediator for GOx oxidation of glucose.

2.2 Mediation of Glucose Oxidase using Iodide

Electrochemical mediation of the oxidation of glucose by GOx was studied using CV of the mediators with and without GOx present and under saturating sugar concentration (100 mM) conditions. The simplest case is that of FcTMATos, which in the presence of the GOx and glucose shows the oxidation peak of the ferrocene with no discernible reverse reduction peak (Figure 2.9).

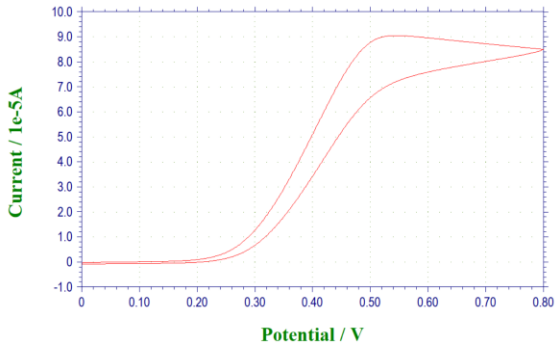

Figure 2.9 Cyclic voltammogram of 2.5 mM FcTMATos, 20 µM GOx and 123 mM glucose in 50 mM phosphate buffer pH 7.0 scanned at 50 mV/s using an SCE reference, a glassy carbon working electrode and a platinum wire counter electrode.

This occurs because the ferrocenium produced by oxidation at the electrode is immediately reduced back to ferrocene by GOX's $FADH_2$ center and thus is not available to be reduced in the reverse potential scan. The oxidation peak is amplified relative to that of the FcTMATos alone because the ferrocenium reduced by the GOx $FADH_2$ can immediately be oxidized again (and subsequently reduced by the glucose/GOx multiple times), increasing the current until it reaches an approximate steady state that is limited by reaction and diffusion kinetics.

A similar behavior can be seen using sodium iodide as the mediator, although analysis is somewhat more complicated (Figure 2.10). The sodium iodide with glucose oxidase and glucose present clearly shows a significant amplification of the first oxidation at ca. 0.5 V when compared to the sodium iodide voltammogram (Figure 2.6). This indicates that the iodine produced by oxidation of iodide at the electrode is getting reduced, at least partially, by the glucose/GOx and these iodide molecules are then reoxidized to iodine by the electrode. The current amplification is

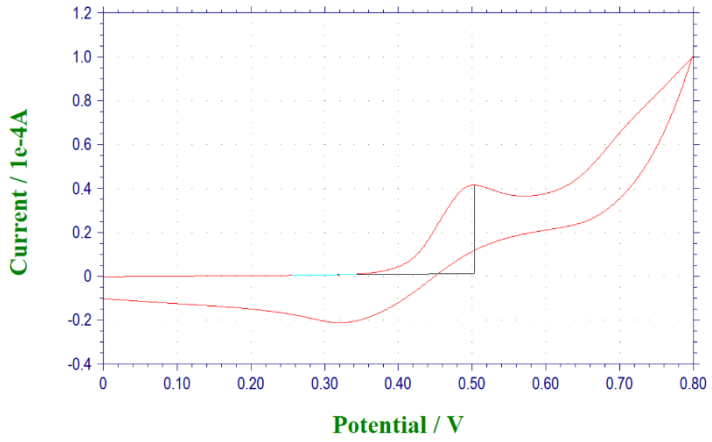

Figure 2.10 Cyclic voltammogram of 2.5 mM NaI, 20 µM GOx and 123 mM glucose in 50 mM phosphate buffer pH 7.0 scanned at 50 mV/s using an SCE reference, a glassy carbon working electrode and a platinum wire counter electrode.

attenuated by competition with formation of less easily oxidized triiodide, and which decreases the available iodide concentration. At higher oxidation potentials, oxidation of the triiodide to iodine contributes to the availability of iodine and an increase in current (as shown in Scheme 2.1), and by the continued rise in current at higher potentials. The process may be further complicated

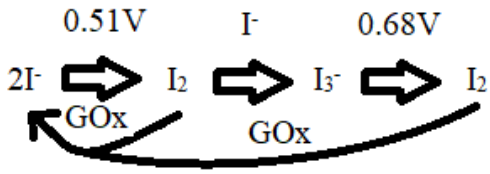

Scheme 2.1 A proposed route for iodide's oxidations and subsequent reduction by GOx.

by deposition of polyiodide species on the electrode, making them unavailable for mediation. The observation of a reduction peak at a lower reduction potential of ca. 0.32 V is consistent with a desorption process.

Perhaps not unexpectedly, the CVs for FcTMAI with (Figure 2.11) glucose/GOx present appear to be a hybrid of the FcTMATos (Figure 2.9) and NaI (Figure 2.10) CV's with glucose/GOx present with a small synergistic effect on the current maxima. The main noticeable feature in the

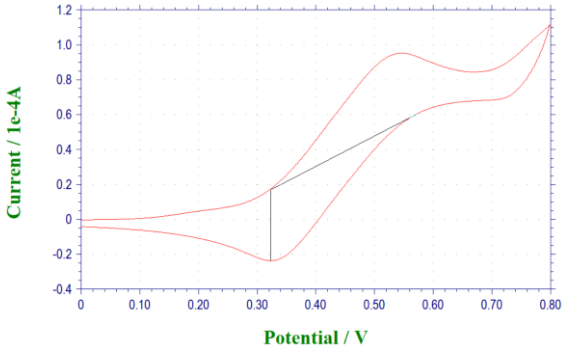

Figure 2.11 Cyclic voltammogram of 2.5 mM FcTMAI, 20 µM GOx and 123 mM glucose in 50 mM phosphate buffer pH 7.0 scanned at 50 mV/s using an SCE reference, a glassy carbon working electrode and a platinum wire counter electrode.

FcTMAI mediated CV (Figure 2.11) when compared to NaI with glucose/GOx (Figure 2.10), is that it has a higher current at iodide's first oxidation and shares the catalytic second oxidation with no apparent corresponding reduction beginning at around 0.7 V. The reduction at ca. 0.32 V for the NaI mediated system is larger and shifted to somewhat higher potentials for FcTMAI mediated CV's. Assuming this reduction is from adsorbed triiodide that did not participate in the GOx mediation, the FcTMAI behavior is consistent with the presence of the ferrocene/ferricenium

moiety somewhat inhibiting the absorption of the polyiodide species. Ferrocenium-triiodide salts are known and could explain this phenomenon[24]. The reduction potential of the ferrocinium and (adsorbed) triiodide occur at a similar potential and their formation may go unnoticed in the unmediated CVs. The presence of the I_3^-/I_2 oxidation and reduction peaks in the mediated NaI and FcTMAI voltammograms demonstrates that not all of the I_2 is utilized in the mediation of the glucose oxidase, and that there is some available for side reactions, of which iodine and polyiodide species have many. These results are consistent with the iodide/iodine couple functioning directly as a mediator for the electrochemical oxidation of glucose by GOx. The results also suggest the ferrocene moiety somewhat inhibits polyiodide species formation, perhaps through complexation with the triiodide.

In order to study these systems amperometrically as steady-state sensors or as half-cells for biofuel cell applications, the earlier results suggested that the anode potential should be carefully chosen to minimize polyiodide deposition. Steady-state mediation by the FcTMATos, FcTMAI, and NaI were studied by constant potential experiments with GOx and varying amounts of glucose to generate the Michaelis-Menten curves. In order to compare the three mediators, a constant potential of 0.60 V was chosen for these experiments as this was approximately 200 mV above $E_{1/2}$ for both the ferrocene moiety oxidation and the first iodide oxidation [see the Experimental Section 2.3] to maximize their contribution to catalytic currents, and before significant triodide oxidation processes were occurring (see Figures 2.10 and 2.11) to minimize their contribution and any deposition complications. Michaelis-Menten curves were then constructed for each of the mediators to ensure they are mediating the enzyme and determining whether they inhibit enzyme function (Figure 2.12). As expected, null experiments using only glucose, GOx, and phosphate buffer solution without a mediator did not show any appreciable catalytic current. However, the

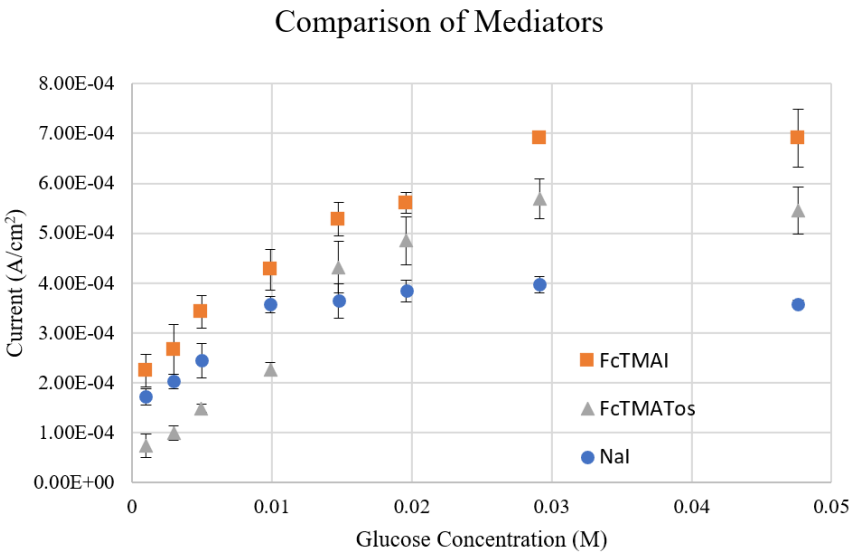

Figure 2.12 The Michaelis-Menten curves of GOx with each mediator NaI, FcTMATos, and FcTMAI made using the current output after exposure to 0.60 V for 200 s at each glucose concentration using 50 mM pH 7 Phosphate buffer 2.5 mM mediator and 20 µM GOx using a glassy carbon working electrode, a platinum wire counter electrode and an SCE reference.

resulting curves show definitively that FcTMATos, NaI, and FcTMAI all act as mediators for the catalytic oxidation of glucose by GOx. A summary of the results is shown in Table 2.1. This data shows that the NaI mediator has the lowest J_{max}, that there is an increase in J_{max} with the FcTMATos, and another increase with the FcTMAI, showing that the I_2 and ferrocene are working either together or independently adding to the total current. This is also consistent with the small synergistic effect between the ferrocene/ferricenium and iodide/iodine couple noted in the earlier CV studies. It is also evident that the K_M values of the NaI and the FcTMAI are lower (1.92 mM

and 2.29 mM respectively, see Table 2.1), meaning that they work somewhat more efficiently at low glucose concentrations than the FcTMATos (7.92 mM). The composite mediator FcTMAI has the upside of its respective isolated mediators, with the highest J_{max} and a relatively low K_M.

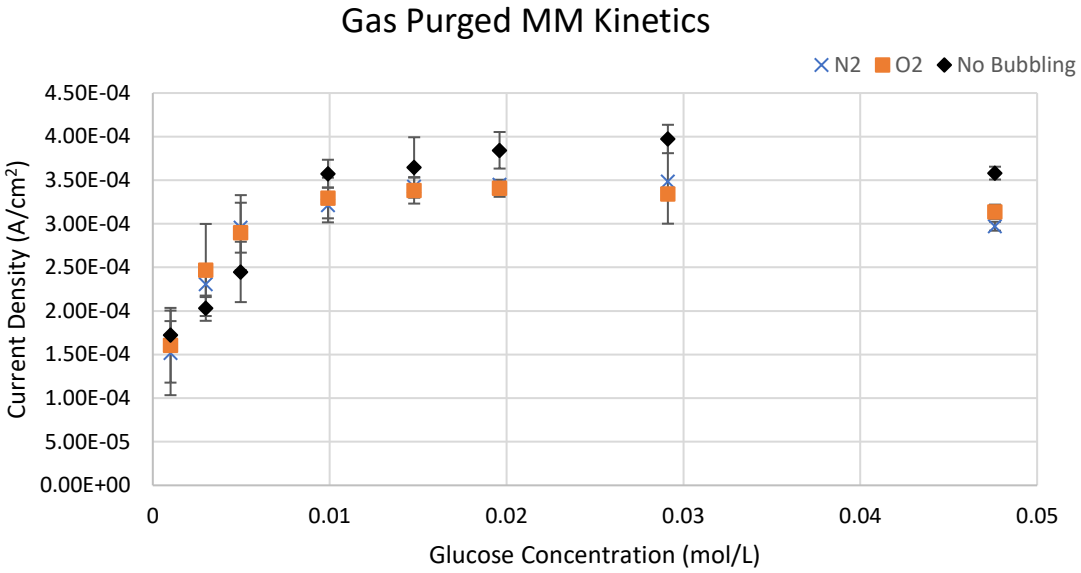

Figure 2.13: Michaelis-Menten Curves of GOx with NaI with and without solution purging made using the current output after exposure to 0.60 V for 200 s at each glucose concentration using 50mM pH 7 Phosphate buffer 2.5 mM NaI and 20 µM GOx using a glassy carbon working electrode, a platinum wire counter electrode and an SCE reference.

While the above results demonstrate that the iodide/iodine couple functions to mediate electrochemical glucose oxidation by GOx, there was still a question as to whether the oxygen/hydrogen peroxide couple played any role in the process. To further probe this question, steady-state amperometric experiments were carried out again using sodium iodide as the mediator as normal, after bubbling air through the through the mediator/glucose/GOx solution for 10 min,

Mediator	Km (mM)	J_{max} (A/cm²*s)
FcTMATos	7.92	5.69E-04
FcTMAI	2.29	6.91E-04
NaI	1.92	3.97E-04
NaI (N2 purge)	1.46	3.49E-04
NaI (O2 purge)	1.22	3.41E-04

Table 2.1 The K_M and J_{max} of GOx with each Mediator

and after bubbling N_2 through the solution (Figure 2.13). These curves are nearly identical, with many of their points within a standard deviation of one another. These results are consistent with the conclusion that dissolved O_2 is not significantly participating in the mechanism of mediation for the iodide under these conditions. The results are also consistent with the hypothesis that the iodide mediator interacts directly with the glucose oxidase and demonstrates that it must be acting almost exclusively as a second-generation mediator.

Although it is unlikely that the iodide/iodine redox couple will be useful as a solo mediator for sensor or biofuel cells, iodide has been used as a putative hydrogen peroxide scavenger in biofuel cells[11]. As has been shown here, the actual function of the iodide is likely more complicated and it would be good to understand the effect of having iodide present in a working glucose/GOX biofuel cell. This would also be useful in explaining some of the anomalous biofuel cell results our group has observed when iodide was present and justify its exclusion in most cases to simplify the results.

Biofuel cells were constructed using mediated glucose/GOx oxidation for the anodic reaction and dissolved oxygen reduction at a platinum electrode as the cathodic reaction. The working electrode was set as the cathode and the electrode was scanned from the open circuit

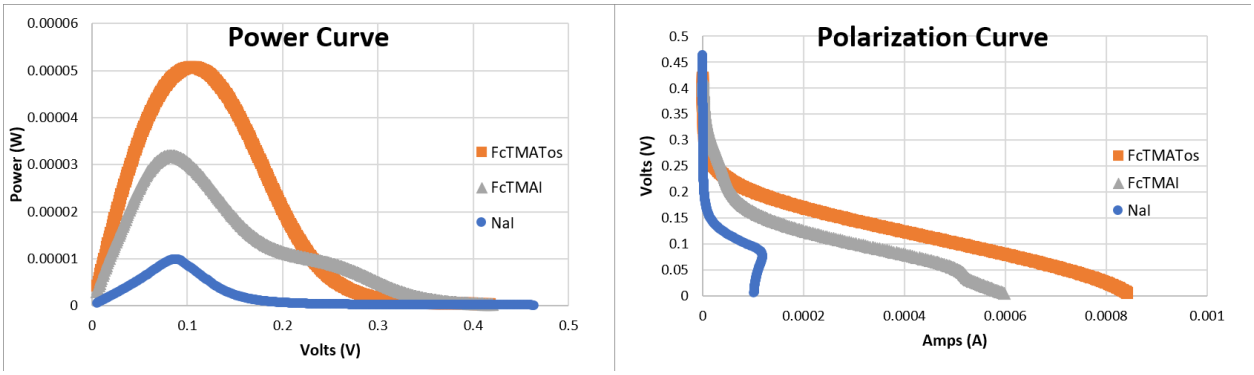

Figure 2.14: Power and polarization curves of GOx with FcTMATos, FcTMAI, NaI on a glassy carbon electrode poised against a platinum cloth air breathing electrode in pH 7 50 mM phosphate buffer with 2.5 mM mediator and 20 µM GOx and 100 mM glucose. All solutions purged with N_2 gas for 15 min before testing.

potential to 0.005V at 2 mV/s to simulate scanning through different resistances. From these experiments polarization and power curves were constructed to summarize and compare the results using the FcTMATos, FcTMAI, and NaI mediators as shown in Figure 2.14. The FcTMATos was clearly the best mediator, giving the most current and power, and having its power maximum (50 $\mu W/cm^2$) at a higher potential. It is apparent that the presence of iodide in the FcTMAI lowers the voltage at which the maximum power is generated from 0.110 V in the FcTMATos to 0.091 V which is the same as for the NaI. The lower operating potential is not surprising as the iodide/iodine couple has a somewhat more positive potential, increasing the overvoltage at the anode and decreasing the overall cell potential. The currents at equivalent potentials also decrease, suggesting that the iodide is limiting mediation in the FcTMAI system and further attenuating the performance of the fuel cell. While these results seem to contradict the synergistic effects discussed earlier, it should be noted that in the biofuel cell experiments the electrode potentials are not kept constant as they were for the steady-state studies, and polyiodide participation and deposition effects likely play a role in attenuating the biofuel cell's performance. While the mediators discussed here will probably never be used in practical biofuel cells, these studies show that the presence of iodide interferes with ferrocene's ability to mediate GOx in biofuel cells. Further, these results suggest that care should be taken before attempting to use iodide to scavenge hydrogen peroxide in biofuel cells, and in evaluating the results if it is used.

2.3 Conclusion

In this study, the mechanism of iodine's mediation of glucose oxidase was probed using electrochemical methods, and it was determined that the iodide/iodine couple acts as a second-generation mediator, interacting directly with the glucose oxidase FAD/$FADH_2$ redox site. It was

found that gas bubbling (O_2 and N_2) had no effect on iodine's mediation of glucose oxidase, ruling out O_2 as a participant in iodine's catalytic electron transport from GOx to the electrode surface. Since some sensors rely on the production of the H_2O_2 intermediate from oxygen, implying a first-generation oxygen mediated mechanism, the presence of iodide complicates the process and may not be beneficial.

2.4 Materials and Methods

2.4.1 Chemicals and Solutions.

Glucose oxidase (GOX) from Aspergillus niger (EC 1.1.3.4, type X-S, 117 units/mg solid, 75% protein), and methyl tosylate, purchased from Sigma-Aldrich and used as recieved. Ferrocenylmethyl-N,N-dimethylamine and ferrocenylmethyl-N,N,N-trimethylammonium iodide were synthesized using a previously reported method[20].

2.4.2 Synthesis of Ferrocenylmethyl-N,N,N-trimethylammonium salts

The synthesis of ferrocenylmethyl-N,N,N-trimethylammonium iodide performed as in 1957 by Lindsay and Houser[20]. The tosylate analogue was also synthesized in this same manner, replacing the methyl iodide with methyl tosylate. The NMR spectra of both compounds (the iodide and tosylate salts) matched what would be expected from literature and are shown in Figures A1 and A2. The ferrocenylmethyl-N,N,N-trimethylammonium tosylate had the following ^{1}H-NMR peaks. ^{1}H-NMR CD_3COD, (300 MHz): δ 2.25 (s, 3H), 2.47 (s, 12h), 4.26 (s, 5H), 4.34 (s 2H), 4.36 (t, 2H), 4.45 (s, 2H), 7.08 (d 2H), 7.43 (d, 2H).

2.4.3 Cyclic Voltammetry

Cyclic voltammetry was performed using a bipotentiostat (CHI 832) and a three-electrode setup with a platinum counter electrode, a saturated calomel reference electrode and a 2 mm diameter glassy carbon working electrode at a scan rate of 50 mV/s (unless otherwise specified). All electrochemical experiments were done at room temperature (ca. 25 °C) in 100 mM phosphate buffer at a pH of 7.0 unless otherwise stated. GOx 20 μM and 2.5 mM mediator concentrations were used unless stated otherwise.

2.4.4 Michaelis-Menten Curves

Michaelis-Menten Curves were produced using GOx and iodide, FcTMAI, or FcTMATos mediators by applying 600 mV to a glassy carbon working electrode with a Pt counter electrode and a SCE reference electrode in a pH 7.0 50 mM phosphate buffer, with 20 μM GOx and 2.5 mM mediator concentrations. The voltage was held for 200 seconds to allow the current to stabilize and the current was recorded. Glucose was added in aliquots from a 1 M glucose stock solution before each current measurement was taken. This process was repeated to give concentrations of glucose from 0-150 mM to produce the Michaelis-Menten curves. The solution was bubbled with nitrogen or air for 15 min after addition of each glucose aliquot and immediately before each measurement if noted as a gas bubbled sample for these experiments. This entire experiment was repeated 3 times to produce the curve in triplicate with each mediator and averaged to produce the Michaelis-Menten curves seen in Chapter 2.

2.4.5 Fuel Cells.

To simulate sweeping through resistances a glassy carbon electrode was used as the anode and a Pt cloth air breathing electrode used as the cathode. The working electrode lead was attached to the Pt cloth and the reference and counter electrode leads were attached to the glassy carbon electrode dipped in a solution of 20 uM GOx, 100 mM Glucose and 2.5 mM mediator (NaI, FcTMAI, or FcTMATos respectively) in pH 7 50 mM phosphate buffer. The circuit was scanned from the open circuit potential to 0.005 V at 2 mV/s to generate the polarization curves shown in Chapter 2.

2.5 Chapter 2 Bibliography

1. Peng, Z.; Xie, X.; Tan, Q.; Kang, H.; Cui, J.; Zhang, X.; Li, W.; Feng, G., Blood glucose sensors and recent advances: A review. *Journal of Innovative Optical Health Sciences* **2022,** *15* (02), 2230003,10.1142/s1793545822300038.

2. Hassan, M. H.; Vyas, C.; Grieve, B.; Bartolo, P., Recent advances in enzymatic and non-enzymatic electrochemical glucose sensing. *Sensors* **2021,** *21* (14), 4672

3. Pardue, H. L.; Simon, R. K.; Malmstadt, H. V., An automatic potentiometric method for the determination of the absolute activity of glucose oxidase. *Analytical Chemistry* **1964,** *36* (4), 735-737,10.1021/ac60210a012.

4. Kalaycı, S.; Somer, G.; Ekmekci, G., Preparation and application of a new glucose sensor based on iodide ion selective electrode. *Talanta* **2005,** *65* (1), 87-91,10.1016/j.talanta.2004.05.015.

5. Nagy, G.; Von Storp, L. H.; Guilbault, G. G., Enzyme electrode for glucose based on an iodide membrane sensor. *Analytica Chimica Acta* **1973,** *66* (3), 443-445,https://doi.org/10.1016/S0003-2670(01)82564-2.

6. Zhong, Q.; Chen, Y.; Qin, X.; Wang, Y.; Yuan, C.; Xu, Y., Colorimetric enzymatic determination of glucose based on etching of gold nanorods by iodine and using carbon quantum dots as peroxidase mimics. *Microchimica Acta* **2019,** *186* (3), 161,10.1007/s00604-019-3291-2.

7. Liu, Y.; Lei, L.; Zhang, Z., An ultrasensitive colorimetric immunoassay based on glucose oxidase catalyzed cascade formation of blue–black iodine–starch complex. *Sensors and Actuators B: Chemical* **2017,** *248*, 195-200,https://doi.org/10.1016/j.snb.2017.03.142.

8. Liebhafsky, H. A., The catalytic decomposition of hydrogen peroxide by the iodine-iodide couple. Ii and iii. The rate of oxidation in neutral, and in acid, solution of hydrogen peroxide by iodine. *Journal of the American Chemical Society* **1932,** *54* (9), 3499-3508,10.1021/ja01348a003.

9. Liebhafsky, H. A., The catalytic decomposition of hydrogen peroxide by the iodine-iodide couple at 25°. *Journal of the American Chemical Society* **1932,** *54* (5), 1792-1806,10.1021/ja01344a011.

10. Punnoy, P.; Preechakasedkit, P.; Aumnate, C.; Rodthongkum, N.; Potiyaraj, P.; Ruecha, N., Polyvinyl alcohol/starch modified cotton thread surface as a novel colorimetric glucose sensor. *Materials Letters* **2021,** *299*, 130076,https://doi.org/10.1016/j.matlet.2021.130076.

11. Li, H.; Münchberg, U.; Oughli, A. A.; Buesen, D.; Lubitz, W.; Freier, E.; Plumeré, N., Suppressing hydrogen peroxide generation to achieve oxygen-insensitivity of a [nife] hydrogenase in redox active films. *Nature Communications* **2020,** *11* (1), 920,10.1038/s41467-020-14673-7.

12. Merchant, S. A.; Tran, T. O.; Meredith, M. T.; Cline, T. C.; Glatzhofer, D. T.; Schmidtke, D. W., High-sensitivity amperometric biosensors based on ferrocene-modified linear poly(ethylenimine). *Langmuir : the ACS journal of surfaces and colloids* **2009,** *25* (13), 7736-7742,10.1021/la9004938.

13. Merchant, S. A.; Meredith, M. T.; Tran, T. O.; Brunski, D. B.; Johnson, M. B.; Glatzhofer, D. T.; Schmidtke, D. W., Effect of mediator spacing on electrochemical and enzymatic response of ferrocene redox polymers. *The Journal of Physical Chemistry C* **2010,** *114* (26), 11627-11634,10.1021/jp911188r.

14. Tran, T. O.; Lammert, E. G.; Chen, J.; Merchant, S. A.; Brunski, D. B.; Keay, J. C.; Johnson, M. B.; Glatzhofer, D. T.; Schmidtke, D. W., Incorporation of single-walled carbon nanotubes into ferrocene-modified linear polyethylenimine redox polymer films. *Langmuir : the ACS journal of surfaces and colloids* **2011,** *27* (10), 6201-6210,10.1021/la104999f.

15. Meredith, M. T.; Hickey, D. P.; Redemann, J. P.; Schmidtke, D. W.; Glatzhofer, D. T., Effects of ferrocene methylation on ferrocene-modified linear poly(ethylenimine) bioanodes. *Electrochim. Acta* **2013,** *92*, 226-235,10.1016/j.electacta.2013.01.006.

16. Hickey, D. P.; Giroud, F.; Schmidtke, D. W.; Glatzhofer, D. T.; Minteer, S. D., Enzyme cascade for catalyzing sucrose oxidation in a biofuel cell. *ACS Catal.* **2013,** *3* (12), 2729-2737,10.1021/cs4003832.

17. Hickey, D. P.; Halmes, A. J.; Schmidtke, D. W.; Glatzhofer, D. T., Electrochemical characterization of glucose bioanodes based on tetramethylferrocene-modified linear poly(ethylenimine). *Electrochim. Acta* **2014,** *149*, 252-257,10.1016/j.electacta.2014.10.077.

18. Godman, N. P.; DeLuca, J. L.; McCollum, S. R.; Schmidtke, D. W.; Glatzhofer, D. T., Electrochemical characterization of layer-by-layer assembled ferrocene-modified linear poly(ethylenimine)/enzyme bioanodes for glucose sensor and biofuel cell applications. *Langmuir : the ACS journal of surfaces and colloids* **2016,** *32* (14), 3541-3551,10.1021/acs.langmuir.5b04753.

19. Bamper, D. 2019. A binding isotherm between ferrocene mediators and glucose oxidase for use in bioanode development and intitial studies of an electrocatalytic deoxydehydration reaction. Doctoral Dissertation, University of Oklahoma, ShareOK.org

20. LINDSAY, J. K.; HAUSER, C. R., Aminomethylation of ferrocene to form n, n-dimethylaminomethylferrocene and its conversion to the corresponding alcohol and aldehyde1. *The Journal of organic chemistry* **1957,** *22* (4), 355-358

21. Boschloo, G.; Gibson, E. A.; Hagfeldt, A., Photomodulated voltammetry of iodide/triiodide redox electrolytes and its relevance to dye-sensitized solar cells. *The Journal of Physical Chemistry Letters* **2011,** *2* (24), 3016-3020,10.1021/jz2014314.

22. Bentley, C. L.; Bond, A. M.; Hollenkamp, A. F.; Mahon, P. J.; Zhang, J., Voltammetric determination of the iodide/iodine formal potential and triiodide stability constant in conventional and ionic liquid media. *The Journal of Physical Chemistry C* **2015,** *119* (39), 22392-22403,10.1021/acs.jpcc.5b07484.

23. Nicholson, R. S.; Shain, I., Theory of stationary electrode polarography. Single scan and cyclic methods applied to reversible, irreversible, and kinetic systems. *Analytical Chemistry* **1964,** *36* (4), 706-723,10.1021/ac60210a007.

24. Neuse, E. W.; Loonat, M. S., Ferricenium polyiodides. *Journal of Organometallic Chemistry* **1985,** *286* (3), 329-341,https://doi.org/10.1016/0022-328X(85)80049-8.

Chapter 3

3.1 Introduction

Layer-by-layer (LBL) modification of surfaces is an important method for the fabrication of sensors, fuel cells and photovoltaics[1-3]. Many of these applications depend on the flow of electrons from an upper layer to an electrode surface through an attachment layer. Ferrocene-modified linear polyethylenimine (Fc-LPEI) has been used by our group to produce a variety of sensors[4-16] including LBL electrodes for glucose sensing[10-14]. These LBL electrodes utilize the sulfur in cystamine hydrochloride as the first layer (attachment layer) to establish an amine surface on a gold electrode for functionalization of gold surfaces (Scheme 3.1)[17]. After this first layer, a second layer of negatively charged GOx can be electrostatically immobilized on the surface. The GOx can also be oxidized with sodium periodate to form aldehyde functional groups from the surface sugars of the GOx so that it can react with the amine surface and form covalent bonds as well. The Fc-LPEI can then be used as another positively charged amine layer to form another electrostatically and covalently attached layer. The Fc-LPEI and GOx can be deposited in alternating layers to build up more material on the surface and increase the sensitivity and current output of these glucose sensors. While this is an elegant electrode system that has produced very sensitive electrodes, the cystamine layer does not contribute to the electrode's functionality in any other way. This has led us to search for a better first layer for these electrodes.

PEI has many basic and nucleophilic amines that can be easily functionalized to build functional polymer materials like Fc-LPEI used in the LBL electrodes mentioned above. In solution these amines are in equilibrium with protonated ammoniums and the ratio is dependent

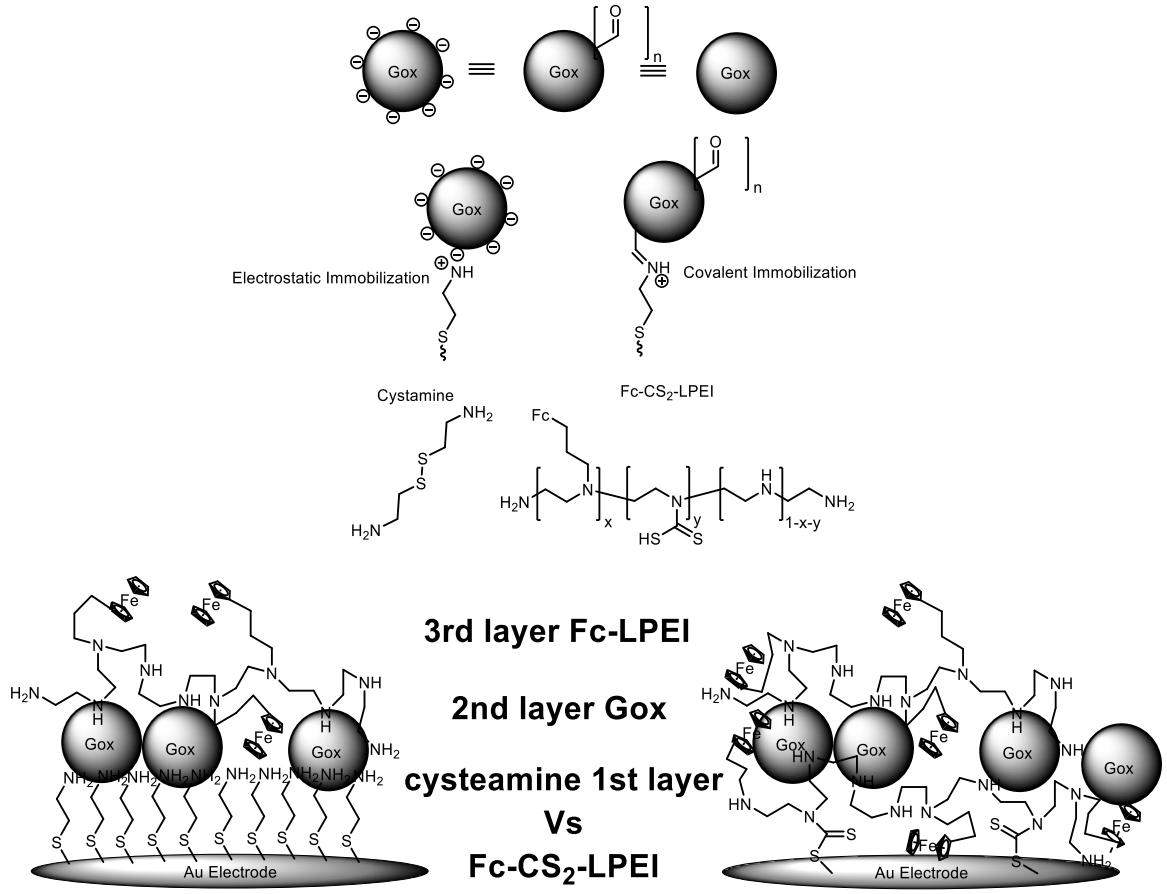

Scheme 3.1 Graphical comparison of cysteamine first layer vs modified Fc-CS_2-LPEI first-layer in a 3-layer LBL system.

on the pH of the solution. Amines in other polymers and bio-molecules have been reacted with carbon disulfide to form dithiocarbamate moieties that can be used to link them to and functionalize gold surfaces and nanoparticles[18-20]. In this chapter, carbon disulfide was used to react with the amine backbone[21] of Fc-LPEI which can then be attached to gold electrodes. This material was used as the first layer in LBL-fabricated enzymatic glucose biosensors. We hypothesized that using a large redox-active polymer first layer, instead of a small molecule like cystamine, could provide the LBL electrode with large dendritic molecules with a high surface area for a better attachment to the large GOx enzymes in the second layer. This polymer could also act as an efficient electron transport first layer on the electrode surface since it is redox active.

This first layer was synthesized, and the material factors such as deposition pH and time were investigated. The substitution percentages of carbon disulfide, and ferrocene in these materials were also investigated. The small-molecule cystamine first electrode layer was directly compared to electrodes with CS_2-LPEI and Fc-CS_2-LPEI first-layer electrodes using ferrocene salts to study how the diffusion/electron transfer processes were different for each system. This polymer first layer was then used to fabricate 9-layer enzymatic glucose sensors that matched the sensitivity and current outputs of 32-layer (16-bilayers) cystamine first layer electrodes. These polymeric first layer electrodes were also used in fuel cells and found to be more stable, and produced much more current than their small molecule cystamine electrodes.

3.2 Results and Discussion

3.2.1 Fc-CS_2-LPEI synthesis and electrochemical characterization

Fc-LPEI was functionalized with carbon disulfide by dissolving the polymer in methanol and adding 5-50 mole percent (per LPEI repeat unit) of carbon disulfide to the solution. The polymer quickly precipitates out of solution due to the electrostatic attraction between the anionic dithiocarbamate groups and ammonium backbone groups, making crosslinks and forming an insoluble salt-bridged crosslinked network (as shown in Scheme 3.2 below). After the solvent was evaporated the polymer was dried in a vacuum oven to a constant weight. The weight was

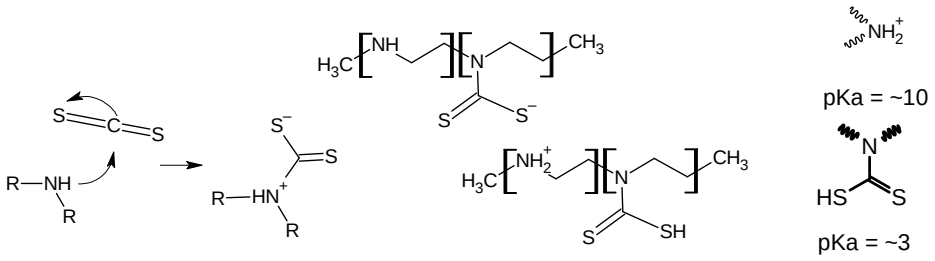

Scheme 3.2 Graphical representation of an amine reaction with CS_2 and the electrostatic crosslinking between CS_2 modifications and ammoniums in the LPEI backbone.

consistent with the amount of carbon disulfide added, indicating that all the added carbon disulfide was incorporated essentially quantitatively into the co-polymer. The resulting polymer was insoluble in neutral and acidic water. To further use or analyze the polymer it needs to be dissolved by breaking up the ionic crosslinks between the dithiocarbamate and ammonium groups. This could be done by either protonating all of the dithiocarbamates, or deprotonating all of the ammoniums. Given that there are many more amines than dithiocarbamate groups one might assume it would be easier to dissolve the polymer with acidic conditions by protonating the few dithiocarbamates. However, the pK_a of thiocarbamic acid is approximately ~3.4 pK_a[22], while the pKa of an ammonium is in the range of 8.4-9.6[23]. While the Fc-LPEI dissolves in acidic solutions around pH 6 when the amines are protonated, the Fc-CS_2-LPEI polymer does not dissolve under acidic conditions even in 1M HCl (aq.) indicating an extremely low pKa for the dithiocarbamate moieties. However, because the amines can be deprotonated, forming the free amine and reducing electrostatic crosslinks between the ammonium and thiocarbamate groups, the polymer can be dissolved in aqueous solutions under highly basic conditions around pH 11.

Using D_2O and sodium hydroxide the polymers were dissolved and ^{1}H-NMR spectra were obtained for several different CS_2 addition percentages (Figure 3.1). These spectra show new peaks above the ferrocene peaks at δ 4.0-4.1 ppm, from δ 4.15-4.55 ppm, indicating a highly electronegative group has been added to the polymer. These peaks are likely due to the LPEI -C_2H_4- backbone hydrogens that are adjacent to the CS_2 moieties. This is consistent with the chemical shifts observed for the methylene hydrogens of sodium diethyldithiocarbamate in D_2O at ca. δ 4.1[24]. While the integration keeps rising with higher CS_2 addition percentages, it is difficult to use these to correlate quantitatively to the CS_2 substitution percentages since these peaks are broadened significantly, likely affected by proton exchange to neighboring nitrogens, and because

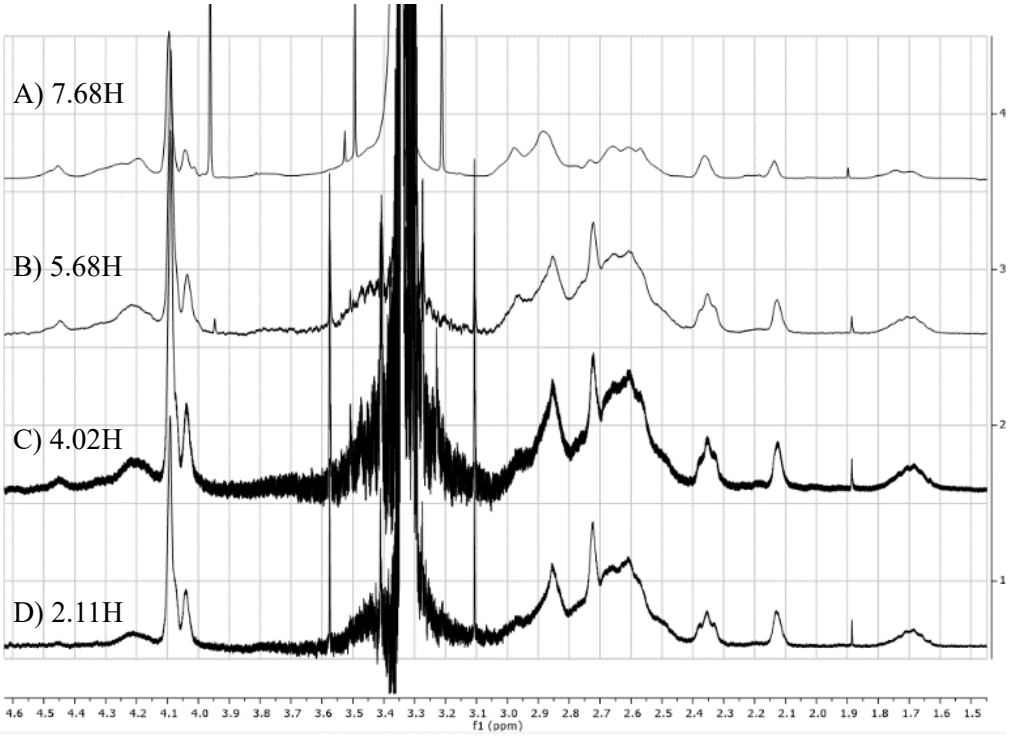

Figure 3.1 ^{1}H NMRs of the Fc-CS_2-LPEI obtained using a 300MHz instrument in D_2O having A) 50%, B) 9%, C) 7.5%, and D) 2.5% CS_2 addition by molarity. The integration of the 4.15-4.55 ppm region relative to that of the normalized 9H ferrocene peak is shown to the left of the spectra.

of possible overlap with the ferrocene signals from the N-3-ferrocenylpropyl groups that are also on the LPEI. Because of this, the CS_2 substitution percentages on the Fc-LPEI were from 5-50% and were determined using gravimetric analysis.

Since the dithiocarbamic acid groups on the polymer are in the anionic state when dissolved in a high pH environment, the basic solution is also ideal for attaching the material to gold surfaces through the dithiocarbamate groups. Because 20-25% ferrocenyl substitution had been used by our group previously for layers 3-34 in LBL systems, a 20% ferrocenyl and 10% CS_2 substituted Fc-CS_2-LPEI was used for the initial studies. Gold electrodes were coated with Fc-CS_2-LPEI by dipping in the Fc-CS_2-LPEI solution for 5 minutes. After this, the electrodes were washed gently with DI water and CVs were run in a phosphate buffer to determine whether or not any material was attaching to the electrode surface (see Figure 3.2 below). While the Fc-CS_2-LPEI clearly

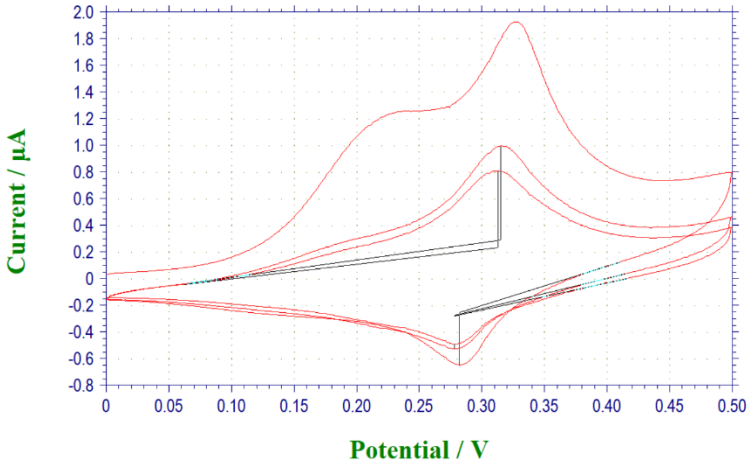

Figure 3.2, Cyclic voltammogram of Fc-CS_2-LPEI (20% Fc, and 10 % CS_2) on a gold electrode scanned at 50 mV/s in 50 mM pH 7 phosphate buffer with a Pt wire counter electrode and a SCE reference electrode.

sticks to the gold and can be detected electrochemically on the surface of the electrode (Figure 3.2), the CV possesses several interesting features. First is the fact that it has a broad shoulder before the sharper surface wave peak at higher potential, indicating that there are at least two different types of ferrocene environments seen by the electrode. For example, some could be dendritic and farther from the electrode and CS_2 groups, while others could be more tightly held next to the electrode surface near the CS_2 attachment points. This model is consistent with what is seen in the CV above. There is a significant loss in ferrocene response between the first and second scans of the electrode. However, most of this loss occurs in the broad shoulder and could be explained by those being loosely bound ferrocene groups diffusing away from the surface of the electrode and tearing loose some of the surface bound ferrocenes as well. The second scan is used in the studies outlined below to obtain more consistent results since the electrodes are more stable after 1 scan. It should be noted that the dip time-current response relationships were often inconsistent, and that dip-times longer than 5 minutes only occasionally resulted in significantly more current response. It was determined that a consistent monolayer builds up quickly in the first 5 min, with an inconsistent doubling of the ferrocene depositing on the electrode from 6 to 30 min

of deposition (see Figure 3.3). Electrodes with similar surface coverage to the 30 min electrodes showed up after 400 min of deposition time and the results were very inconsistent. Since more material can be built up quickly and consistently using more layers rather than longer dipping times, 5 min was settled on as a consistent deposition time for the first layer to build the rest of the

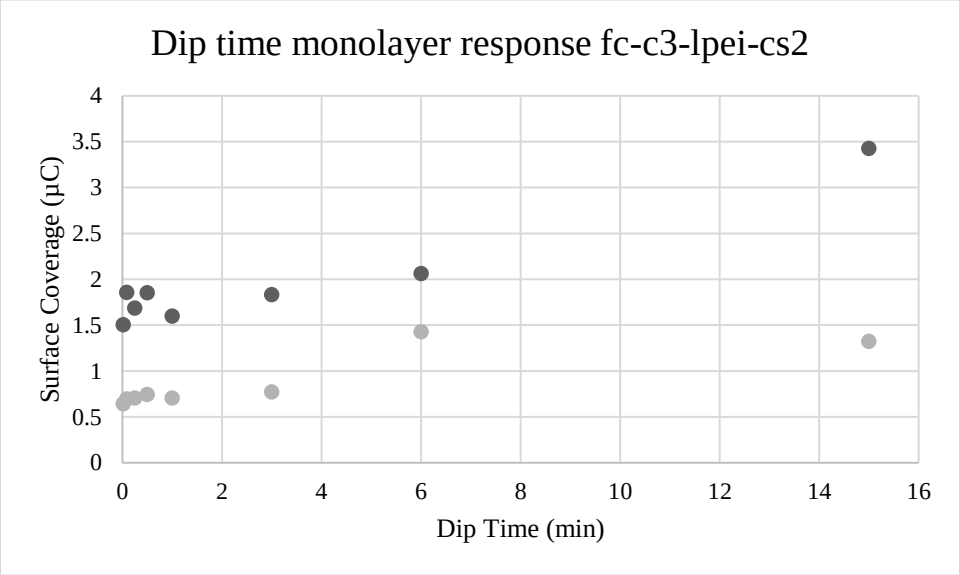

Figure 3.3 The surface charge (Coulombs) detected on the Fc-CS_2-LPEI (20% Fc, and 10 % CS_2) on gold electrodes measured through integration of the anodic peak with varying dip time using CV in 50 mM phosphate buffer at 50 mV/s with a Pt wire counter electrode and a SCE reference. The black dots are the first scan, and the gray are the second.

multilayered electrode on.

The Randle-Sevcik equation[25-26] below (Equations 3.1) shows that the current should vary linearly with the square root of the scan rate (i_p is peak current in amps, n is the number of electrons

$$\text{Randle-Sevcik Equation: } i_p = 0.4463nFAC\left(\frac{nF\nu D}{RT}\right)^{\frac{1}{2}}$$

$$\text{Langmuir Adsorption Isotherm: } i_p = \nu\frac{n^2F^2A\Gamma_{O,m}}{4RT}$$

$$log(i_p) = log\left(0.4463nFAC\left(\frac{nF\nu D}{RT}\right)^{\frac{1}{2}}\right) = log\left(c_1\left(\frac{c_2\nu}{c_3}\right)^{\frac{1}{2}}\right) = \frac{1}{2}log(c_4\nu)$$

Equations 3.1 Randle-Sevcik Equation, the Langmuir Adsorption Isotherm and the Randle Sevcik equation after taking the Log of both sides.

in the redox event, A is the area of the electrode in cm^2, F is the Faraday constant in C/mol, D is the diffusion coefficient in cm^2/s, C is the concentration in mol/cm^3, ν is the scan rate, R is the gas constant in J/K*mol, and T is the temperature in kelvin). However if the process is surface bound the peak current should vary linearly with the scan rate[27-28] following the Langmuir adsorption isotherm[29] where $\Gamma_{O,m}$ is the coverage of the electroactive species in mol/cm^2. Given these relationships, if the logarithm is taken of both sides of the equation, the log(i_p) vs log(ν) graph should have a slope of ½ if it is diffusion controlled and 1 if it is surface bound given the exponent on the scan rate in the equations. This is a much greater difference and can be used to differentiate between surface-bound and diffusion-controlled phenomena with certainty. As shown below (Figure 3.4) for an electrode prepared using a 5 min dip time it can be difficult to decipher whether the peak current is linear with the square root of the scan rate or the scan rate itself with R^2 values

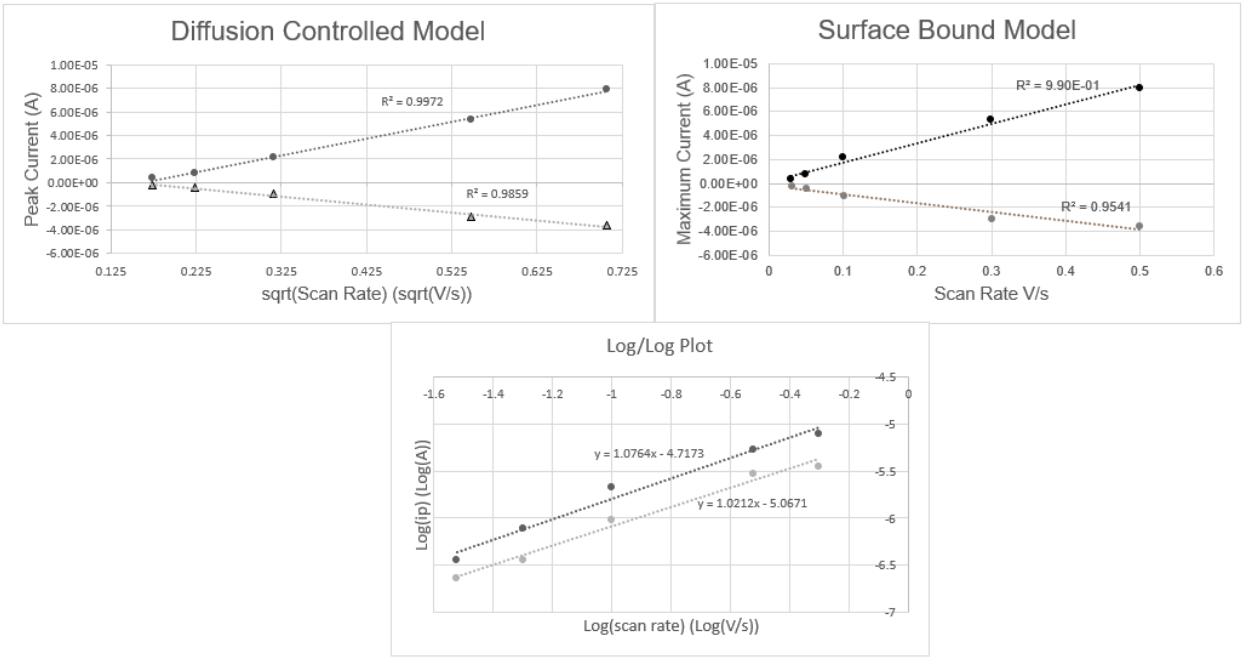

Figure 3.4 One layer of Fc-CS_2-LPEI (20% Fc, and 10 % CS_2) on a gold disk electrode scanned in 100 mM phosphate buffer using Pt counter and SCE reference electrodes, and using the second scan and a fresh electrode for each scan rate: A) Plotted according to the Randle-Sevcik equation using the peak current and the square root of the scan rate. B) According to the Langmuir adsorption isotherm where i_{pa} and ν are proportional and C) Plotted Log(i_{pa}) Vs. Log(ν). Both the oxidation and reduction peak currents are shown.

above 0.9. Therefore, the log(i) vs. log(v) plot is used and as shown, the plot has a slope of 1.08, showing that the ferrocene behaves as though it is surface bound (the slope would be 0.5 if it were diffusion controlled).

Since this first-layer could have a large impact on the performance of the electrode it was important to standardize the ferrocene and carbon disulfide substitution percentages, as well as the dipping conditions used, to produce the first layer in order to study multi-layered electrodes. To do this, the variables of the dip time and dip pH, as well as the carbon disulfide and ferrocene content of the copolymer needed to be considered. The CS_2-Fc-LPEI dissolves around pH 11.7 making this the logical pH to begin deposition pH testing. While the dipping pH did not have a dramatic effect on the amount of ferrocene deposited on the surface the optimal pH appeared to be around pH 13 (see Figure 3.5). After the dipping pH and dip time (Figure 3.3) had been

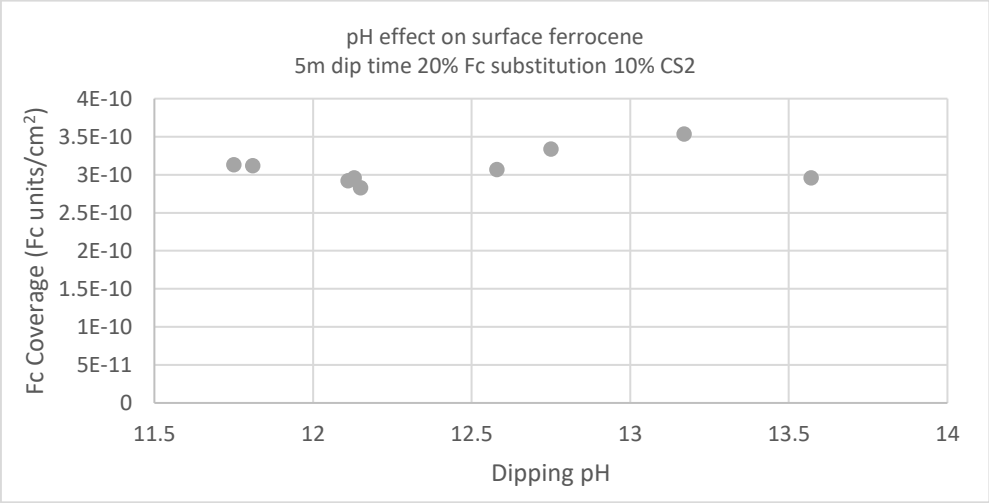

Figure 3.5 Number of ferrocenes (or surface charge) per cm of gold electrode vs dipping pH used for the construction of the Fc-CS_2-LPEI (20% Ferocenyl and 10% CS_2) monolayer, constructed using a 5 min dip time and scanned against a Pt wire electrode with an SCE reference at 50 mV/s in 50 mM pH 7 phosphate buffer.

standardized, the optimal substitution percentages of the polymer could be studied.

The ferrocenyl substitution percentage was tested by synthesizing several different Fc-CS_2-LPEI polymers with ferrocenyl content from 9-24 mol% and 10 mol% CS_2 substitution and testing

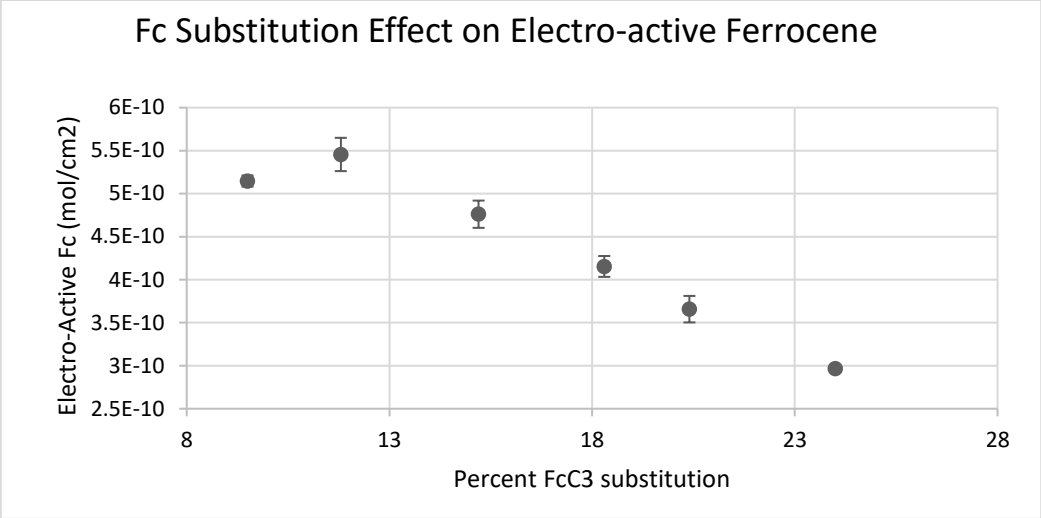

Figure 3.6 Number of ferrocenes per cm on a gold electrode varying the Fc substitution percentage of an Fc-CS_2-LPEI with 10 % CS_2 substitution fabricated using a 5 min dip time at pH 13 scanned against a Pt wire electrode with a SCE reference at 50 mV/s in 50 mM pH 7 phosphate buffer.

a 5 min dip time gold electrode using CV. The ferrocene content chosen for continued studies was around 11.5% substitution (see Figure 3.6) since this gave the highest response. The carbon disulfide substitution percentage was the next important variable to set before continuing to produce a layered electrode. This was studied using the 11.5 mol% ferrocenyl Fc-LPEI and substituting it with 5-15 mol% CS_2 and using CV to determine the surface ferrocene concentration. We found that a 7 mol% CS_2 substitution was close to the peak of the most observable ferrocene

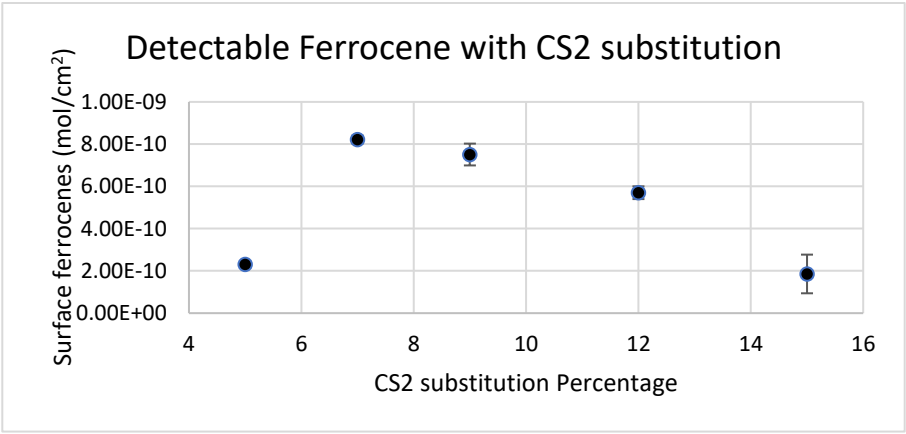

Figure 3.7 Number of ferrocenes (or surface charge) per cm on a Fc-CS_2-LPEI gold electrode, modified using a 5 min dip time at pH 13 and 12 % Fc substitution, scanned against a Pt wire electrode with a SCE reference at 50 mV/s in 50 mM pH 7 phosphate buffer and varying the CS_2 substitution percentage.

on the surface of a gold electrode (Figure 3.7). Because the changes made in the first attachment layer could greatly affect multilayered electrodes, the varying CS_2 substitution percentage was also tested as a 2- and 3-layer electrode using saturating glucose conditions. Cyclic voltammograms were taken and the steady state current was plotted against the CS_2 substitution percentage to validate that the high ferrocene surface concentration in the first layer correlated with higher current outputs from the multi-layered catalytic system. It can be seen in Figure 3.8 that the current at saturating glucose concentration is the highest at 7% CS_2 substitution. The 3L electrode glucose response graph resembles the monolayer CS_2 substitution percent graph (Figure 3.7) indicating the importance of tuning the first layer to contain as much ferrocene as possible.

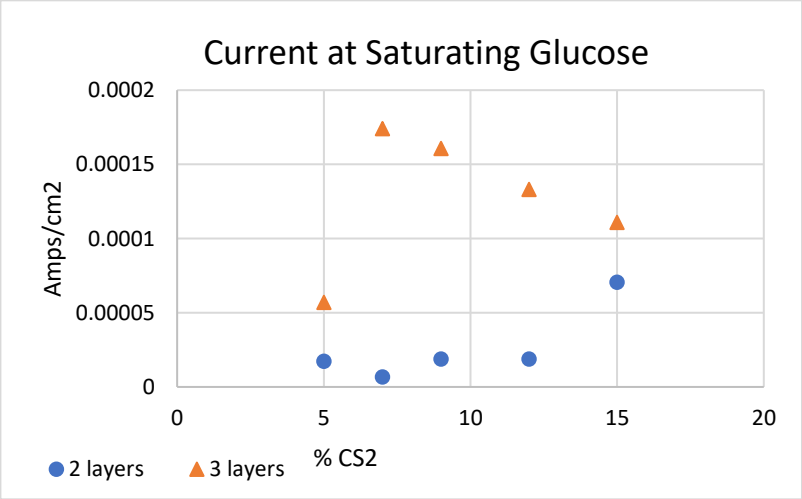

Figure 3.8 Steady state current of a gold electrode with 2 and 3 layers (p-GOx and Fc-LPEI respectively) using a Fc-CS_2-LPEI (12% Fc Substitution) using varying the CS_2 substitution percentage found using an electrode scanned against a Pt wire counter electrode with a SCE reference at 50 mV/s in 50 mM pH 7 phosphate buffer with 150 mM glucose.

Increasing the percentage of electron withdrawing carbon disulfide units showed a small but significant increase in the potential required to oxidize the ferrocene as seen in Figure 3.10 below. This is likely due to the thiocarbamate moieties withdrawing electrons from the surrounding environment better and protecting the ferrocene from oxidation, causing the oxidation peak to shift to higher potentials. While higher oxidation potentials for the ferrocenes lessens the voltage

generated by a biofuel cell, the potential is less important in bio-sensing applications. A 9 mol% CS_2 substitution was chosen to proceed with in the multilayer system studies in order to avoid the sharp changes in performance seen between the 7 and 5 CS_2 mol% materials.

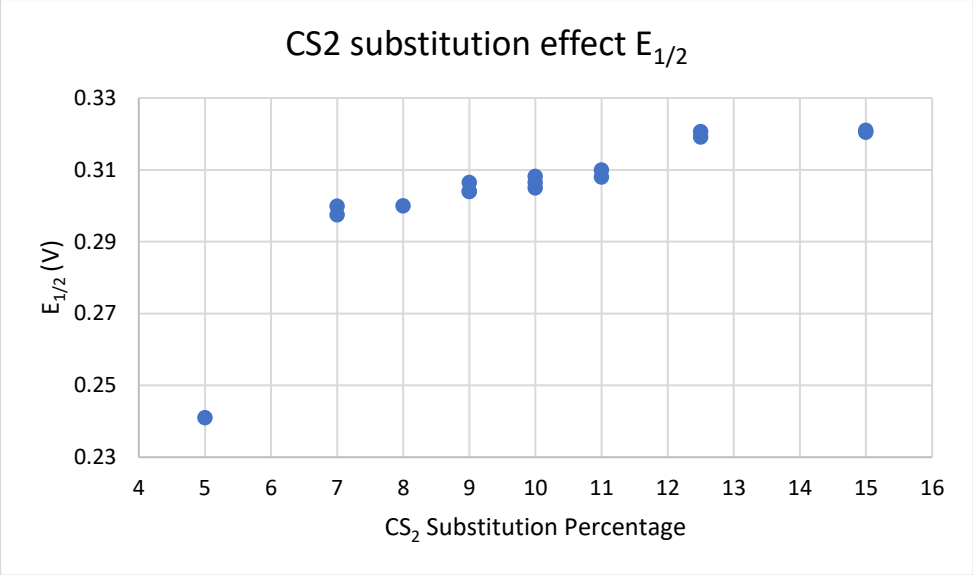

Figure 3.10 The $E_{1/2}$ of Fc-CS_2-LPEI (12% Fc substitution) on a gold electrode with varying CS_2 substitution, fabricated using a 5 min dip time scanned against a Pt wire electrode with a SCE reference at 50 mV/s in 50 mM pH 7 phosphate buffer.

3.2.2 Low-Layer Characterization

Although each dip does not result in a completely uniform monolayer[14], each dip will be described as a layer. For example, an electrode dipped in a cystamine or a Fc-CS_2-LPEI solution will be described as a 1-layer (1L) system and an electrode dipped in cystamine or Fc-CS_2-LPEI

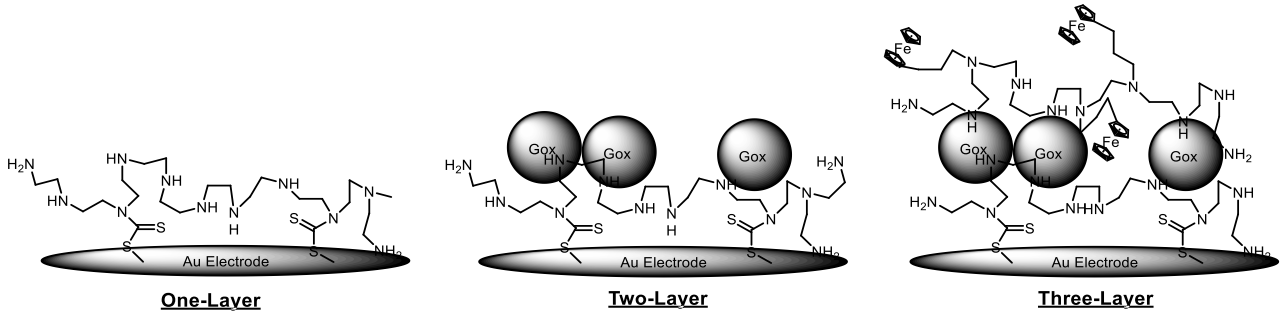

Scheme 3.3 One-, two-, and three-layer electrodes shown with a CS_2-LPEI first layer, a p-GOX second layer, and a Fc-LPEI third layer.

solution and then in the p-GOX solution would be described as a 2-layer (2L) system (see Scheme 3.3).

There were two main ways we hypothesized that the functionalized polymer in the first layer could change the performance of the sensor. The first was that the polymer is large and dendritic and porous, allowing for many attachment points for the large enzymes. The small molecule cystamine, in contrast, forms a relatively flat and low surface area attachment layer on the electrode surface for the large enzymes in the second layer (see Scheme 3.1). The second way it could affect the sensor is that the cystamine has no electrochemically active component and could partially insulate the surface from interacting with the upper layers, while the CS_2-Fc-LPEI could effectively wire the upper layers to the electrode surface with its incorporated ferrocene moiety. In order to determine the effect the material used in the first layer has on the electrode's behavior, we first studied 1L & 2L system on their own, outside of their use in a sensor or fuel cell.

The insulating effect of the first layer materials was studied by layering one and two layers of material on an electrode surface and determining diffusion coefficients (D) for ferrocene salts in solution using these electrodes. These studies were carried out using cystamine, CS_2-LPEI, and Fc-CS_2-LPEI as the first layer (see Figure 3.10). Diffusion coefficients for FcTMATos were calculated using the Randles-Sevcik equation (Equation 3.1). It was found that one- and two-layered cystamine coated electrodes' diffusion coefficients were within experimental error to those of the naked gold electrodes, indicating that the cysteamine does not really insulate or inhibit diffusion of electroactive components to the surface. In contrast, CS_2-LPEI one-layer electrodes showed a significant drop in the diffusion coefficient, indicating that the polymer surface interferes somewhat with access to the electrode surface. While this may initially seem like a negative, it also indicates that there is a significant amount of material on the surface. The 2-layer electrodes

saw no experimental difference when compared to the monolayer electrodes, indicating that the GOx layer is patchy enough that it adds no extra barrier to access to the electrode surface. The Fc in the first layer did not seem to affect the diffusion of electrons through the first layer relative to the CS_2-LPEI first layer.

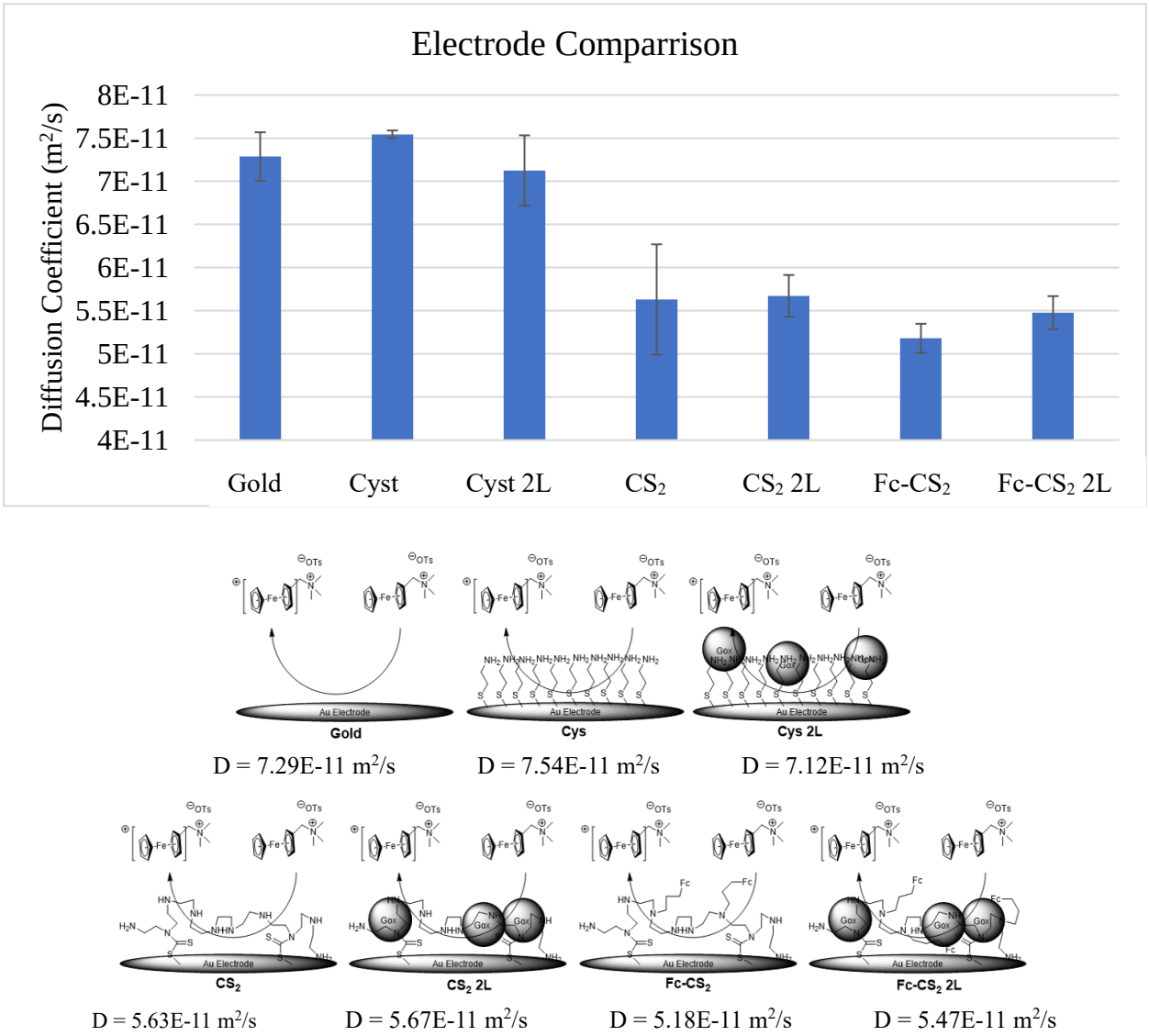

Figure 3.10 The diffusion coeficients of FCTMATos (2.5 mM) on the gold and modified gold electrode with one, and two material layers using cystamine, CS_2-LPEI, and Fc-CS_2-LPEI as the first layers respectively, and GOx as the second layer. These were done on a 2 mm gold electrode in 50 mM phosphate buffer pH 7 and using a SCE reference and Pt counter electrod. The diffusion constants of the FcTMATos salt on each electrode were calculated at scan rates from 10-500 mV/s using the Randle Sevcik equation and then averaged together to obtain the final coefficient.

The Δ_E (E_{pa} - E_{pc}) of an ideal diffusion-controlled process should be 59 mV under standard conditions[30]. Since the surface-bound systems studied here vary greatly from the ideal, the diffusional redox behavior of FcTMATos can be compared to the bare gold electrode rather than the theoretical standard (Figure 3.11). Here the cystamine shows almost no difference from the standard gold electrode, while the CS_2-LPEI 1 and 2-layered electrodes show a significant increase in delta E, indicating some retardation of the redox process. The Fc-CS_2-LPEI 1 and 2-layered electrodes are somewhere between the small molecule and non-electroactive polymer, suggesting that the ferrocene inclusion in the first layer is electrically wiring the surface to the solution through a reasonably diffusion-controlled process.

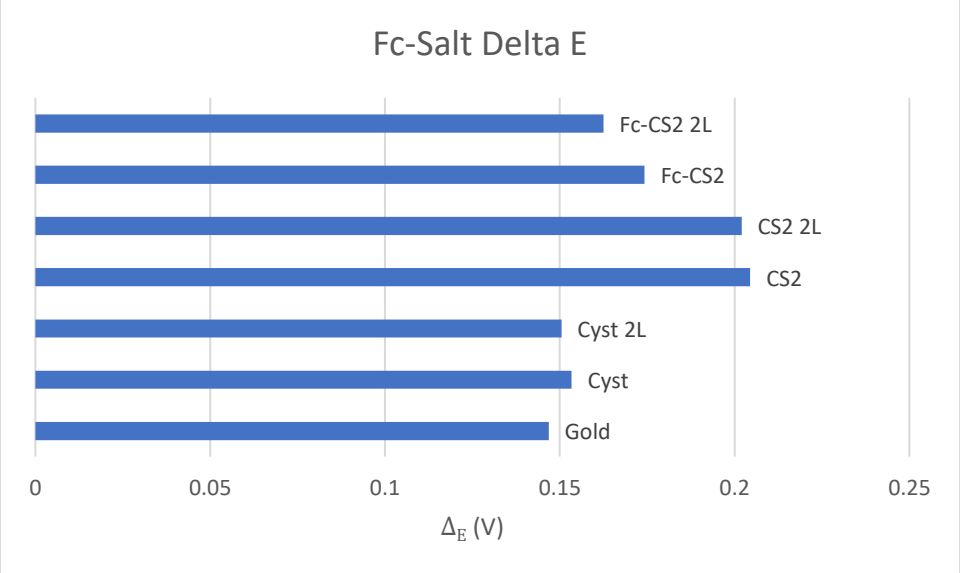

Figure 3.11 The Δ_E of the cyclic voltammograms of FcTMATos (2.5 mM) on the one-, and two-layer electrodes using cystamine, CS_2-LPEI (9% substituted) and Fc-CS_2-LPEI (12% Fc and 9% CS_2 substitution) as the first layer, respectively, on a 2 mm gold electrode in 50 mM phosphate buffer pH 7 using a SCE reference and Pt counter electrode scanned at 50 mV/s.

The $E_{1/2}$ of a redox process is indicative of how difficult it is to oxidize or reduce the compound involved in the redox process. If something is harder to oxidize its $E_{1/2}$ will be higher. It is apparent from Figure 3.12 below that the $E_{1/2}$ decreases slightly but consistantly with the addition of the negatively charged glucose oxidase layer. The presence of the negative charges

around the electrode surface could aid in the oxidation of the ferrocene to ferrocenium. It is also apparent that the presence of the ferrocene in the first layer of the electrode material induces a better connection of the electrode surface to the ferrocene in solution, aiding in the oxidation of the ferrocene salt. Models in the literature suggest that ferrocene polymers can pass electrons through these polymers in a hopping mechanism from the outer layers to the electrode surface[31]. This mechanism could aid in the oxidation of the ferrocene salt in solution since the ferrocene of the Fc-CS_2-LPEI on the electrode surface oxidizes at a lower voltage around 0.3 V.

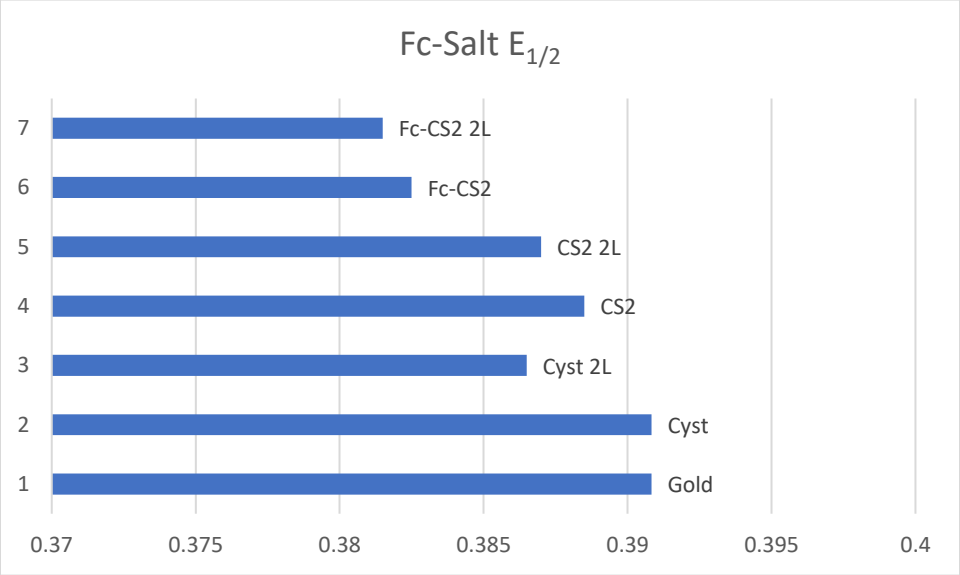

Figure 3.12 The $E_{1/2}$ of the cyclic voltammograms of FcTMATos (2.5 mM) on the one-, and two-layer electrodes using cystamine, CS_2-LPEI (9% substituted) and Fc-CS_2-LPEI (12% Fc and 9% CS_2 substitution) as the first layer, respectively, on a 2 mm gold electrode in 50 mM phosphate buffer pH 7 using a SCE reference and Pt counter electrode scanned at 50 mV/s.

These results show that our first hypothesis was correct; the polymer first layer makes a much better attachment surface for the large enzymatic second-layer than the small cysteamine molecule by immobilizing more material on the electrode surface. This material can be seen by it's effects on the cyclic voltammetry of FcTMATos in solution. It also shows that the first layer is important in the oxidation of upper layers by the way that it facilitates the oxidation of the

ferrocene salts in solution. These hypotheses were further confirmed by results from the use of Fc-CS_2-LPEI as the first layer of a glucose biosensor as discussed below.

In order to further study the effect that incorporating ferrocene into the first layer of these biosensors, cystamine, CS_2-LPEI, and CS_2-Fc-LPEI 3-layer electrodes were made on gold electrodes (see Scheme 3.4) and tested as sensors amperometrically at a potential of 0.45 V in pH 7 50 mM phosphate buffer with an SCE reference and a platinum wire counter electrode. Aliquots

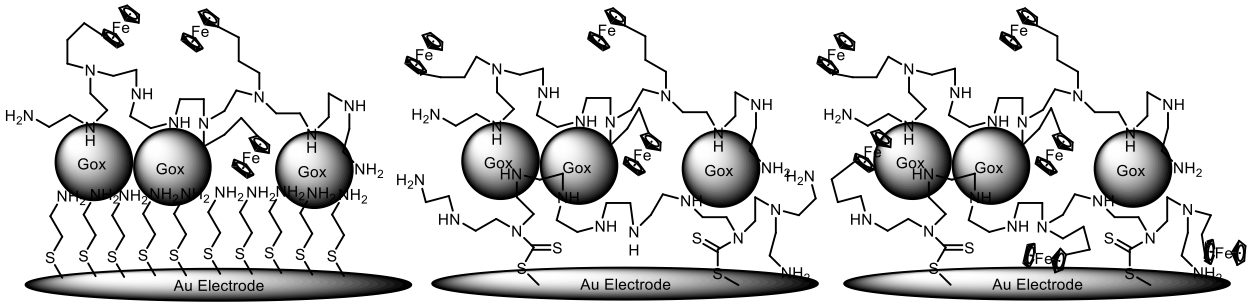

Scheme 3.4 Three-layer electrodes shown with a CS_2-LPEI first layer, a p-GOX second layer and a Fc-LPEI third layer.

of 1 M glucose were added to generate current and a Michaelis-Menten[32-33] (MM) curve which gave the K_M and current at saturating conditions as seen in Table 3.1. The ferrocene coverage was also compared to estimate the amount of material deposited in the 3L systems using cyclic voltammetry, scanned at 50 mV/s and the same phosphate buffer and a 3-electrode set up as used for the MM experiments. While the cysteamine electrode had the middle ferrocene coverage and lowest current at saturating glucose concentrations, it also had the lowest $E_{1/2}$ indicating that it

All electrodes tested were 3 layers	Current w/Glucose (uA/cm^2)	Fc Coverage ($nmol/cm^2$)	K_m (M)	$E_{1/2}$ (mV)
Cystamine	30	.71	0.0130	185
CS_2-LPEI	44	.64	0.0218	195
CS_2-Fc-LPEI	**174**	**1.76**	0.0239	196

Table 3.1 The 3-layer cystamine, CS_2-LPEI and Fc-CS_2-LPEI electrodes compared using Fc surface coverage, current with saturating glucose concentrations, enzyme kinetics and oxidation potential (see text for conditions).

inhibits the oxidation of ferrocene the least. It also has the lowest K_M, meaning that it inhibits the enzymatic reaction of the least of the three electrodes. While the CS_2-LPEI shows the lowest ferrocene content of the three electrodes, it also has 1.5 times the response to glucose when compared with the cysteamine electrode, likely due to a greater GOx content on the electrode. The ferrocene in the first layer had a drastic effect on the response to glucose with more than a seven-fold increase in current over the CS_2-LPEI. The increased K_M of the CS_2-LPEI and CS_2-Fc-LPEI shows some inhibition of the enzyme, but is outweighed by the increase in response to glucose and make much more sensitive glucose sensors than the cysteamine 3-layer electrode. The greater amount of material deposited on the surface, as well as its more efficient wiring to the surface, makes the CS_2-Fc-LPEI a better overall choice as the first layer when immobilizing large enzymes on a surface when compared to cystamine.

These promising electrodes were used in galvanic cells at saturating glucose concentrations to produce polarization and power curves. In order to set up a galvanic cell, a Nafion® coated platinum cloth electrode was used as the working O_2 cathode , and the ferrocene/GOx electrode is connected as the counter and reference electrode in a 2-electrode configuration. The potential between the two electrodes is scanned from the open circuit voltage to 0.005 V at 2 mV/s. This simulates moving through different resistences from high to low and generating a current/voltage (I/V) curve[34]. Since P=IV, a power curve can be generated that shows the power generated at a given voltage. This was done as shown in Figure 3.13A below. After these polarization curves were generated, the electrodes were allowed to run at 0.3 V for 2 hours, and another polarization curve was generated to monitor the stability of the bio-anodes. The 3L-LPEI electrode has the highest power at 100 $\mu W/cm^2$ of power at around 0.5 V followed by the 3L-LPEI electrode after decay. Not only did the 3L-LPEI electrode produce more power than the cystamine first-layered

electrode, it also retained 50% of it's original current after 2 hours of use, where as the cystamine electrode only retained about 15%, showing clearly that the Fc-CS_2-LPEI first layer allows the electrodes to perform better and last longer than the cystamine first-layer electrodes.

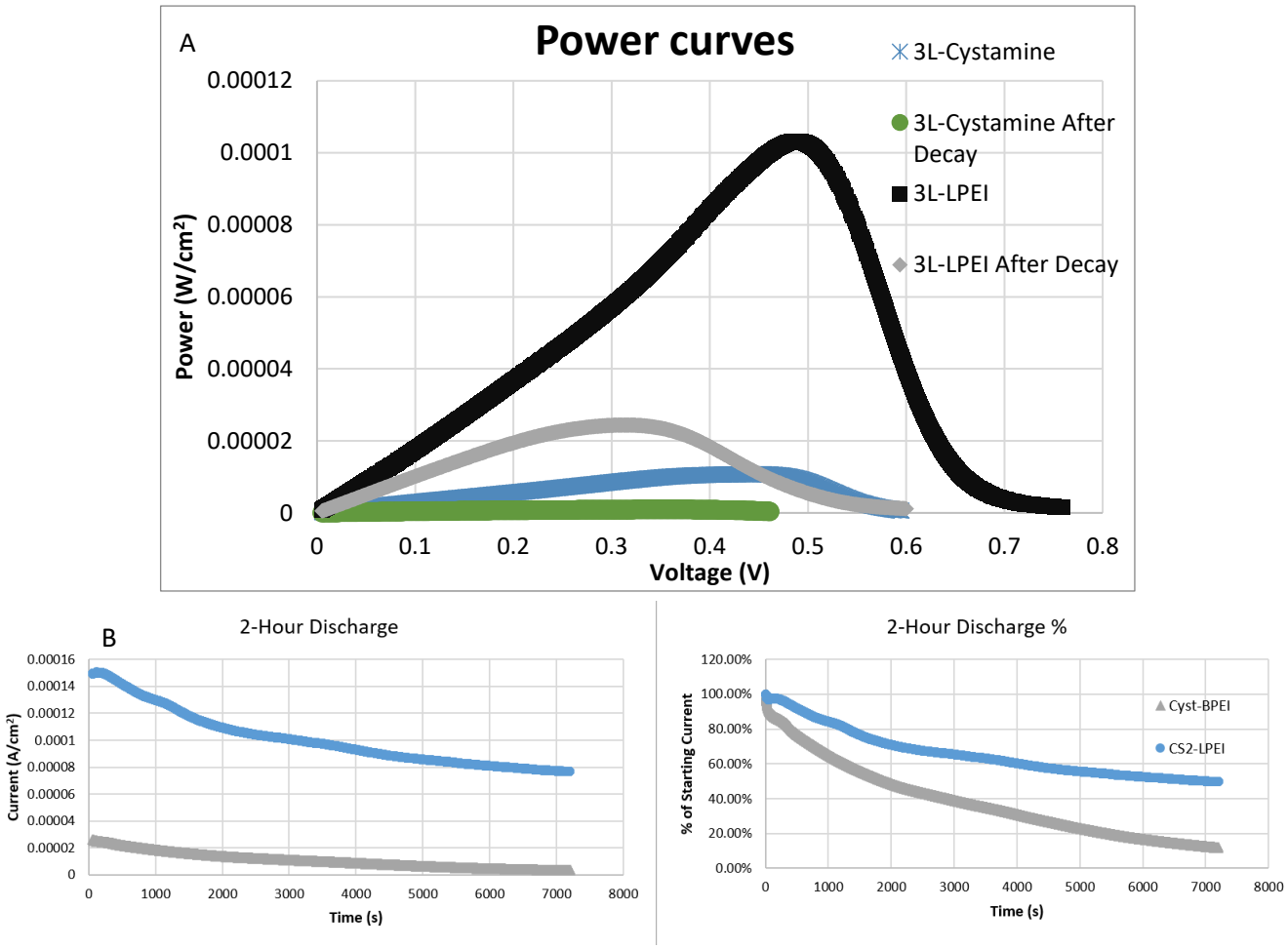

Figure 3.13 The 3-layer cystamine, and Fc-CS_2-LPEI electrodes compared to one another using the: (A) power curves before and (B) after a 2-hour discharge at 0.3 V. Both experiments were run in 150 mM glucose 50 mM phosphate buffer pH 7 using a 2 electrode setup with a functionalized gold electrode anode connected to the counter electrode and reference electrode leads and an air breathing Pt cloth electrode as the working electrode.

3.2.3 Multi-Layer Analysis

Because the CS_2-Fc-LPEI showed great improvement as the first layer in the 3-layer glucose bio-anode as shown above, more layers were placed on the electrode and compared to the analogous cysteamine first-layer systems. Just like in Table 3.1 the buildup of layers was

monitored by cyclic voltammetry of the multi-layered electrodes in phosphate buffer, and the sensing ability was determined by the addition of glucose and the construction of MM curves. The active ferrocene detected by cyclic voltammetry showed an alternating relationship between odd

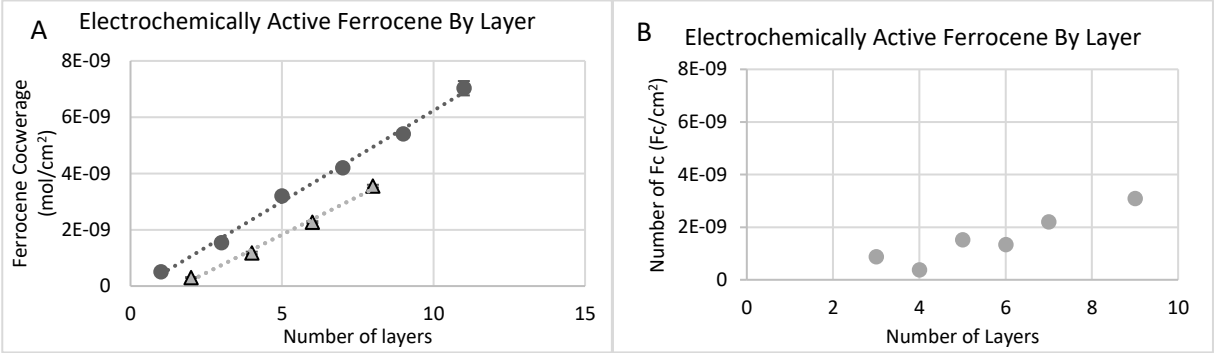

Figure 3.14 The ferrocene on the surface of the gold electrodes compared by the number of layers using: A) Fc-CS_2-LPEI as the first layer and B) Cystamine as the first layer. All electrodes were analyzed using the specified modified gold electrode with a Pt counter electrode, and an SCE reference in 50 mM phosphate buffer pH 7 using 50 mV/s scan rate.

and even numbers of layers. The odd layers (Fc-LPEI) show an increase in ferrocene on the surface of the electrode, giving an indication of buildup of material from layer to layer (Figure 3.14). This buildup of material is linear with the number of layers, indicating that roughly the same amount of ferrocene material (~.8 nmol) is deposited in each odd layer. The cysteamine system builds up roughly half of this amount per odd layer. The even layers show a regular marked dip in detectable ferrocenes compared to the previous odd layer. Since there is no ferrocene in the even layers (made up of p-GOx) it makes sense that they would have at the very most the same amount of ferrocene as the previous odd layer. However, since the GOx is known to bind to ferrocene[35], impeding it's oxidation, and there is a possibility that some of the material could wash off through the dipping and washing processes, it makes sense that there would be a decrease in the measured ferrocene in each of the even layers. The linear relationship of the even layers indicates that roughly the same

amount of enzyme is binding to the ferrocene layer each dip, or that our dipping and washing process is consistent at the very least.

The oxidation of the ferrocene appears to get easier as more layers are added, with the $E_{1/2}$ dropping from 0.461 at one layer to 0.357 V at 11 layers (Figure 3.15). As was discussed earlier, the high oxidation potential of the monolayer may be due to the inclusion of the carbon disulfide groups on the polymer. The first two layers are the only two to have $E_{1/2}$'s around 0.45 V with the rest of them dropping to around 0.4 V from 3-9 layers. These upper layers may be easier to oxidize since they don't have any carbon disulfide electron withdrawing groups. The oxidation potential is higher in the Fc-CS_2-LPEI than in the cystamine first-layer system, however the Fc-CS_2-LPEI

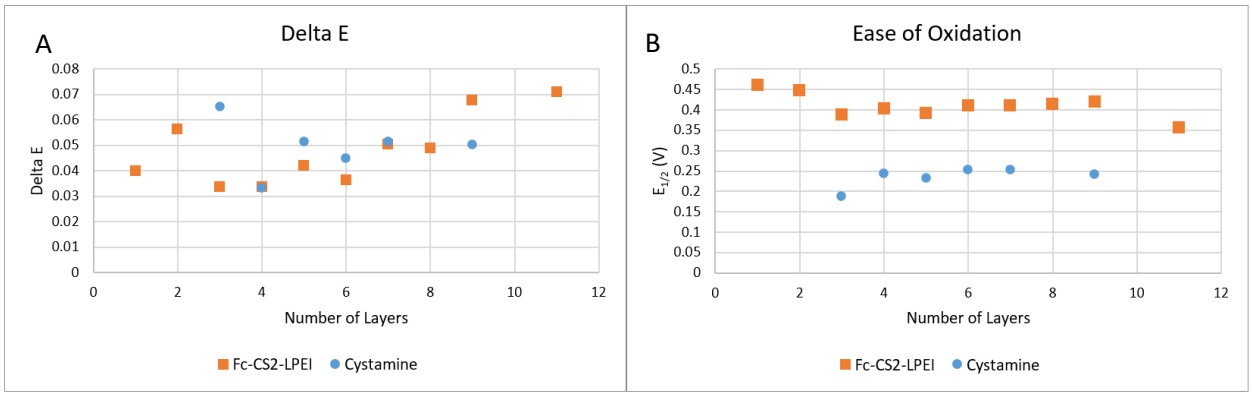

Figure 3.15 Peak voltage behavior using multi-layered cystamine and Fc-CS_2-LPEI electrodes showing A) Delta E and B) $E_{1/2}$ at different numbers of layers. All electrodes were analyzed using the specified modified gold electrode with a Pt counter electrode, and an SCE reference in 50mM phosphate buffer pH 7 using 50 mV/s scan rate.

system performs better in nearly every other metric, making this difference a minor footnote. The delta E of the ferrocene redox process also increases as the ferrocene gets further from the electrode surface from 1-11 layers (0.401 V to 0.710 V). This indicates that the redox process becomes more diffusion-controlled with distance from the gold electrode surface. There is no significant difference between the cystamine and Fc-CS_2-LPEI systems with respect to delta E.

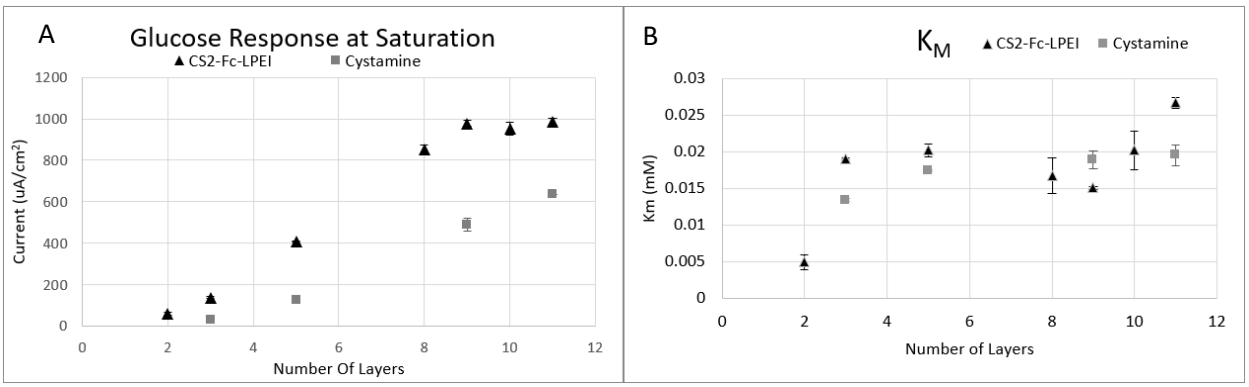

Figure 3.16 A) The current output of the Fc-CS_2-LPEI and the Cystamine electrodes, and B) the K_M of the enzymes in the electrodes shown by layer under saturating glucose concentrations at 0.35 V vs a SCE reference and a platinum wire counter electrode.

The amperometric response at higher than saturating glucose concentrations (~150 mM for these electrodes, measured at 176 mM glucose) builds with each layer, odd and even (Figure 3.16). This buildup of current is roughly linear with the number of layers indicating that after each dip, the last material put on the electrode, either Fc-LPEI or p-GOx, is the limiting factor in the catalytic process and limits the current output of the electrode (see Figure 3.16 A). The cysteamine system builds slowly to around 650 $\mu A/cm^2$ at 11 layers and continues to build to ~1.4 mA/cm^2 at 32 layers[13] (not shown). The Fc-CS_2-LPEI first-layer electrodes build up much more quickly to ~1 mA/cm^2 at 9 layers. Although the CVs show that the Fc-CS_2-LPEI electrodes continue to build up material on the surface up to 11 layers (see Figure 3.16A) the maximum current obtained from these electrodes with glucose present plateaus at ~1 mA/cm^2 from 9-11 layers. The K_m of the Fc-CS_2-LPEI system at 9 layers is 15.1 mM, which is just over half of the K_M for the cystamine system at 9 layers, increasing to 27 mM at 11 layers, indicating a loss of efficiency of the enzyme. This jump in K_M lines up with the plateau of the current output and could, in fact, be causing the plateau. Little increase in K_M is observed in the cystamine first-layered electrodes from 5-11L, while the current density continues to build all the way up to 32-layers. The high current output and low K_M of the 9-Layered Fc-CS_2-LPEI first layered electrodes leads to 3 times the sensitivity in the

physiological range compared to a cystamine electrode (Table 3.2). This is a significant improvement to produce highly sensitive electrodes that are only 13 μA/mM*cm^2 less sensitive than the 32-layer cystamine electrodes fabricated in less than 1/3 of the time (~45 min for the Fc-CS_2-LPEI compared to nearly 3 hours for the cystamine electrodes).

	9 Layer Electrodes		
	Fc-CS2-LPEI 1st Layer	Cystamine 1st Layer	
Fc Coverage	7.0	3.0	(nmol/cm^2)
Sensitivity at 5mM	47	16	(uA/(mM*cm^2))
Saturated Response	978	290	(uA/cm^2)
K_m	15.1	18.8	(mM)

Table 3.2 A comparison of the 9-Layered cystamine and Fc-CS_2-LPEI electrodes using key attributes.

3.3 Conclusions

In this chapter the novel material Fc-CS_2-LPEI was synthesized, characterized and used in GOx based glucose bio-electrodes in comparison to cystamine as the first layer of LBL constructed electrodes utilizing p-GOx. The material was made using a known Fc-LPEI polymer reacted with carbon disulfide in methanol that was characterized using gravimetric analysis as well as ^{1}H NMR and behavioral observations. It was found that the CS_2 adds quantitatively to the Fc-LPEI up to 25% and the material dissolves under highly basic conditions. The diffusion of ferrocene salts through this material adsorbed onto gold in 1L and 2L electrodes was compared to the cystamine and it was found that the material inhibits ferrocene's access to the gold electrode surface. However, the ferrocene's inclusion into the first layer increased the ferrocene surface coverage (from 0.71 to 1.76 nM/cm^2) and the current density of the bio-electrodes when used in saturating glucose conditions, from 30 to 174 μA/cm^2 in the 3-layered electrodes. The Fc-CS_2-LPEI 3-layer

electrodes outperformed the cystamine electrodes by ~10 times producing ~100 μW/cm^2 peak power compared to the cystamine electrode's 10 μA/cm^2 in a fuel cell. The Fc-CS_2-LPEI first layered electrodes also lasted longer, retaining ~50% of their current density after discharging for 2 hours at 0.3 V compared to cystamine electrode's ~15%.

In multilayers, the Fc-CS_2-LPEI electrodes also builtup ferrocene coverage in fewer layers than the cystamine electrodes producing 9.0 nmol/cm^2 Fc coverage to cystamine's 3.0 nmol/cm^2, and producing ~3 times the current density under saturating glucose concentrations (978 to 290 μA/cm^2). While the Fc-CS_2-LPEI electrodes outperform the cystamine electrodes up to 9-layers, the Fc-CS_2-LPEI electrodes current density plateaus at this point and the K_M of the GOx in these electrodes increases while the cystamine electrodes continue to build current density up to 32-layers. While the maximum current density of the Fc-CS_2-LPEI electrodes is only 978 μA/cm^2 compared to cystamine's ~1600 μA/cm^2, the advantages of electrode stability and construction time make the Fc-CS_2-LPEI electrodes an attractive alternative to the cystamine electrodes when considering the use of these materials in LBL glucose bio-anodes.

3.4 Materials and Methods

3.4.1 Chemicals and Solutions

Methanol, acetonitrile, sodium carbonate, cysteamine hydrochloride, sodium metaperiodate, and carbon disulfide were purchased from Sigma-Aldrich and used as recieved. (3-Bromopropyl)ferrocene was synthesized as previously reported in literature[10]. Ferrocenylmethyl-N,N,N-trimethylammonium tosylate was synthesized as noted in Chapter 2. Glucose oxidase (GOx) from Aspergillus niger (EC 1.1.3.4, type X-S, 117 units/mg solid, 75% protein), was bought

from Millipore sigma and oxidized using sodium metaperiodate to form periodate modified GOx (p-GOx) as previously reported in literature[10].

3.4.2 Synthesis of N-(3-Ferrocenylpropyl)-linear polyethylenimine.

N-(3-Ferrocenylpropyl)linear polyethylenimine (Fc-LPEI) was synthesized as reported in the literature[10] with varying 3-ferrocenylpropyl on nitrogen substitution percentages. These substitution percentages were confirmed by ^{1}H-NMR as done previously in literature. While the previously established literature used CD_3OD as the solvent, this work shows that the ferrocene substitution percentages can determined using $CDCl_3$ as the solvent and the method previously established in the literature[6] by setting the ferrocene integration (δ 3.9-4.35 ppm) to 9 and dividing 4 by the LPEI backbone integration (δ 2.2-2.9 ppm) minus 2 (2 is subtracted to compensate for the 3 carbon linker from the LPEI backbone to the ferrocene (see ^{1}H-NMR in Figures A3-5 in the Appendix). ^{1}H NMR ($CDCl_3$, δ): ca. 1.5-1.6 (br,-CH2-), 2.3-2.4 (br t, -CH2Fc), 2.5-3.0 (br, -CH2N-),4.1-4.35 (br, Fc ring H).

$$Fc\ substitution\ \% = 100 * \left(\frac{4}{Backbone\ Hs - 2}\right)$$

3.4.3 Synthesis of N-Dithiocarbamato-N-(3-ferrocenylpropyl)-linear polyethylenimine (Fc-CS_2-LPEI).

Fc-LPEI (~13 mol percent Fc-substituted, 50.0 mg, 67 g/mol) was dissolved in 5 mL of methanol and 9 mol percent carbon disulfide (4.5 mg in 237 uL methanol using a 0.25 M solution) was added to the rapidly stirred solution. The vessel was immediately capped and the reaction was allowed to proceed for 20 minutes. Over the course of this time the yellow solution became cloudy, and a precipitate formed. The solvent was removed on a rotary evaporator in a water bath at 60 C and the residue dried to a constant weight of 54.5 mg. This weight indicated a quantitative addition

of the carbon disulfide to the Fc-LPEI. Because the polymer is insoluble due to the electrostatic crosslinking between the ammonium cation groups and the dithiocarbamato anionic groups, NaOH was added to dissolve the polymer in water. This process was adjusted for different Fc-LPEI substitution percentages and desired CS_2 substitution percentages. This same process was followed for the functionalization of LPEI with CS_2.

3.4.4 Fabrication of Fc-LPEI and Cysteamine Electrodes.

Gold electrodes (2.0 mm diameter, CH instruments, Austin, TX) were polished on a microcloth pad with 0.05 mm alumina and thoroughly rinsed to prepare the surface for functionalization. The first modification layer (e.g. CS_2-LPEI or CS_2-Fc-LPEI or cystamine) was deposited by dipping the cleaned gold disk electrode into a solution of CS_2-LPEI 5 mg/mL in water at a pH of 13 for 5 min. The electrode was gently washed quickly by spraying DI water over the electrode for <1 second with a lab spray bottle between each layer. The second layer of p-GOx was deposited by dipping in a 20 μM solution of p-GOx at pH 6.8 for 5 min (this solution was prepared using a previously reported method[10]). To deposit the 3rd layer of Fc-LPEI the electrode was dipped in a solution of 25 mol% ferrocene substituted Fc-LPEI (5 mg/mL pH 5) for 5 min. More layers were built up by alternating between the p-GOx and Fc-LPEI solutions for the even and odd numbered layers, respectively, until the desired number of layers were reached. The same method was used for the cysteamine electrodes but instead of a CS_2-LPEI first layer, a cysteamine first layer was deposited by dipping a bare gold electrode in a 20 mM solution of cysteamine hydrochloride for 5 min.

3.4.5 Cyclic Voltammetry.

Cyclic voltammetry was performed using a bipotentiostat (CHI 832) and a three-electrode setup with a platinum counter electrode, a saturated calomel reference electrode and a 2 mm gold disc electrode (coated or not, as specified). All electrochemical experiments were done at room temperature (ca. 22 °C) using samples in 0.1 M phosphate buffer at a pH of 7.0 unless otherwise noted.

3.4.6 Michaelis-Menten Curves.

The Michaelis-Menten curves were produced using the same 3-electrode setup with a platinum wire counter electrode, a saturated calomel reference and a coated gold disc working electrode (see Electrode fabrication above). Each Michaelis-Menten curve was produced using 5 mL of 50 mM phosphate buffer (pH 7.0) at a stir rate of 120 rev/min. To generate the MM curves a voltage of 0.4 V was applied to the working electrode and the current outeput was graphed as aliquots of 1 M glucose were added to produce points from 4-150 mM glucose. The current was recorded after it had stabilized after each aliquot addition. Each electrode's curve was produced in triplicate using a freshly prepared electrode each time. Each concentration point was averaged together across the three curves and one average curve was produced from these experiments.

3.4.7 Power Curves.

Power curves were produced using a LBL-assembled glucose electrode as the anode, and a Pt cloth electrode hot pressed onto a Nafion® membrane as the cathode. The buffer and glucose concentrations are specified in the data where the power curve is presented. The glucose anode was connected to the potentiostat through the counter and reference electrode leads while the Pt

cloth electrode was connected to the working electrode lead. The open circuit voltage (OCV) was measured, and the working electrode was then scanned from the OCV to 0.05 V at 1 mV/s. Differently sized areas of the Pt air breathing electrode were exposed to air and no difference in performance was observed; therefore, it was assumed not to be the rate limiting electrode.

3.4.8 2-Hr Power Discharge.

Each specific LBL-assembled glucose anode was placed in 100 mM phosphate buffer at pH 7.0 with 100 mM glucose and paired with a Pt cloth ELAT electrode hot pressed to a Nafion® membrane as the cathode. A voltage of 0.3 V was applied for 2 hours, and the current was recorded for the duration of the time.

3.5 Chapter 3 Bibliography

1. Sun, R.; Wu, Q.; Guo, J.; Wang, T.; Wu, Y.; Qiu, B.; Luo, Z.; Yang, W.; Hu, Z.; Guo, J.; Shi, M.; Yang, C.; Huang, F.; Li, Y.; Min, J., A layer-by-layer architecture for printable organic solar cells overcoming the scaling lag of module efficiency. *Joule* **2020,** *4* (2), 407-419,https://doi.org/10.1016/j.joule.2019.12.004.

2. Campos, P. P.; Moraes, M. L.; Volpati, D.; Miranda, P. B.; Oliveira, O. N., Jr.; Ferreira, M., Amperometric detection of lactose using β-galactosidase immobilized in layer-by-layer films. *ACS Appl Mater Interfaces* **2014,** *6* (14), 11657-64,10.1021/am5024463.

3. Zhang, H.-X.; Abe, M.; Zhang, Y.; Li, G.; Ye, S.; Osawa, M.; Sasaki, Y., Proton-coupled electron transfer and lewis acid recognition at self-assembled monolayers of an oxo-bridged diruthenium(iii) complex functionalized with two disulfide anchors. *Langmuir : the ACS journal of surfaces and colloids* **2013,** *29* (32), 10110-10119,10.1021/la401736f.

4. Merchant, S. A.; Glatzhofer, D. T.; Schmidtke, D. W., Effects of electrolyte and ph on the behavior of cross-linked films of ferrocene-modified poly(ethylenimine). *Langmuir : the ACS journal of surfaces and colloids* **2007,** *23* (22), 11295-11302,10.1021/la701521s.

5. Merchant, S. A.; Tran, T. O.; Meredith, M. T.; Cline, T. C.; Glatzhofer, D. T.; Schmidtke, D. W., High-sensitivity amperometric biosensors based on ferrocene-modified linear

poly(ethylenimine). *Langmuir : the ACS journal of surfaces and colloids* **2009,** *25* (13), 7736-7742,10.1021/la9004938.

6. Merchant, S. A.; Meredith, M. T.; Tran, T. O.; Brunski, D. B.; Johnson, M. B.; Glatzhofer, D. T.; Schmidtke, D. W., Effect of mediator spacing on electrochemical and enzymatic response of ferrocene redox polymers. *The Journal of Physical Chemistry C* **2010,** *114* (26), 11627-11634,10.1021/jp911188r.

7. Tran, T. O.; Lammert, E. G.; Chen, J.; Merchant, S. A.; Brunski, D. B.; Keay, J. C.; Johnson, M. B.; Glatzhofer, D. T.; Schmidtke, D. W., Incorporation of single-walled carbon nanotubes into ferrocene-modified linear polyethylenimine redox polymer films. *Langmuir : the ACS journal of surfaces and colloids* **2011,** *27* (10), 6201-6210,10.1021/la104999f.

8. Minson, M.; Meredith, M. T.; Shrier, A.; Giroud, F.; Hickey, D.; Glatzhofer, D. T.; Minteer, S. D., High performance glucose/o2 biofuel cell: Effect of utilizing purified laccase with anthracene-modified multi-walled carbon nanotubes. *J. Electrochem. Soc.* **2012,** *159* (12), G166-G170,10.1149/2.062212jes.

9. Chen, J.; Tran, T. O.; Ray, M. T.; Brunski, D. B.; Keay, J. C.; Hickey, D.; Johnson, M. B.; Glatzhofer, D. T.; Schmidtke, D. W., Effect of surfactant type and redox polymer type on single-walled carbon nanotube modified electrodes. *Langmuir : the ACS journal of surfaces and colloids* **2013,** *29* (33), 10586-10595,10.1021/la401158y.

10. DeLuca, J. L.; Hickey, D. P.; Bamper, D. A.; Glatzhofer, D. T.; Johnson, M. B.; Schmidtke, D. W., Layer-by-layer assembly of ferrocene-modified linear polyethylenimine redox polymer films. *Chemphyschem : a European journal of chemical physics and physical chemistry* **2013,** *14* (10), 2149-2158,10.1002/cphc.201300146.

11. Hickey, D. P.; Giroud, F.; Schmidtke, D. W.; Glatzhofer, D. T.; Minteer, S. D., Enzyme cascade for catalyzing sucrose oxidation in a biofuel cell. *ACS Catal.* **2013,** *3* (12), 2729-2737,10.1021/cs4003832.

12. Meredith, M. T.; Hickey, D. P.; Redemann, J. P.; Schmidtke, D. W.; Glatzhofer, D. T., Effects of ferrocene methylation on ferrocene-modified linear poly(ethylenimine) bioanodes. *Electrochim. Acta* **2013,** *92*, 226-235,10.1016/j.electacta.2013.01.006.

13. Hickey, D. P.; Halmes, A. J.; Schmidtke, D. W.; Glatzhofer, D. T., Electrochemical characterization of glucose bioanodes based on tetramethylferrocene-modified linear poly(ethylenimine). *Electrochim. Acta* **2014,** *149*, 252-257,10.1016/j.electacta.2014.10.077.

14. Godman, N. P.; DeLuca, J. L.; McCollum, S. R.; Schmidtke, D. W.; Glatzhofer, D. T., Electrochemical characterization of layer-by-layer assembled ferrocene-modified linear poly(ethylenimine)/enzyme bioanodes for glucose sensor and biofuel cell applications. *Langmuir : the ACS journal of surfaces and colloids* **2016,** *32* (14), 3541-51,10.1021/acs.langmuir.5b04753.

15. Chen, J.; Munje, R.; Godman, N. P.; Prasad, S.; Glatzhofer, D. T.; Schmidtke, D. W., Improved performance of glucose bioanodes using composites of (7,6) single-walled carbon nanotubes and a ferrocene-lpei redox polymer. *Langmuir : the ACS journal of surfaces and colloids* **2017,** *33* (31), 7591-7599,10.1021/acs.langmuir.7b00718.

16. Hickey, D. P.; Godman, N. P.; Schmidtke, D. W.; Glatzhofer, D. T., Chloroferrocene-mediated laccase bioelectrocatalyst for the rapid reduction of o_2. *Electrochimica Acta* **2021,** *383*, 138130,https://doi.org/10.1016/j.electacta.2021.138130.

17. Ionescu, R. E., Use of cysteamine and glutaraldehyde chemicals for robust functionalization of substrates with protein biomarkers-an overview on the construction of biosensors with different transductions. *Biosensors (Basel)* **2022,** *12* (8),10.3390/bios12080581.

18. Almeida, I.; Cascalheira, A. C.; Viana, A. S., One step gold (bio)functionalisation based on cs2-amine reaction. *Electrochim. Acta* **2010,** *55* (28), 8686-8695,10.1016/j.electacta.2010.07.084.

19. Wang, L.; Wang, X.; Chen, X.; Liu, J.; Liu, S.; Zhao, C., Development of an electrochemical DNA biosensor with the DNA immobilization based on in situ generation of dithiocarbamate ligands. *Bioelectrochemistry* **2012,** *88*, 30-35,https://doi.org/10.1016/j.bioelechem.2012.04.003.

20. Zhao, Y.; Pérez-Segarra, W.; Shi, Q.; Wei, A., Dithiocarbamate assembly on gold. *Journal of the American Chemical Society* **2005,** *127* (20), 7328-7329,10.1021/ja050432f.

21. Gergaly, Š., Investigation of thermal decomposition of ethylenebisdithiocarbamate acid, its diammonia salt and β-amino-ethyl-dithiocarbamate. *Thermochimica Acta* **1985,** *93*, 137-140,http://dx.doi.org/10.1016/0040-6031(85)85035-8.

22. Humeres, E.; Sun Lee, B.; Debacher, N. A., Mechanisms of acid decomposition of dithiocarbamates. 5. Piperidyl dithiocarbamate and analogues. *The Journal of organic chemistry* **2008,** *73* (18), 7189-7196,10.1021/jo801015t.

23. Ziebarth, J. D.; Wang, Y., Understanding the protonation behavior of linear polyethylenimine in solutions through monte carlo simulations. *Biomacromolecules* **2010,** *11* (1), 29-38,10.1021/bm900842d.

24. (SDBS), S. D. f. O. C., Sdbs-1h nmrsdbs no. 527hpm-00-409, 300 mhz, . *National Institute of Advanced Industrial Science and Technology (AIST),*

25. Randles, J. E. B., A cathode ray polarograph. Part ii.—the current-voltage curves. *Transactions of the Faraday Society* **1948,** *44* (0), 327-338,10.1039/TF9484400327.

26. Ševčík, A., Oscillographic polarography with periodical triangular voltage. *Collection of Czechoslovak Chemical Communications* **1948,** *13*, 349-377

27. Laviron, E., General expression of the linear potential sweep voltammogram in the case of diffusionless electrochemical systems. *Journal of Electroanalytical Chemistry and Interfacial Electrochemistry* **1979,** *101* (1), 19-28,https://doi.org/10.1016/S0022-0728(79)80075-3.

28. Zare, H. R.; Golabi, S. M., Caffeic acid modified glassy carbon electrode for electrocatalytic oxidation of reduced nicotinamide adenine dinucleotide (nadh). *Journal of Solid State Electrochemistry* **2000,** *4* (2), 87-94,10.1007/s100080050006.

29. Garrido, J. A.; Rodríguez, R. M.; Bastida, R. M.; Brillas, E., Study by cyclic voltammetry of a reversible surface charge transfer reaction when the reactant diffuses to the electrode. *Journal of Electroanalytical Chemistry* **1992,** *324* (1), 19-32,https://doi.org/10.1016/0022-0728(92)80033-Z.

30. Elgrishi, N.; Rountree, K. J.; McCarthy, B. D.; Rountree, E. S.; Eisenhart, T. T.; Dempsey, J. L., A practical beginner's guide to cyclic voltammetry. *Journal of Chemical Education* **2018,** *95* (2), 197-206,10.1021/acs.jchemed.7b00361.

31. Battaglini, F.; Calvo, E. J.; Danilowicz, C.; Wolosiuk, A., Effect of ionic strength on the behavior of amperometric enzyme electrodes mediated by redox hydrogels. *Anal Chem* **1999,** *71* (5), 1062-7,10.1021/ac971253m.

32. Johnson, K. A.; Goody, R. S., The original michaelis constant: Translation of the 1913 michaelis–menten paper. *Biochemistry* **2011,** *50* (39), 8264-8269,10.1021/bi201284u.

33. Lineweaver, H.; Burk, D., The determination of enzyme dissociation constants. *Journal of the American Chemical Society* **1934,** *56* (3), 658-666,10.1021/ja01318a036.

34. Hickey, D. P.. 2014, Ferrocene-modified linear poly(ethylenimine) bioelectrode materials for use in glucose/O_2 biofuel cells. Doctoral Dissertation, *University of Oklahoma,* ShareOK.org

35. Bamper, D. 2019. A binding isotherm between ferrocene mediators and glucose oxidase for use in bioanode development and intitial studies of an electrocatalytic deoxydehydration reaction. Doctoral Dissertation, University of Oklahoma, ShareOK.org

Chapter 4

4.1 Introduction

As shown in Chapter 3, our group has used Fc-LPEI with GOx to construct LBL glucose bio-electrodes. However, branched polyethylenimine (BPEI) has been used more often than LPEI in LBL applications[1-2]. BPEI has been used extensively as a matrix material the production of sensors for a variety of analytes including cocaine[3], thrombin and lysozymes[4], glucose[5-6], cancer cells[7], and lactose[2, 8-9] sensors. Our group has used Fc-BPEI (N-ferrocenylmethyl-branched polyethylenamine) crosslinked with GOx to produce glucose biosensors[10]. Because the Fc-LPEI had worked better than Fc-BPEI in electrodes made by crosslinking, it was assumed that it would also work better in the LBL-constructed electrodes[11-12] and Fc-BPEI has not been used in fabricating LBL electrodes. In this chapter, the assumption that Fc-LPEI performed better than Fc-BPEI was tested by building LBL Fc-BPEI electrodes and comparing them to LBL Fc-LPEI electrodes.

BPEI can be thought of on the molecular level as a "fuzzy caterpillar" when it comes to their morphology. These oblong polymers are made of usually around 25% primary amines located on the outer surface with secondary and tertiary amines comprising the inner core. When these long bunches of polymer are crosslinked using epoxides (as was done by our group using ethyleneglycol diglicydyl ether (EGDGE)) the polymer will crosslink quickly and randomly due to the ready availability of primary amines on their surface, potentially leading to non-homogeneously crosslinked BPEI molecules and large non-crosslinked domains within the polymer matrix (see Scheme 4.1 below). This non-homogeneous structure makes parts of the matrix functionally useless since they are disconnected from any catalytic activity in the

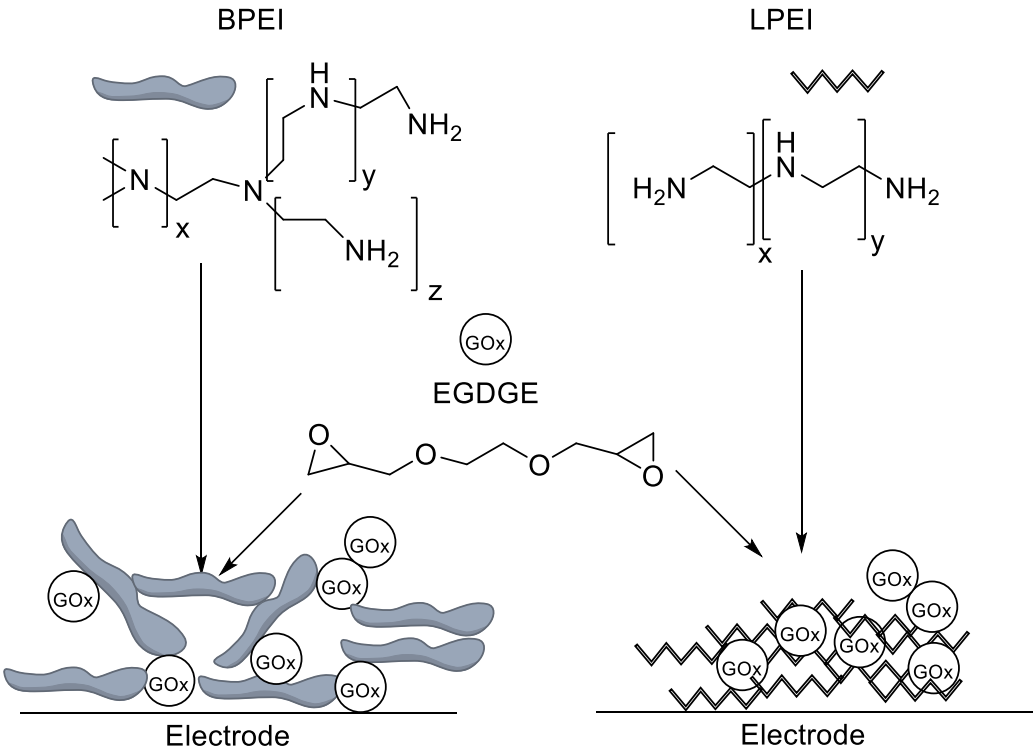

Scheme 4.1: The cross-linking of BPEI vs LPEI with EGDGE and GOx, showing the potential for voids and isolated GOx active sites.

crosslinked networks. Due to the granular structure of these "fuzzy caterpillar" BPEI networks, stress points form between each BPEI/GOx domain and the material breaks apart upon swelling. These drawbacks are largely sidestepped with the use of LPEI. Because the LPEI is comprised of mostly secondary amines, it will react with the EGDGE more slowly allowing time to bend and weave together to form a homogeneous closely packed network. Because it is a more homogeneous, lacking weak points and grain boundaries, the LPEI network can distribute the stress of swelling after soaking in water better than its BPEI counterpart. The LPEI is also less prone to have parts of the network not contributing to the catalytic process since it is more homogeneous. Since Fc-LPEI had worked so well, outperforming the Fc-BPEI electrodes in the crosslinked systems, the Fc-LPEI material was initially used to construct LBL electrodes. While

originally overlooked, the BPEI material could have some key advantages in LBL electrodes over its LPEI counterpart.

Because of the differences in the assembly process, the disadvantages BPEI faced in crosslinked systems are conveniently absent in the LBL construction. In a LBL assembly, Fc-CS_2-BPEI is deposited on the electrode and the periodate treated p-GOx can then be immobilized on the Fc-CS_2-BPEI. After this, the 3rd layer of Fc-BPEI can be immobilized on the p-GOx layer. Because the BPEI is immobilized electrostatically, and through reacting with aldehydes on the p-GOx, each BPEI molecule will be covalently bound to a p-GOx active site unlike the random crosslinking process using EGDGE (see Scheme 4.2 below). Our hypothesis was the use of the Fc-BPEI polymer could lead to higher sensitivity LBL assembled glucose sensors than its LPEI counterpart for two reasons. Firstly, because of the order of material deposition and the nature of the crosslinking mechanism, it is certain that each immobilized Fc-BPEI molecule will be in contact with a GOx and that the GOx will be arranged in "veins" between the BPEI molecules. Due to the size of the BPEI molecules there should be more space in these veins for diffusion of sugar into the electrode matrix than was available in the LPEI electrodes. Second, the ferrocene on the BPEI will also be mostly localized on the surfaces of the BPEI, and therefore the surfaces

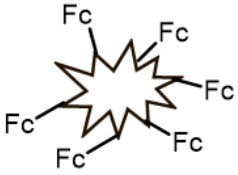

Ferrocene Lined BPEI

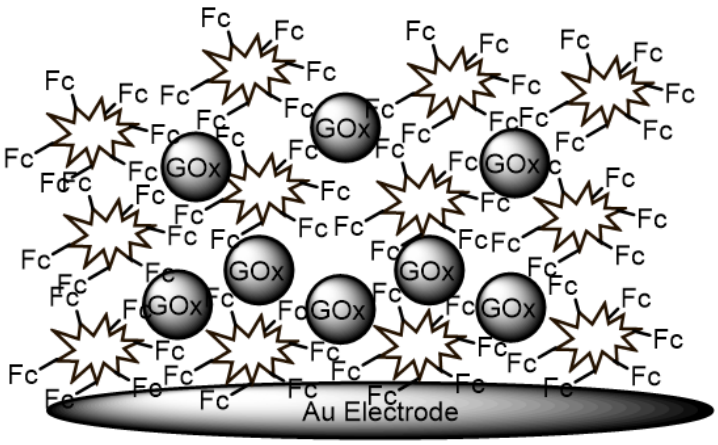

electrode surface.

of the domain interfaces, since they will most readily functionalize the more reactive and available primary amines on the BPEI. These ferrocene-lined veins of GOx are ideal for shuttling electrons from the GOx enzymes, funneling them to the gold electrode surface where they can be pulled through the circuit. This proposed morphology should be much more efficient when compared with the Fc-LPEI molecules that have more homogeneous and random Fc functionalization, and a relatively less porous material structure. In this chapter, Fc-CS_2-BPEI and Fc-BPEI were synthesized and used to construct LBL glucose bioanode sensors and compared to their Fc-LPEI counterparts. The BPEI electrodes were shown to have 50% more sensitivity and current than their LPEI counterparts. These BPEI electrodes were also used in glucose powered fuel cells and compared to cystamine first-layer electrodes, as well as the 3L CS_2-LPEI first-layer electrodes.

4.2 Results and Discussion

4.2.1 Fc-CS_2-BPEI synthesis and Characterization

BPEI was functionalized using (3-bromopropyl)ferrocene resulting in Fc-BPEI in the same way Fc-LPEI was synthesized. The high availability and reactivity of the primary nitrogens on the surface of the BPEI molecules leads to the formation of two different environments in the polymer, the BPEI core, with the largely unsubstituted secondary and tertiary amines, and the ferrocene functionalized surface amines. This Fc-BPEI was then treated with carbon disulfide in the same way as the CS_2-Fc-LPEI to produce CS_2-Fc-BPEI for use as the first layer of the multi-

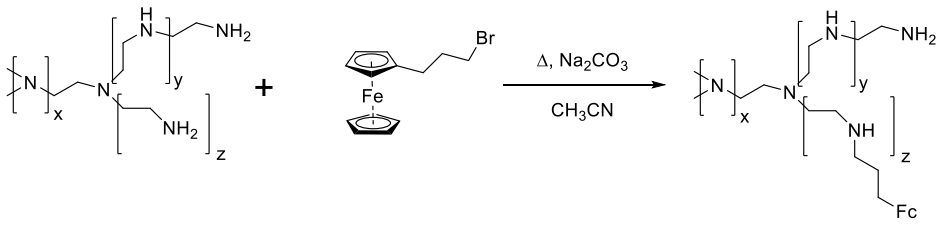

Scheme 4.3: Synthesis of Fc-BPEI from (3-bromopropyl)ferrocene and BPEI.

layered sensors built on gold electrodes. The percent substitution was determined gravimetrically and was found to be consistent with the complete reaction of all the carbon disulfide added. The ferrocene and CS_2 substitution percentages used in this chapter were the same 13 and 9 percent, respectively as used for the LPEI material in Chapter 3. This CS_2-Fc-BPEI polymer can be dissolved in water using sodium hydroxide just like the CS_2-Fc-LPEI material.

The CS_2-Fc-BPEI was characterized on a gold electrode surface by dipping the gold electrode in the basic CS_2-Fc-BPEI solution, quickly washing the electrode off with DI water and running cyclic voltammetry in a phosphate buffer solution to verify that it had chemisorbed onto the electrode surface. While the voltammogram of the CS_2-Fc-BPEI electrodes does not appear at a first look to be surface bound, the scan rate study shows the slope of the $\log(i_{pa})/\log(\nu)$ plot is 0.94 (close to 1), indicating that the peak results from more of a surface bound phenomenon than a diffusion controlled redox event (see Figure 4.1 below). The shoulder appearing at ~230 mV, 95 mV lower than the main peak at ~340 mV, indicates that the ferrocene in this shoulder is farther from any electron-withdrawing carbon disulfide units also attached to the polymer backbone. This loosely bound material with less carbon disulfide diffuses away from the surface after the first scan (the charged ferrocenium is more soluble in the buffer solution than the uncharged ferrocene), leaving the surface bound material with higher carbon disulfide content and a higher oxidation voltage at ~330 mV. Because all of these electrodes have this loosely bound material, all of the

points for analysis were taken from the second more stable scan of the electrodes after the loose material was not present.

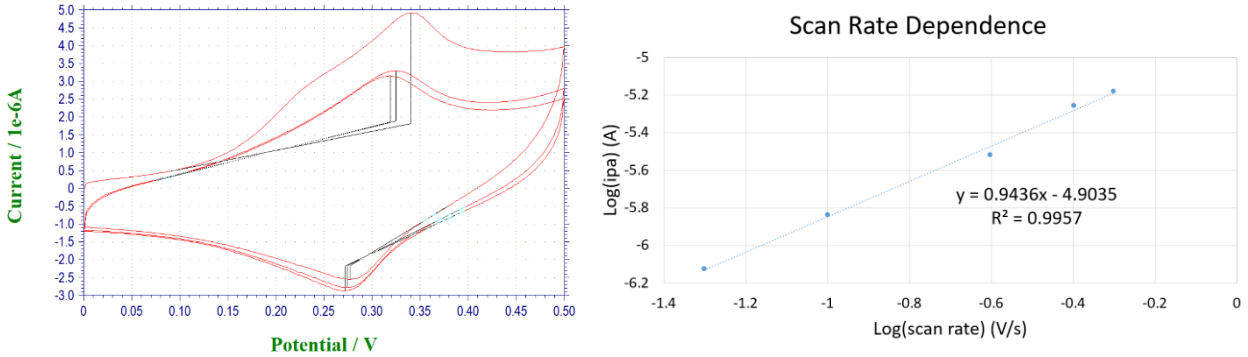

Figure 4.1: Characterization of Fc-CS_2-BPEI on a gold working electrode in 50mM Phosphate buffer with a platinum counter electrode and a SCE reference electrode shown with a cyclic voltammogram at A) 50 mV/s and B) showing the Log(i_{pa})/Log(scan rate) of the second anodic wave at several scan rates.

4.2.2 CS_2-Fc-BPEI Multi-Layered Biosensor Construction and Testing

Multi-layered sensors using CS_2-Fc-BPEI and Fc-BPEI and p-GOx were constructed in the same way as the LPEI electrodes discussed in Chapter 3, using the carbon disulfide substituted polymer as the first layer and then alternating p-GOx and Fc-BPEI to build up the successive layers. The electrochemical analyses of these electrodes are summarized in Figure 4.2. The amount of ferrocene detected on the surface scaled roughly linearly with the number of layers just as the LPEI material in Chapter 3. The peak Δ_E and $E_{1/2}$ increased with increasing layers, indicating that the material is getting thicker and the material at the edge takes longer to respond to the voltage of the electrode. The Δ_E of a pure surface wave should theoretically be 0, and for a reversible diffusion controlled process it should ideally be 57 mV. However, this is for electroactive species adsorbed onto electrode surfaces. Our material is different from this scenario with the ferrocene simply immobilized near the surface of the electrode. While it would be

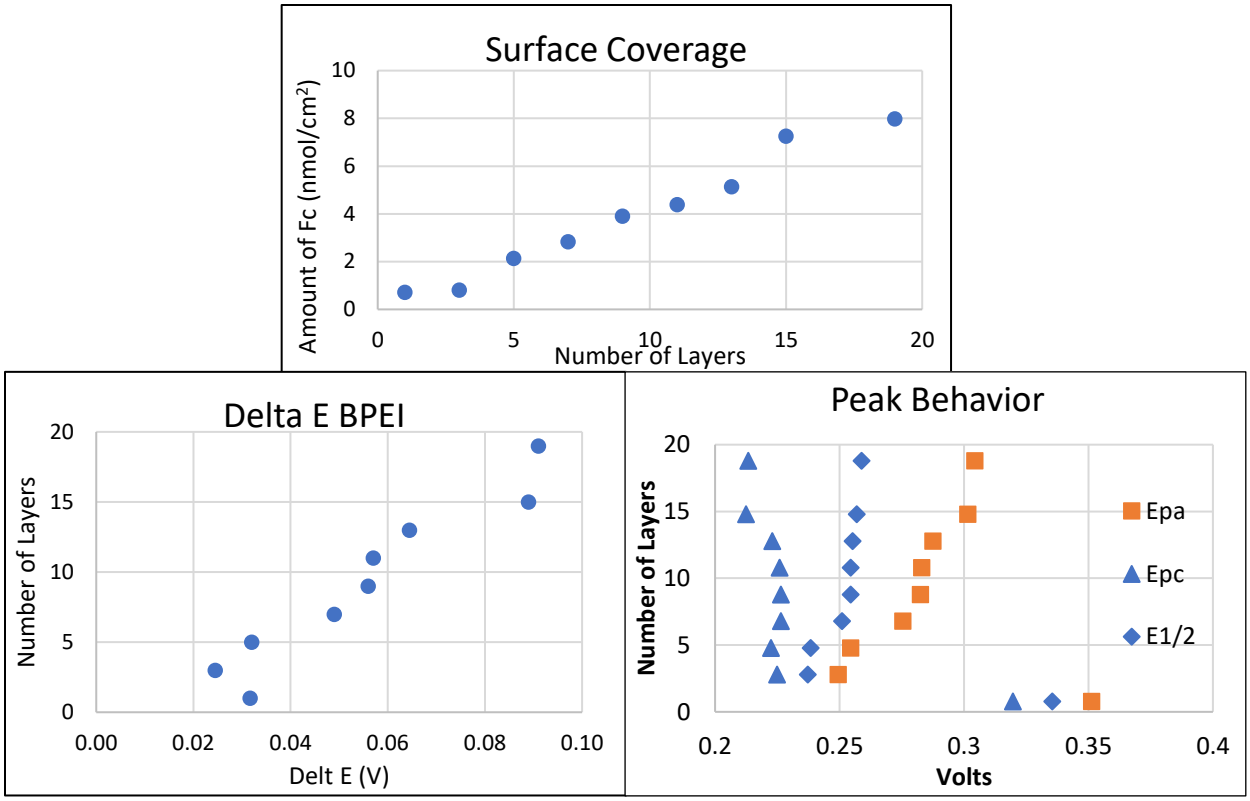

Figure 4.2: Characterization of multi-layered Fc-BPEI/GOx on a gold working electrode in 50 mM phosphate buffer with a platinum counter electrode and a SCE reference electrode comparing A) the amount of avtive ferrocene, B) ΔE and C) the $E_{1/2}$.

unreasonable to assume that the hydrogel on the surface would follow the surface wave characteristics, it would also be surprising if it were a purely diffusion controlled process due to it's attachment to the surface. In fact what is seen in the data is a Δ_E starting lower than 57 mV at ~30 mV in the monlayer and moving up to 90 mV in the 19L electrode, indicating a shift from surface bound phenomenon in the lower layers to diffusion controlled as more layers are deposited on the electrode. Interestingly the Log(i_{pa})/Log(v) relationship has a slope of 0.94, indicating surface bound behavior in the monolayer and a slope of 0.52 indicating diffusion controlled behavior on the 19-layer electrode. This makes sense since the monolayer is similar to an adsorbed species, and the 19-layer electrode has material far away to the electrode, similar to a dissolved species. The first layer also has a higher $E_{1/2}$ when compared to the higher layer number electrodes

since the first layer has the carbon disulfide unit pulling electron density away from the ferrocene, making it harder to oxidize. The upper layers are dominated by the Fc-BPEI material, making the $E_{1/2}$ lower in these layers. All of this behavior is consistent with what was seen in the analogous LPEI electrodes studied in Chapter 3. However, when the FcBPEI electrode systems were tested with glucose some favorable differences were noted.

These BPEI-based electrodes were tested with glucose to determine their sensitivity and maximum response to glucose. Although the LPEI-based electrodes from Chapter 3 matched the BPEI electrodes' responses to glucose at saturating glucose conditions up to 9 layers, the BPEI electrodes continued to grow all the way up to 19 layers where it eventually plateaued (see Figure 4.3 below). This growth up to 19 layers allowed the Fc-CS_2-BPEI first layer electrodes to outpace the Fc-CS_2-LPEI first layer electrodes and offer much greater sensitivity in the physiological range (46.8 $\mu A/cm^2$ mM for the 9L Fc-LPEI and 64.2 $\mu A/cm^2$ mM for the 19L Fc-BPEI) even though the K_M of the Fc-CS_2-BPEI electrodes is higher (25 mM compared to 15 mM in the Fc-CS_2-LPEI first layer). This increase in activity through 19-layers (compared to the LPEI material topping out at 9-layers) could be due to the wider channels of ferrocene and GOx in the BPEI material

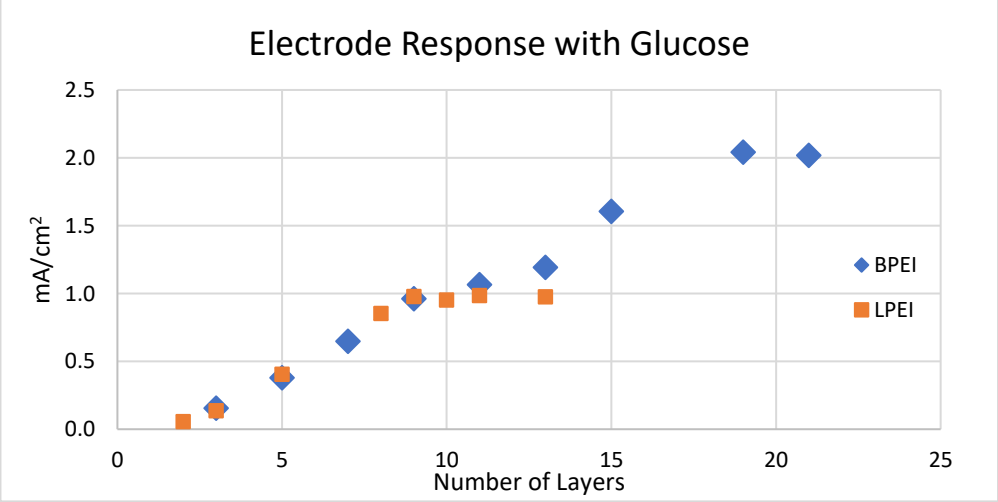

Figure 4.3: Comparison of the LBL-constructed Fc-CS_2-BPEI and Fc-CS_2-LPEI first layer electrodes response to 100 mM glucose with the build-up of layers using an SCE reference and a platinum counter electrode in 50 mM phosphate buffer.

allowing glucose to permeate the the electrode more efficiently and quickly. While this data clearly identifies the properties of these sensors we wanted to also characterize them as fuel cells as well.

Polarization and power curves were generated using the same platinum cloth working electrode and gold modified electrode as the combined counter and reference electrode set up in Chapter 3 for the Fc-LPEI LBL power curves. The polarization and power curves for the 19-layer Fc-BPEI electrode are compared to the Fc-LPEI 9-layered electrodes in Figure 4.4 and shows that the Fc-LPEI and Fc-BPEI generate as much current as they did in the applied voltage experiments from ~0.25 V to 0 V, ~1 mA/cm^2 for the Fc-LPEI and ~2 mA/cm^2 for the Fc-BPEI. This translates to current densities of 1.01 mA/cm^2 at 261 mV for the 9L Fc-LPEI, and 2.14 mA/cm^2 at 286 mV for the Fc-BPEI. The maximum power of 677 µW/cm^2 occurred at 354 mV for the Fc-BPEI with an open circuit voltage (OCV) of 639 mV and for the Fc-LPEI a maximum power of 271 µA/cm^2 at 0.290 V was observed with an OCV of 629 mV as shown in Table 4.1. This shows that the OCV generated by the two electrodes are essentially the same, however the maximum power and voltage at maximum power are higher in the Fc-BPEI. Since these differences aren't due to differences in material makeup, (both electrodes are made of PEI, ferrocene and p-GOx) they must be due to the

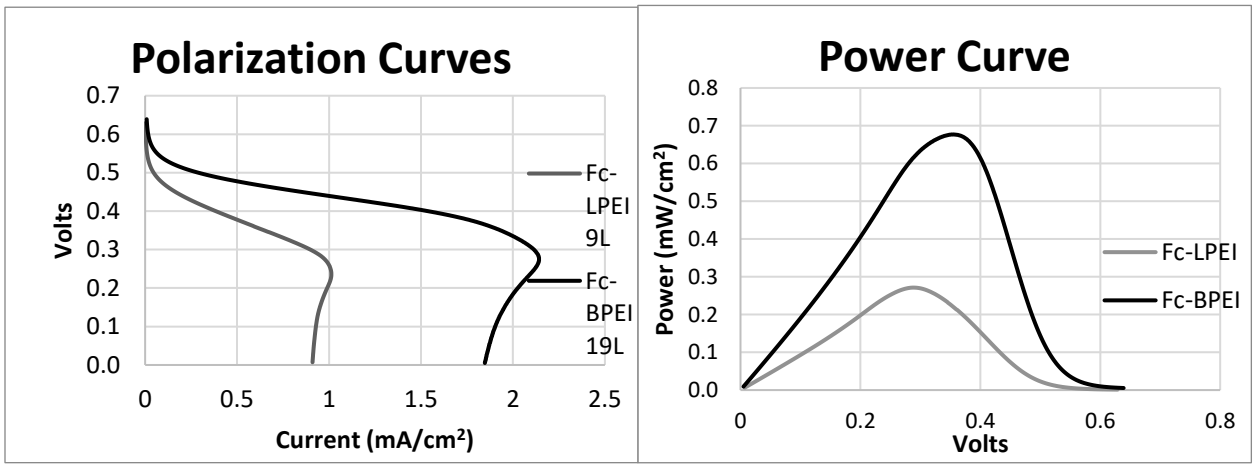

Figure 4.4: Comparison of the LBL-constructed 19L-BPEI and 9L-LPEI electrodes performance in A) polarization curves and B) power curves using a platinum working electrode and the constructed electrode as a combined counter and reference electrode in 100 mM glucose and a 50 mM phosphate buffer

morphology of the materials. It is likely that the diffusion of glucose through the channels of the Fc-BPEI to the p-GOx active sites allows the Fc-BPEI to function more efficiently and to build performance through more layers than the LPEI.

While the 19L-BPEI curve was substantially higher than the 9L-LPEI power curve a like-to-like comparison was used to study the stability of these two different materials. For this comparison power curves were measured for 3L electrodes of each material (see Figure 4.5). Each power curve measurement was run, after which the fuel cell was allowed to run at 0.3 V (near peak power) for 2 hours. After this time another polarization curve was collected to determine how stable the electrode material was. This was also done with a cystamine-first layer Fc-BPEI material to determine the effect using a polymer has on the stability of these bio-anodes. While the

Power Curves	OCV	Max Power (uA/cm^2)	Voltage at Max Power (V)
Fc-BPEI	0.639	677	0.354
Fc-LPEI	0.629	271	0.290

Table 4.1: A selection of relevant points taken from the comparison of the LBL-constructed 19L-BPEI and 9L-LPEI power curves in Figure 4.4.

cystamine produced much less current and lost ~80% of its current over the 2 hours, the degradation experienced by both the 3L-LPEI and BPEI electrodes was comparable to each other with the BPEI system losing ~60% of its current, and the LPEI system losing ~50% of its current over that time. When comparing the Fc-CS_2-BPEI and Fc-CS_2-LPEI pre- and post-degradation power curves, the Fc-CS_2-BPEI electrode lost 0.16 V of OCV, and only had 24% of its peak power

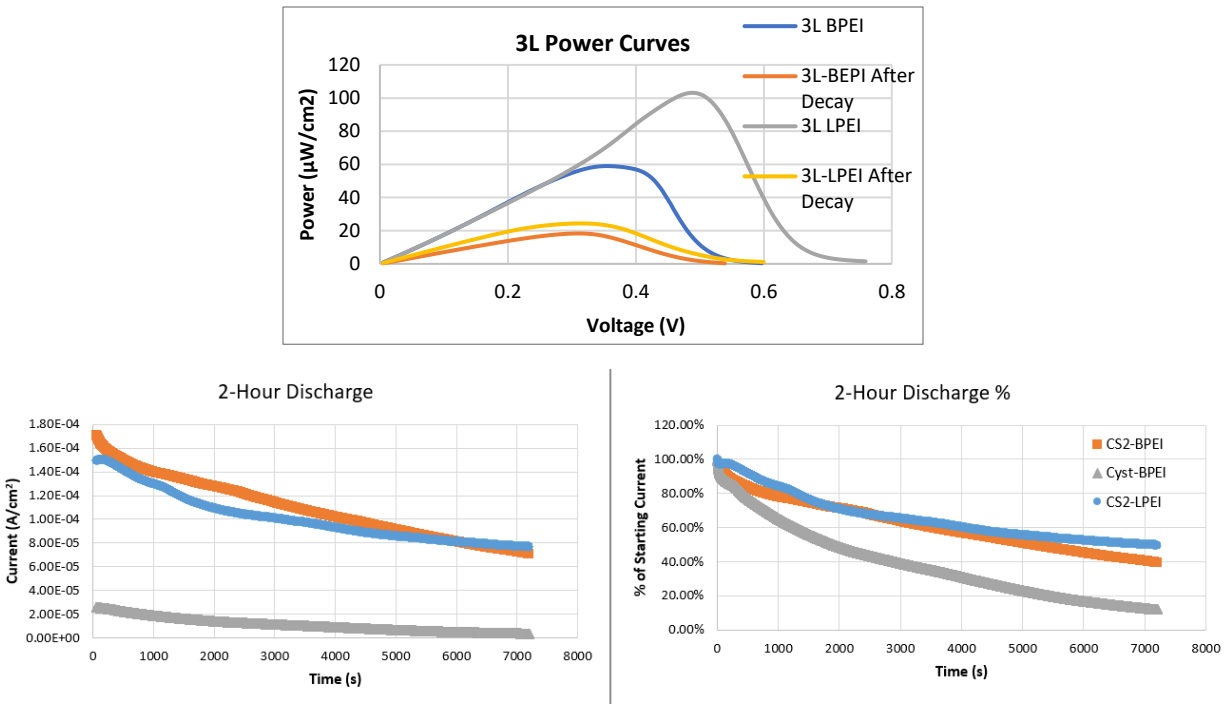

Figure 4.5: A) Power Curves of 3-layer Fc-CS_2-BPEI and Fc-CS_2-LPEI compared before and after 2 hr decay and their 2hr current graphs at 0.3V compared by B) their raw current values and C) the percentage of the starting current.

remaining, whereas the LPEI electrode lost only 0.06V in OCV and had 30% of its peak power remaining, only losing 0.05 V of its peak power voltage. The Fc-CS_2-BPEI electrode still somewhat outperformed the Fc-CS_2-LPEI despite losing a greater percentage of its performance parameters. The results are shown in Table 4.2.

These differences (Table 4.2) are again attributable to the morphological differences between the BPEI and LPEI. The LPEI will swell homogeneously since it is a more homogeneously crosslinked. The LPEI would then have fewer stress points compared to the BPEI. Since the BPEI has all 3 types (3', 2', and 1') of amines, there will be regions that swell more and some that swell less. This could cause channels of swelling in the regions comprised of primary amines, introducing stress points. The BPEI is more porous when compared to more homogeneous LPEI electrodes. This leads to established channels of GOx and ferrocene for efficient transport of electrons to the electrode surface from the GOx active site. This is because the ferrocene groups

will have mostly reacted with the primary amines, ensuring the ferrocene is in close proximity to the GOx catalytic sites which will be immobilized between BPEI molecules. This may also be why the BPEI system continues to build current density through 19L compared to the LPEI system's 9L.

First Layer (3L Electrodes)	Pmax ($\mu W/cm^2$)	V at Pmax (V)	OCV (V)	Pmax After 2 hr Run ($\mu W/cm2$)	V at Pmax After 2 hr Run (V)	OCV After 2 hr Run (V)	Starting Current (uA/cm^2)	Current after 2 hr Run (uA/cm^2)	Current % Remaining
CS2-Fc-LPEI	59.0	0.355	0.597	1.83	0.309	0.539	16.1	7.67	49.75%
CS2-Fc-BPEI	103	0.489	0.759	2.44	0.315	0.600	17.9	7.10	39.58%
Cyst-LPEI	10.8	0.440	0.595	0.0927	0.356	0.461	2.88	0.346	12.02%

Table 4.2: A selection of relevant points taken from the comparison of the LBL-constructed Fc-CS_2-BPEI and Fc-CS_2-LPEI and cystamine first-layered 3-layer power and 2 hr usage curves in Figure 4.5.

The differences outlined above show that the BPEI continues to grow through more layers and produce the highest current and power densities in a LBL electrode built by our group. Although they degraded more quickly than the LPEI electrodes in the 2 hr usage study, the BPEI electrodes maintained a better power curve with higher peak power and OCV than the LPEI electrodes after the 2-hour discharge. This establishes the BPEI LBL electrodes as a most promising and worthwhile system to improve upon and study further.

4.2.3 Literature Comparisons

Comparing literature examples of these glucose sensors can be a challenge since there are no standards when it comes to what is tested and how the electrodes are tested. It can get particularly difficult to compare stability/durability of these systems since they can be analyzed at different constant voltages, or are sometimes tested at constant currents, particularly when they are used as fuel cells. While each author has their reasons for testing under certain conditions, and

certain systems may call for particular conditions and tests that others may not, it can be difficult to find like-like comparisons for many examples. Most publications choose not to include any stability or durability analysis at all. There are however two properties that are nearly always reported when these glucose electrodes are used as sensors; the sensitivity of the electrodes to glucose and the range over which the response to glucose is linear. While sensitivity is important and intuitive and overall, a great point of comparison for these sensors, the range of linearity is not as straightforward as it may initially seem. For example, healthy blood-glucose levels in the human body are roughly from 5-10 mM, so it would seem that a linear response in this range is necessary for an adequate glucose sensor. However, if the response is not quite linear in this range but is predictable (as is the case with enzymatic kinetics) this may not matter quite as much (Figure 4.6). Different authors may use different statistical analyses and have different tolerances for their definition of linearity in their sensors.

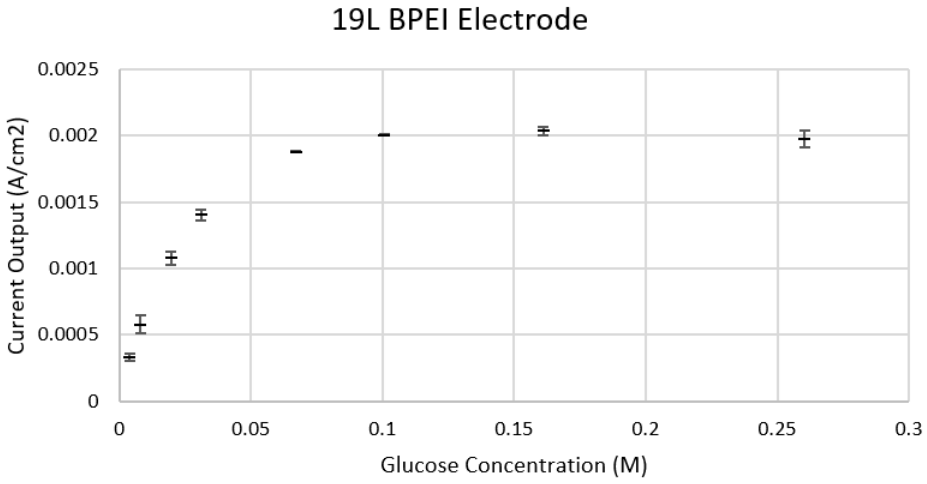

Figure 4.6 A Michaelis-Menten kinetics curve generated by the addition of 1M glucose aliquots to 50 mM phosphate buffer pH 7, with a 19-L Fc-BPEI working electrode, a SCE reference and a platinum counter electrode held at a constant potential of 0.40 V.

A selection of recent literature examples of glucose sensors is shown below and is compared to the sensors made in this work (Table 4.3). Because our enzymatic sensors are linear when plotted as 1/current vs 1/concentration, the response is predictable, and the linear range is irrelevant. The sensitivity was taken as the slope of the curve at 5 mM glucose concentration. While the sensitivity of our PEI electrodes is better than four of the chosen examples, they are 1/10-1/20th of the sensitivity of the other two. However, these high sensitivity examples have extremely low ranges of linearity, outside the normal physiological blood-glucose range. The sensitivities of these electrodes were also taken near what would be the bottom of a Michaelis-Menten curve where the slope is the steepest, inflating the sensitivity value. This work used the slope of the Michaelis-Menten curve from 5-20 mM glucose concentrations to obtain the sensitivity of the electrodes at physiological glucose concentrations. When compared to previous electrodes made by our group, the highest sensitivity LBL electrode was the 32-layer cystamine

Material	Sensitivity (μA/mM*cm^2)	Linear Range (mM)
Recent Literature		
Au-SiO_2NP/GOx[13]	9.69	0.2 - 7.0
Nf-GOx-fMWCNTs-Ppy[14]	54.2	0 - 4.1
Nf-CoS-MWCNTS/GOx[15]	15,000	.008 - 1.5
(CQDs)-AuNPs/GOx[16]	626.06	0.16 - 4.32
(Con A/GOx)$_5$[17]	68	.001-1
Our Group		
Cystamine/Fc-LPEI/GOx 32L[18]	60	N/A
Fc-LPEI/GOx (X-linked)[10]	43	N/A
Fc-LPEI/SWNT/GOx (X-linked)[19]	93	N/A
This Work		
LBL-CS_2/LPEI/GOx 9L	47	N/A
LBL-CS_2/BPEI/GOx 19L	64	N/A

Table 4.3: A selection of recent literature references chosen to compare to the materials prepared in this work. The sensitivities of our group's electrodes used the slope of the Michaelis-Menten curve from 5-20 mM as the sensitivity.

first-layer Fc-LPEI electrode at 60 μA/cm^{2}mM. This is a mark beaten by the CS_2-Fc-BPEI first-layer 19-layer Fc-BPEI electrode at 64 μA/cm^{2}mM. These FcBPEI 19L electrodes produced 2 mA/cm^2 outperforming the 32L cystamine first-layered Fc-LPEI electrodes that produced 1.4 mA/cm^2.

4.3 Conclusion

This chapter explored the use of the CS_2-Fc-BPEI and Fc-BPEI materials in the construction of bioanodes in conjunction with p-GOx, similar to those described in Chapter 4 using the Fc-LPEI materials. The BPEI material continues to build functionally active material through 19 layers where it tops out with double the current density of the LPEI version at 2 mA/cm^2 under saturating glucose condititons. The BPEI electrodes also had 36% more sensitivity to glucose (64 mA/cm^2 mM compared to 47 mA/cm^2 mM) at physiological glucose concentrations (4-15 mM). The BPEI systems also produced more power at higher voltages than the LPEI electrodes in a galvanic discharge under saturating glucose concentration conditions. Although these electrodes are not ideally suited for long term power generation, this does show that they work more efficiently, likely due to the morphology of the BPEI electrodes. These electrodes performance are at least on par with and better than much of what has been reported in the literature within physiological blood-glucose concentrations.

4.4 Materials and Methods

4.4.1 Chemicals and Solutions.

Glucose oxidase (GOX) from Aspergillus niger (C 1.1.3.4, type X-S, 117 units/mg solid, 75% protein), methanol, acetonitrile, sodium carbonate, cysteamine hydrochloride, carbon disulfide, and 25k MW BPEI was purchased from Sigma-Aldrich and used as recieved.

4.4.2 Synthesis of N-(3-Ferrocenylpropyl)-branched polyethylenimine

N-(3-Ferrocenylpropyl)-branched polyethylenimine [Fc-BPEI] was synthesized in the same way as the Fc-LPEI in Chapter 3. A solution of 100 mg (2.32 mmol repeat units) of 25k MW BPEI in 10 mL of a 6:4 mixture of acetonitrile and methanol in a flask fitted with a reflux condenser. (3-Bromopropyl)ferrocene (177 mg, 0.575 mmol or 25 mol% relative to the BPEI) was added along with 1 equivalent of K_2CO_3, and the mixture was heated to reflux solvent overnight. The solvent was removed under reduced pressure, and diethylether was used to wash the polymer of any ferrocenyl impurities (3 washes of 15mL). The polymer was dissolved in benzene and the mixture was filtered through Celite to remove any residual salt impurities. The solvent was removed under reduced pressure to yield ca. 120 mg Fc-C3-BPEI. The yield was 78%, and the Fc substitution percentage was determined by ^{1}H-NMR as was done in Chapter 3 with the Fc-LPEI.

4.4.3 Synthesis of N-Dithiocarbamato-N-ferrocenylpropyl-branchedpolyethylenimine (Fc-CS_2-BPEI

N-Dithiocarbamato-N-(3-ferrocenylproplyl)-branched polyethylenimine was synthesized by dissolving N-(3-ferrocenylproplyl)-branched polyethylenimine (50 mg, 614 nmol repeat units) in 5 mL of methanol and 9 mol percent carbon disulfide (4.2 mg, 55 nmol) was added with rapid

stirring. The vessel was immediately capped and the reaction was carried out for 20 minutes. Over the course of this time the yellow solution became cloudy, and a precipitate formed. The solvent was removed on a rotary evaporator in a water bath at 60° C and dried to a constant weight of 54.3 mg. This weight indicates a quantitative addition of the carbon disulfide to the BPEI. The polymer is insoluble due to the electrostatic crosslinks between the ammonium cations groups and the carbon disulfide anionic groups. Therefore, NaOH was needed to dissolve the polymer in water.

4.4.4 Electrochemical Experiments

All electrode construction and electrochemical characterizations were carried out as described in Chapter 3, substituting CS_2-Fc-BPEI for CS_2-Fc-LPEI and Fc-BPEI for Fc-LPEI.

4.5 Bibliography

1. Takahashi, S.; Anzai, J.-i., Recent progress in ferrocene-modified thin films and nanoparticles for biosensors. *Materials* **2013,** *6* (12), 5742-5762

2. Schulz, C.; Ludwig, R.; Gorton, L., Polyethyleneimine as a promoter layer for the immobilization of cellobiose dehydrogenase from myriococcum thermophilum on graphite electrodes. *Anal Chem* **2014,** *86* (9), 4256-63,10.1021/ac403957t.

3. Du, Y.; Chen, C.; Yin, J.; Li, B.; Zhou, M.; Dong, S.; Wang, E., Solid-state probe based electrochemical aptasensor for cocaine: A potentially convenient, sensitive, repeatable, and integrated sensing platform for drugs. *Analytical Chemistry* **2010,** *82* (4), 1556-1563,10.1021/ac902566u.

4. Du, Y.; Chen, C.; Li, B.; Zhou, M.; Wang, E.; Dong, S., Layer-by-layer electrochemical biosensor with aptamer-appended active polyelectrolyte multilayer for sensitive protein determination. *Biosensors & bioelectronics* **2010,** *25* (8), 1902-7,10.1016/j.bios.2010.01.003.

5. Song, S.; Hu, N., Ph-controllable bioelectrocatalysis based on "on-off" switching redox property of electroactive probes for spin-assembled layer-by-layer films containing branched poly(ethyleneimine). *The journal of physical chemistry. B* **2010,** *114* (10), 3648-54,10.1021/jp910048e.

6. Christwardana, M.; Kim, K. J.; Kwon, Y., Fabrication of mediatorless/membraneless glucose/oxygen based biofuel cell using biocatalysts including glucose oxidase and laccase enzymes. *Scientific Reports* **2016,** *6* (1), 30128,10.1038/srep30128.

7. Liu, J.; Qin, Y.; Li, D.; Wang, T.; Liu, Y.; Wang, J.; Wang, E., Highly sensitive and selective detection of cancer cell with a label-free electrochemical cytosensor. *Biosensors & bioelectronics* **2013,** *41*, 436-41,10.1016/j.bios.2012.09.002.

8. Wong, D. E.; Talbert, J. N.; Goddard, J. M., Layer by layer assembly of a biocatalytic packaging film: Lactase covalently bound to low-density polyethylene. *Journal of Food Science* **2013,** *78* (6), E853-E860,https://doi.org/10.1111/1750-3841.12134.

9. Campos, P. P.; Moraes, M. L.; Volpati, D.; Miranda, P. B.; Oliveira, O. N., Jr.; Ferreira, M., Amperometric detection of lactose using β-galactosidase immobilized in layer-by-layer films. *ACS Appl Mater Interfaces* **2014,** *6* (14), 11657-64,10.1021/am5024463.

10. Merchant, S. A.; Glatzhofer, D. T.; Schmidtke, D. W., Effects of electrolyte and ph on the behavior of cross-linked films of ferrocene-modified poly(ethylenimine). *Langmuir : the ACS journal of surfaces and colloids* **2007,** *23* (22), 11295-11302,10.1021/la701521s.

11. DeLuca, J. L.; Hickey, D. P.; Bamper, D. A.; Glatzhofer, D. T.; Johnson, M. B.; Schmidtke, D. W., Layer-by-layer assembly of ferrocene-modified linear polyethylenimine redox polymer films. *Chemphyschem : a European journal of chemical physics and physical chemistry* **2013,** *14* (10), 2149-2158,10.1002/cphc.201300146.

12. Godman, N. P.; DeLuca, J. L.; McCollum, S. R.; Schmidtke, D. W.; Glatzhofer, D. T., Electrochemical characterization of layer-by-layer assembled ferrocene-modified linear poly(ethylenimine)/enzyme bioanodes for glucose sensor and biofuel cell applications. *Langmuir : the ACS journal of surfaces and colloids* **2016,** *32* (14), 3541-3551,10.1021/acs.langmuir.5b04753.

13. Kumar-Krishnan, S.; Guadalupe-Ferreira García, M.; Prokhorov, E.; Estevez-González, M.; Pérez, R.; Esparza, R.; Meyyappan, M., Synthesis of gold nanoparticles supported on functionalized nanosilica using deep eutectic solvent for an electrochemical enzymatic glucose biosensor. *Journal of Materials Chemistry B* **2017,** *5* (34), 7072-7081,10.1039/C7TB01346A.

14. Shrestha, B.; Ahmad, R.; Shrestha, S.; Park, C.; Kim, C., Globular shaped polypyrrole doped well-dispersed functionalized multiwall carbon nanotubes/nafion composite for enzymatic glucose biosensor application. *Scientific Reports* **2017,** *7*,10.1038/s41598-017-16541-9.

15. Le, C.; Liu, Y.; Tang, X.; Xu, L.; Min, L.; Xue, Y.; Hu, X.; Yang, Z., Multiwalled carbon nanotubes coated with cobalt(ii) sulfide nanoparticles for electrochemical sensing of glucose via direct electron transfer to glucose oxidase. *Microchimica Acta* **2020,** *187*,10.1007/s00604-019-4047-8.

16. Buk, V.; Pemble, M. E., A highly sensitive glucose biosensor based on a micro disk array electrode design modified with carbon quantum dots and gold nanoparticles. *Electrochimica Acta* **2019,** *298*, 97-105,https://doi.org/10.1016/j.electacta.2018.12.068.

17. Sugiyama, K.; Sato, F.; Komatsu, S.; Kamijo, T.; Yoshida, K.; Kawabe, Y.; Nishikawa, H.; Fujimura, T.; Takahashi, Y.; Sato, K., Highly sensitive glucose electrochemical sensor using sugar-lectin interactions. *Electrochemical Science Advances n/a* (n/a), e2300015,https://doi.org/10.1002/elsa.202300015.

18. Godman, N. P.; DeLuca, J. L.; McCollum, S. R.; Schmidtke, D. W.; Glatzhofer, D. T., Electrochemical characterization of layer-by-layer assembled ferrocene-modified linear poly(ethylenimine)/enzyme bioanodes for glucose sensor and biofuel cell applications. *Langmuir : the ACS journal of surfaces and colloids* **2016,** *32* (14), 3541-51,10.1021/acs.langmuir.5b04753.

19. Chen, J.; Munje, R.; Godman, N. P.; Prasad, S.; Glatzhofer, D. T.; Schmidtke, D. W., Improved performance of glucose bioanodes using composites of (7,6) single-walled carbon nanotubes and a ferrocene-lpei redox polymer. *Langmuir : the ACS journal of surfaces and colloids* **2017,** *33* (31), 7591-7599,10.1021/acs.langmuir.7b00718.

Chapter 5

5.1 Introduction

Non-enzymatic glucose bio-cells have many advantages over enzyme containing materials. For example, the GOx containing materials used in Chapters 3 and 4 are great for making sensitive sensors. However, the use of the enzyme in these sensors leaves them prone to degradation over time[1-2]. Enzymes can also become saturated with substrate at relatively low concentrations, which is fine at physiological concentrations, but this limits the power generation of bio-anodes made using enzymes. While non-enzymatic electrodes are not inherently more stable than enzymatic sensors, they can sometimes be engineered to be stable over longer periods of time. Non-enzymatic materials generally lack the specificity to a substrate that the folded protein of an enzyme provides, but they also have the potential to saturate at much higher concentrations and produce much larger current densities than enzymatic electrodes[3]. This lack of substrate specificity can be used as an advantage as well, generating power from things other than the specific substrates the enzymatic materials are designed to metabolize[4]. Some of these non-enzymatic glucose-consuming electrodes have even been shown to break down glucose all the way to carbon dioxide and water, extracting 24 electrons in the process and theoretically producing 4430 Wh/kg[5]. These differences make them ideal for the production of power as opposed to sensing accurately one single substrate concentration[6], as was done with our enzymatic electrodes in the previous chapters.

In the interest of making a non-enzymatic biofuel cell our group has utilized electrodes made by electrodeposition of a polyviologen capable of oxidizing glucose[7]. This reduced polyviologen material can conduct electrons to the electrode surface and through a circuit to

produce power[8-9]. Using a platinum electrode as the cathode, this polyviologen material can be used as the anode to produce a compartmentless biofuel cell utilizing glucose[9]. Our group has already made and tested the polyviologen material using 1,5-bis(4-cyanopyridinium-1-yl)pentane (BIS) dibromide and 1,3,5-tris(methyl)-2,4,6-tris-(4-cyanopyridinium-1-methyl)benzene (TRIS) tribromide salt precursors (Scheme 5.1), along with CB7 encapsulation of the viologen units to improve its stability in basic environments. CB7 is a macrocyclic molecule that has a hydrophobic pocket with an affinity for binding viologens[10-11]. CB7 is known to protect viologens from oxidation[12-13] and keeps it from forming dimers when reduced to the radical cation state[14]. The TRIS salt was incorporated to introduce branch points and voids to produce a more open structure for the diffusion of glucose through the material[15].

Only one method of electropolymerization and one electrode type has previously been tested. Electropolymerization can be somewhat of an iterative and tedious process to optimize. It is our hypothesis that the environments provided by different applied electrical stimuli can induce different morphologies and polymerization behaviors. For example, in the electrocoupling of the two cyanopyridinium salts shown in Scheme 5.1, the final elimination step to reform the dication

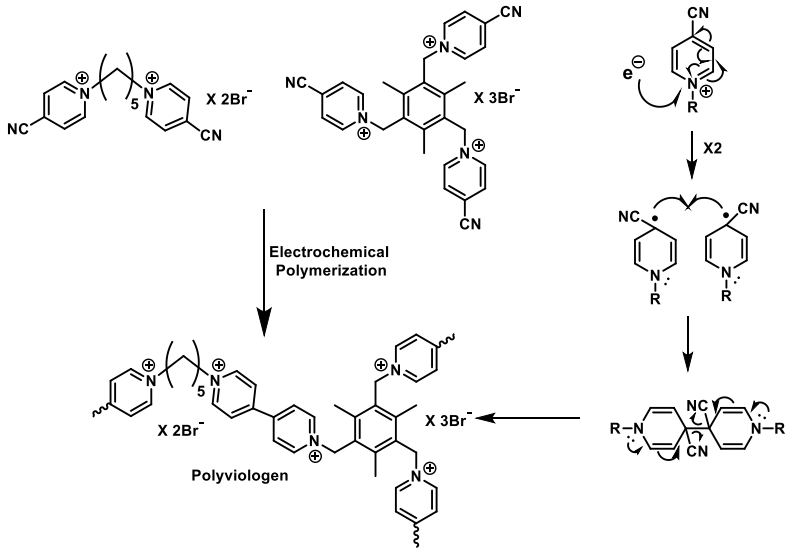

Scheme 5.1: Showing the di- and tri-pyridinium salts and how they reductively electropolymerize to form the viologen polymer.

viologen salt may be hindered if the potential is only held at a reducing voltage and not allow the material to return to more positive potentials where conductive radical cation and the dication forms are favored over the neutral viologen species that would be present in a constant voltage polymerization. If the film were formed by cyclic voltammetry, in which the material is cycled between, there may be "layers" of material deposited on the surface each time the voltage is switched from low to high voltage. The reduction potential of the di- and tri-pyridinium salts are offset by ~0.05V making the cyclic voltammetry electrodes primarily made up of the BIS salt since it reduces at a lower voltage than the TRIS salt. This also could form micro-layer regions solely made from the BIS salts, followed by regions made up of both monomers. If an alternating high and low voltage pulse method is used, then this micro-layering can be avoided to form a more uniform material since both monomers will begin to react at the same time when the voltage is applied. It is also our hypothesis that using a high surface area material such as carbon felt could make compact but high-current producing electrodes.

In previous work our group[7] explored using different concentrations of monomer in the electropolymerizing solution that caused different polymer morphologies on cycling, leading to varying performance of the polymerized material. In this work the electrical stimulus itself is varied to determine the best way to polymerize material for the production of non-enzymatic, viologen-based fuel cells. We also hypothesize that these electrodes could utilize different carbohydrate fuels, increasing their power output from raw sources containing multiple sugars (eg. fruit juice). The different polymerization methods used were cyclic voltammetry, constant voltage and pulsed voltage techniques. The use of high surface area carbon fiber electrodes was also explored, along with stability testing of [CB7]-modified polyviologens to protect the viologen

from oxidation in the high pH environment used for these fuel cells. Sucrose was shown to be an effective alternative fuel for this polyviologen electrode system.

5.2 Results and discussion

In order to study the polymerization method, a known method was used and sequentially modified to study the different polymerization techniques. The only method of polymerization used in our group for making the viologen-modified electrodes has been cyclic voltammetry. Previous work has determined that a 2:3 ratio of TRIS to BIS at concentrations of 1 and 1.5 mM, respectively, is best for the polymerization using this method[7]. Below in Figure 5.1 are shown the polymerization of the viologen material on a glassy carbon electrode using cyclic voltammetry running 1-10, 11-20, 21-30 and 31-40 scans (5.1 A-D) respectively. The initial scans show some

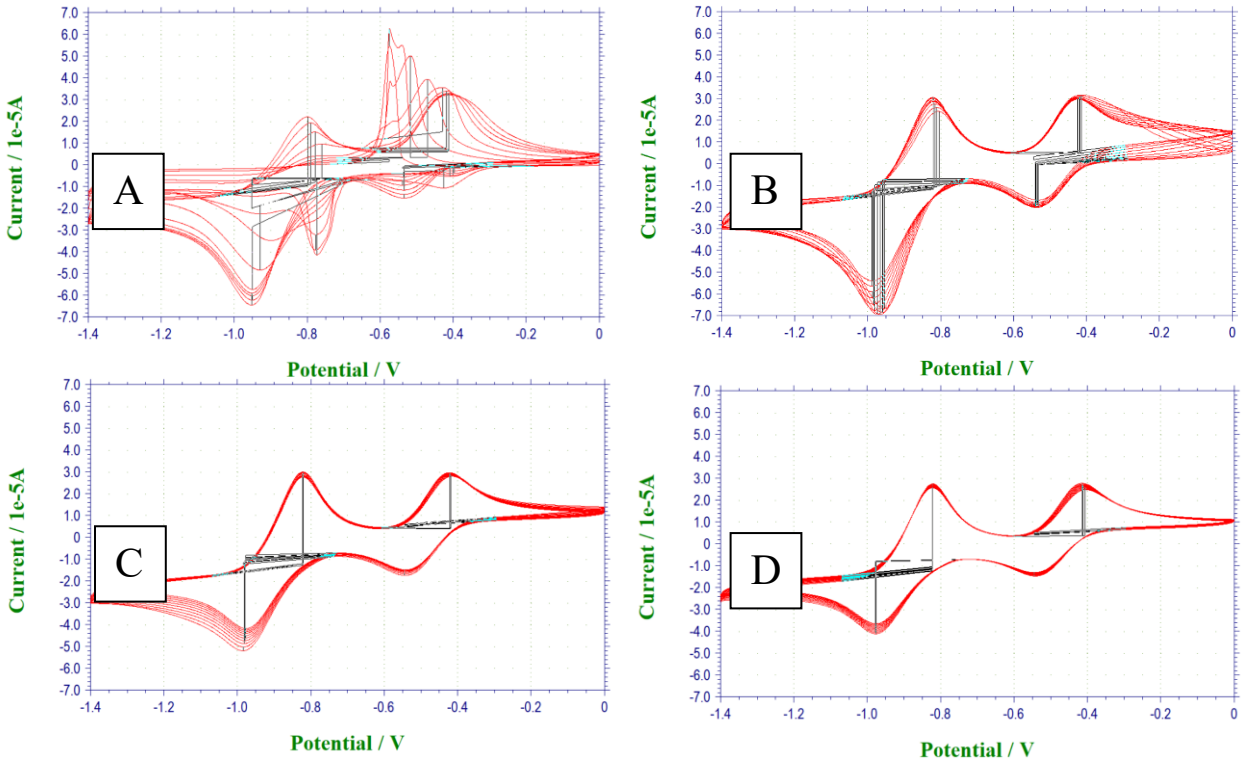

Figure 5.1: The electropolymerization of 1.5 mM and 3 mM di-pyridinium and tris-pyridinium salts on 3 mm glassy carbon electrodes in 50 mM phosphate buffer at a 50 mV/s cyclic voltametric scan rate using a SCE reference and a platinum wire counter electrode A) 1-10 scans B) 11-20 scans C) 21-30 scans and D) 31-40 scans.

pronounced sharp surface wave peaks that diminish as more scans are run. These are the negative reduction peak at ~-0.775 V and the positive oxidation peak at ~-0.575 V. The oxidation and reduction of the viologen can be seen as it is produced from the precursor salts. These are the oxidation/reduction redox couples that have $E_{1/2}$ values of -0.467 V and -0.900 V respectively which grow as more scans are performed. The main peak of interest is the reduction peak at -0.535 V since this is associated with the viologen species that will oxidize the glucose molecules in the operating fuel cell. This peak is seen to only grow in the 1-10 and 11-20 scan polymerizations. In the 21-30 and 31-40 scan polymerizations the peak grows and then begins to diminish slightly as more scans are run. This could be due to the film growing so thick that some of the material is inaccessible to the diffusion of ions through the material that is necessary for the electrochemistry to occur. This is also a sign that the 20 or 30 scan polymerization is the best for the production of this electrode using cyclic voltammetry.

Polyviologen-modified electrodes were also produced at constant voltage by holding the working electrode at -1.0 V for varying amounts of time (Figure 5.2a). The times were chosen to roughly mimic the total amount of time the voltage would be below -0.9 V in the construction of the 20, 30 and 40 scan cyclic voltammetry electrodes, so 270, 580 and 820 second polarization

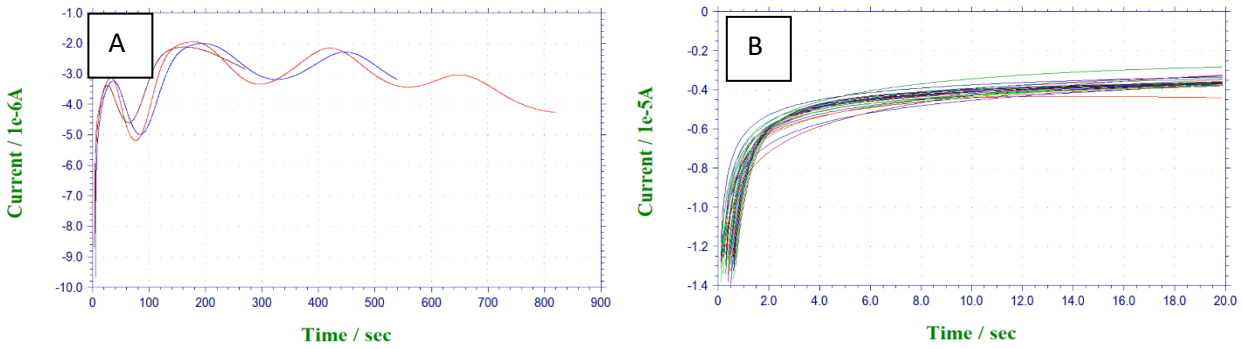

Figure 5.2: The electropolymerization of 1.5 mM and 3 mM BIS and TRIS salts on 3 mm glassy carbon electrodes in 50 mM phosphate buffer using a SCE reference and a platinum wire counter electrode: A) at a constant voltage of -1V for 270, 580 and 820 seconds and B) 30 pulses of -1V.

times were used. The -0.9 V potential was chosen since both the TRIS and the BIS salts would be reduced whenever the scan was below this voltage. Various rises and decreases in current occurred over time and can be seen in Figure 5.2a below, probably due to periods of growth and stagnation. This growth and stagnation could be due to the repeated buildup of neutral reduced polyviologen moieties forming and blocking electron transfer, followed by the elimination to the positively charged viologen species, allowing for electron flow from the electrode surface to the material surface stimulating more growth. Alternatively, it could also be due to a critical concentration at the electrode surface needed for growth to occur and the rate of growth could outpace the diffusion of new material to the electrode inducing these peaks and dips in current over the course of the run.

The pulsed voltage was also designed to mimic somewhat the time frame used in the cyclic voltammetry, holding the electrode at -1.0 V for 20 seconds and then allowing the electrode to rest at 0 V for 40 seconds before pulsing -1.0 V again successively for 30 cycles. This is the amount of time the electrode is below and above -1.0 V in each scan of the CV polymerizations. These pulses seemed to remain roughly the same through the thirty scans with no discernable pattern or growth. In order to judge which polymerization method was the best for our purposes the electrodes were tested as the bioanode in a Pt/air fuel cell, producing polarization and power curves for comparison.

These power curves were generated using the same method as the ferrocene glucose fuel-cells described in Chapters 3 and 4. The working electrode lead was attached to the platinum cloth air breathing electrode and the reference and counter electrode leads were attached to the viologen-coated electrode. The electrode was then scanned from the open circuit potential to 5 mV at a 1 mV/s scan rate to generate a polarization curve. The voltage at each point is then multiplied by

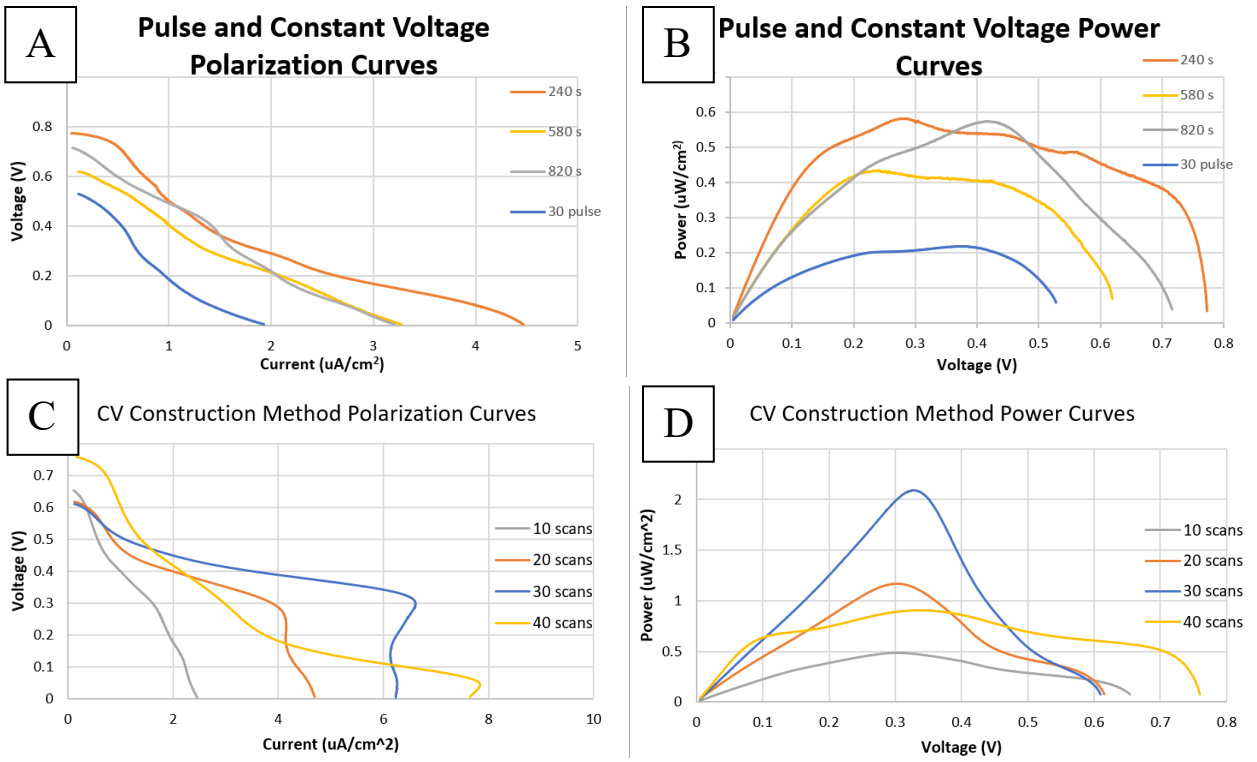

Figure 5.3: Polarization and power curves for the polyviologen anodes on glassy carbon electrodes in 50 mM phosphate buffer pH 7 with 5 mM glucose scanned from the OCV to 5 mV at 1 mV/s using a platinum cloth working electrode with the reference and counter leads attached to the viologen electrode. These electrodes were fabricated using pulsed and constant voltage techniques in A and B and cyclic voltammetry in C and D.

the current at each point to generate a power curve where the maximum power potential and open circuit voltage can then be seen. These are displayed in Figure 5.3 to compare the polarization and power curves of each electropolymerization method. In Figure 5.3C and D, the data from the cyclic voltammetry polymerization method is shown. The OCV of these electrodes all were around the same voltage (~.61-.65 V) with the exception of the 40 total scan method, which was higher (0.75 V). The 30 total scan electrode also has the most normal looking polarization curve with a large ohmic polarization region with a sharp break into the diffusion limited current region of the polarization curve. This large ohmic polarization region at relatively high currents means it also has the most peak power. For these reasons the 30 total scan method was determined to be the best method for CV constructed electrodes. The constant voltage construction methods, while

producing some high OCVs, produced much less current and ~1/4 power of the CV construction method when used in a fuel cell. This information was used to construct an electrode on a high surface area electrode, with and without CB7, to determine if it would stabilize the electrode in highly basic conditions.

Electrodes were constructed using the CV method on carbon felt electrodes, a high surface area/volume material (see Figure 5.4). This was done with CB7 in solution and with a solution not containing any CB7. These polymerization curves are similar with the viologen peaks growing as more scans are performed. One big difference is that the CB7 containing material produces a film with roughly half the peak height of the non-CB7 containing material. This translates into an electrode that produces more current and ~ double the power (Figure 5.5) in the polarization and power curves (~2 vs ~4 uW/cm^2). The non-CB7 material also has a higher OCV (0.85 V vs 0.75V). However these results do not tell the whole story.

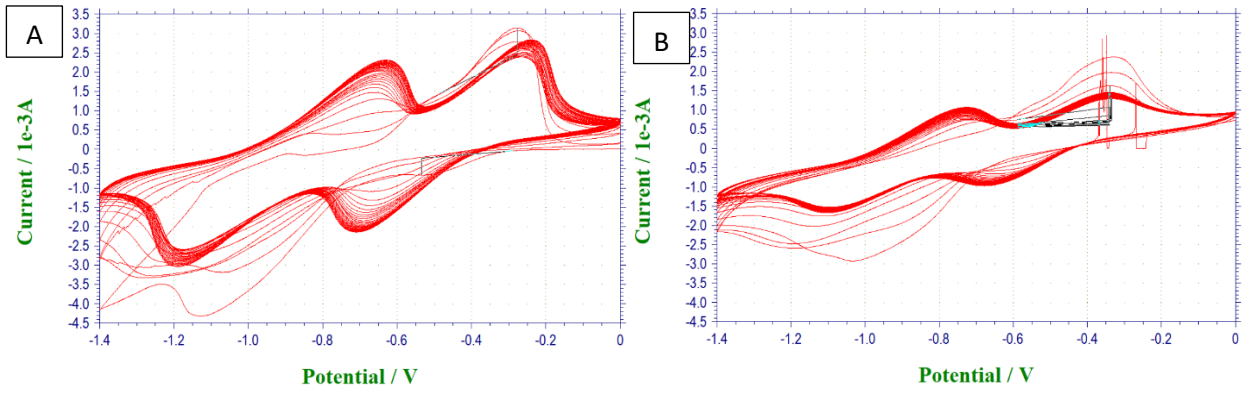

Figure 5.4: Cyclic voltammograms showing the 30-scan electropolymerization of 1.5 mM and 3 mM BIS and TRIS salts on carbon felt electrodes in 50 mM phosphate buffer using a SCE reference and a platinum wire counter electrode: A) without CB7 and B) with 1 mM CB7

While maximum power can be a good indicator of how much power a fuel cell will produce, many batteries and fuel cells are constructed of many cells running at a set voltage to make a high voltage fuel cell since voltage adds when cells are connected in series. Round numbers are often used, for example, many fuel cells connected in series, running at 0.3 or 0.5 V

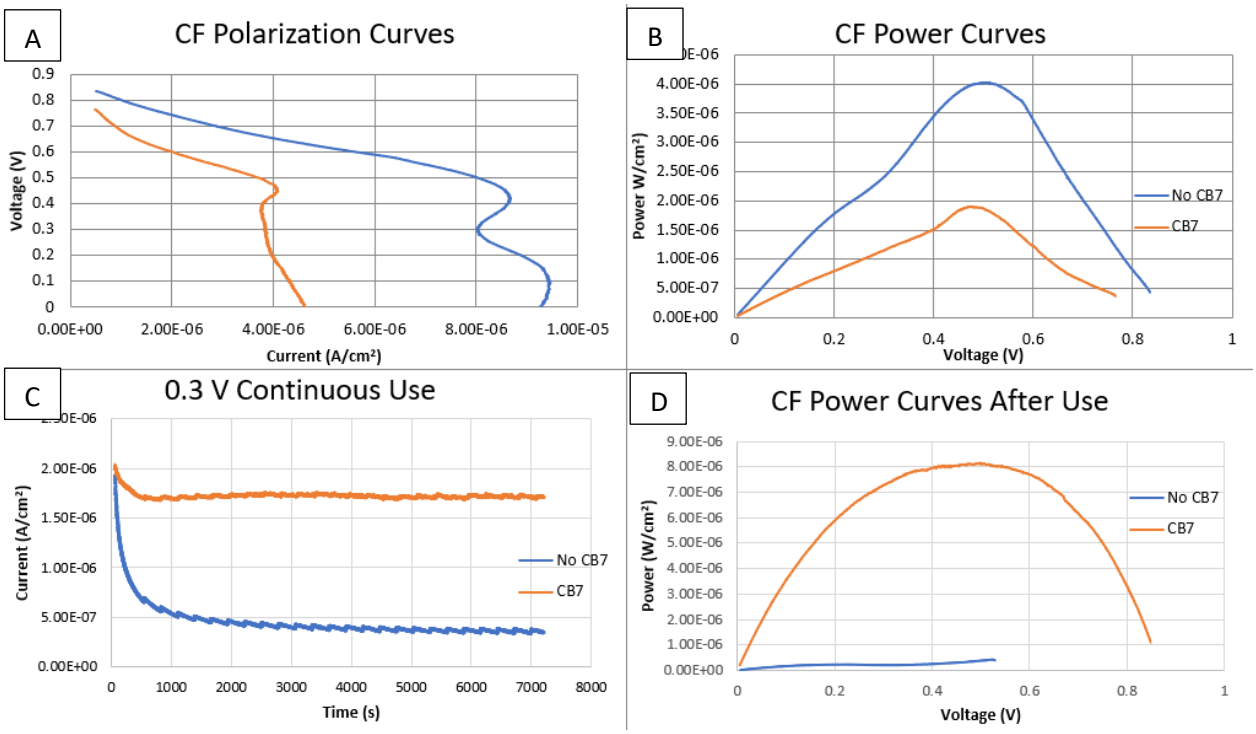

Figure 5.5: Polarization (A) and power curves (B) for carbon fiber viologen electrodes with the current-time 2-Hr 0.3 V usage curve in C and the power curves after the 2-hour discharge in D. These were run in pH 10, 50 mM phosphate buffer.

can be used to easily produce 9 or 12 V batteries. For this reason our degradation test was run at 0.3 V. During this stress test the CB7 protected the viologen from oxidation in the highly basic solution, while the material with no CB7 quickly degraded. The CB7 material maintained 83% of it's starting current and did not seem to lose performance after the first 10 min. The material without the CB7 quickly lost most of it's current and continued to decline down to 18% of it's original current. The power curves of these degraded electrodes show that the CB7 containing material actually gained current, power and OCV in it's polarization and power curves after it's use for 2 hours in a fuel cell, while the non-CB7 containing material lost nearly all ability to catalyze the oxidation of glucose. The doubling (from 4 to 8 uW/cm^2) in power output after the 2 Hr use could be due to electrode break-in, allowing for glucose to flow into and out of the material more easily than in a newly constructed electrode. These carbon fiber electrodes actually outperform the glassy carbon electrodes with respect to performance/surface area (by a factor of

4) as well as raw power output, making them a great option for fuel cell production. CB7 has a large effect on the stability of these electrodes and makes these viologen based electrodes a viable option for use in non-enzymatic glucose biofuel cells.

These non-enzymatic fuel cells have some advantages over their enzymatic counterparts in that they can catalyze the oxidation of other sugars, not just the sugar the enzyme is designed to oxidize. They also continue to add current with much higher concentrations than the 150 mM glucose limiting concentration of our ferrocene containing enzymatic electrodes. The same electrode used in the degradation study was used in a solution of 1M glucose to produce a power curve that more than doubled the power output obtained by the 5 mM solution (from 8 to 20 $\mu W/cm^2$) used in the degradation study (Figure 5.6). This demonstrates that the electrode can operate at high glucose concentrations to produce higher power outputs. These electrodes can also

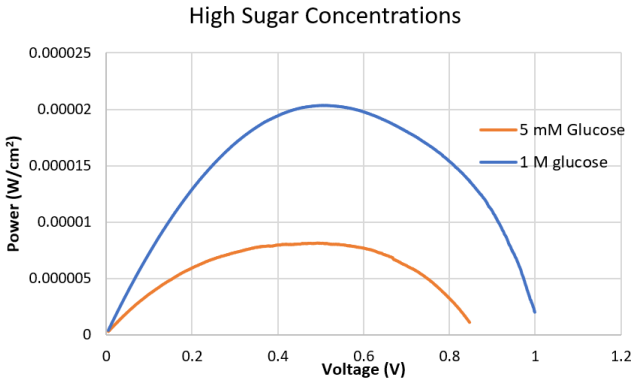

Figure 5.6: The Power curves for a CV-polymerized CB7/polyviologen modified carbon fiber electrode in 50 mM phosphate buffer pH 10 with 5 mM and 1 M glucose.

oxidize other carbohydrates like sucrose. This is shown in Figure 5.7 below with a 2 hour discharge of a CB7-containing electropolymerized polyviologen bio-anode in 5 mM sucrose solution and the power curve of this electrode after use. The data shows that the CB7-polyviologen material on a glassy carbon electrode produced ~3.7 $\mu A/cm^2$ operating at 0.3 V in a 5 mM solution of sucrose. These electrodes also produce ~0.69 OCV and ~4 uW peak current in a polarization

curve. This establishes this polyviologen material as a versatile material that could process raw fruit juice and possibly other bio-fuels into electricity for off-grid or cheap energy production.

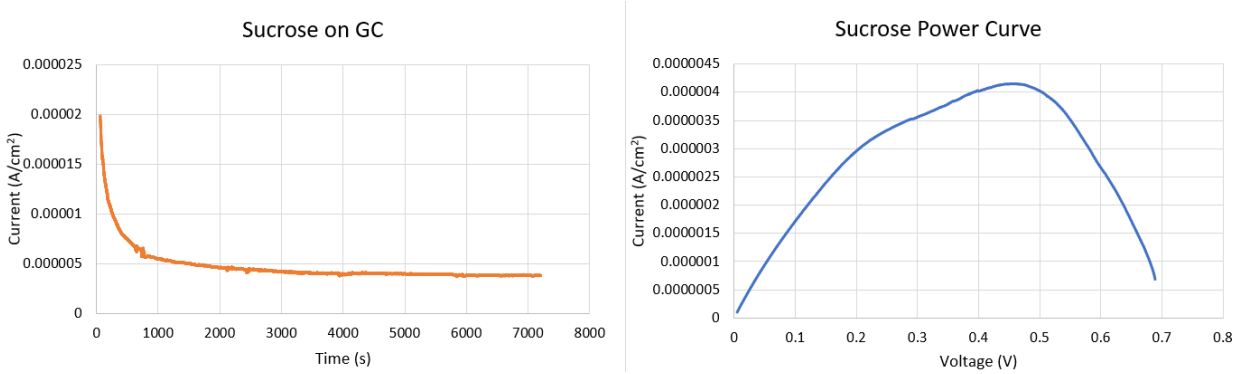

Figure 5.7 Power curve of a carbon fiber CV-polymerized CB7/viologen modified electrode in 5 mM sucrose and 50 mM phosphate buffer pH 10 and a 2-hour discharge of this electrode at 0.3 V.

5.3 Conclusion

In this chapter it was demonstrated that the polyviologen electrodes discussed here are best prepared through cyclic voltametric methods. Cyclic voltammetry was compared to, and found to be better than, both the constant voltage and pulsed voltage techniques used in this chapter. Used in a working bio-fuel cell these electrodes, constructed through cyclic voltammetry, displayed greater stability in relation to non-CB7 containing polyviologens, maintaining much more electrical current output throughout 2 hours of use and actually improving their power output after this period of use. These non-enzymatic electrodes also displayed their versatility in their ability to oxidize high concentrations of glucose as well as sucrose, where many enzymatic electrodes are limited to one substrate.

5.4 Materials and Methods

5.4.1 Chemicals and Solutions.

Sodium phosphate, sodium hydroxide, glucose and sucrose were purchased from Sigma-millipore and used as received. BIS and TRIS salts were prepared as previously reported in literature[7]. The PAN Carbon felt, air breathing 0.1 mg/cm^2 Pt/Vulcan electrode and 0.7 mm thick Nafion membrane were purchased from the Fuel Cell Store website. The Pt cloth and Nafion membrane were hot pressed together at 800 psi and 120 °C for 5 min. A CHI Model 830D potentiostat was used in all electrochemical studies. We thank Profesor R. Halterman for providing us with a sample of CB7

5.4.2 Cyclic Voltammetry.

All scans were performed in 50 mM phosphate buffer at pH 7.0 with a Pt wire counter electrode, an SCE reference, and a glassy carbon working electrode at a scan rate of 50 mV/s unless otherwise stated.

5.4.3 CV Electropolymerization to Form Polyviologen.

A solution of 1.5 mM BIS and 1 mM TRIS was made in 50 mM phosphate buffer at pH 7.0 and cycled 10, 20, 30 and 40 times from 0 to -1.4 V and back to produce the viologen films on 3 mm glassy carbon or PAN carbon felt electrode surfaces as specified in the text. A platinum wire counter electrode and a SCE reference electrode were used in the 3-electrode setup with the glassy carbon working electrode. 1 mM CB7 was added if noted in the text.

5.4.3 Pulsed Voltage Electropolymerization to Form Polyviologen.

A solution of 1.5 mM BIS and 1 mM TRIS was again made in 50 mM phosphate buffer at pH 7.0 and -1 V was applied for 20 s and then 0 V for 40 s. This pulse was repeated 30 times to produce viologen films on 3 mm glassy carbon electrode surfaces. A platinum wire counter electrode and a SCE reference electrode were used in the 3-electrode setup with the glassy carbon working electrode.

5.4.4 Constant Potential Electropolymerization to Form Polyviologen.

A solution of 1.5 mM BIS and 1 mM TRIS was made in 50 mM phosphate buffer at pH 7.0 and -1 V was applied for 270, 580 and 820 s to build the viologen films on 3 mm glassy carbon electrode surfaces. A platinum wire counter electrode and a SCE reference electrode were used in the 3-electrode setup with the glassy carbon working electrode.

5.4.5 Power Curves.

Power curves were produced using an electropolymerized polyviologen as the anode, and a Pt cloth electrode hot pressed onto a Nafion® membrane as the cathode. The buffer and sugar concentrations are specified in the data where the power curve is presented. The glucose anode was connected to the potentiostat through the counter and reference electrode leads while the Pt cloth electrode was connected to the working electrode lead. The open circuit voltage (OCV) was measured, and the working electrode was then scanned from the OCV to 5 mV at 1 mV/s. Differently sized areas of the Pt air breathing electrode were exposed to air and no difference in performance was observed; therefore, it was assumed not to be the rate limiting electrode.

5.4.6 2-Hr Power Discharge

When 2-hr discharge curves were generated, this was done by submersing the specified polyviologen anode in a pH 10, 50 mM phosphate buffer with 1 M, or 5 mM glucose or 5 mM sucrose and paired with a Pt cloth ELAT electrode hot pressed to a Nafion® membrane as the cathode. A voltage of -0.3 V was applied and held for 2 hours; the current was recorded for the duration of the time.

5.5 Bibliography

1. Wei, M.; Qiao, Y.; Zhao, H.; Liang, J.; Li, T.; Luo, Y.; Lu, S.; Shi, X.; Lu, W.; Sun, X., Electrochemical non-enzymatic glucose sensors: Recent progress and perspectives. *Chemical Communications* **2020,** *56* (93), 14553-14569,10.1039/D0CC05650B.

2. Lee, W.-C.; Kim, K.-B.; Gurudatt, N. G.; Hussain, K. K.; Choi, C. S.; Park, D.-S.; Shim, Y.-B., Comparison of enzymatic and non-enzymatic glucose sensors based on hierarchical au-ni alloy with conductive polymer. *Biosensors and Bioelectronics* **2019,** *130*, 48-54,https://doi.org/10.1016/j.bios.2019.01.028.

3. Zhao, Y.; Fan, L.; Gao, D.; Ren, J.; Hong, B., High-power non-enzymatic glucose biofuel cells based on three-dimensional platinum nanoclusters immobilized on multiwalled carbon nanotubes. *Electrochimica Acta* **2014,** *145*, 159-169,https://doi.org/10.1016/j.electacta.2014.09.006.

4. Geetha, M.; Sadasivuni, K. K.; Al-Ejji, M.; Sivadas, N.; Baig, M. Z. K.; Promi, T. J.; Ahmad, S. A.; Alabed, S.; Hijazi, D. A.; Alsaedi, F.; Al-Shaibah, F. N., Review of progress and prospects in research on enzymatic and non- enzymatic biofuel cells; specific emphasis on 2d nanomaterials. *Current Biotechnology* **2022,** *11* (3), 212-229,10.2174/2211550112666221201152211.

5. Fujiwara, N.; Yamazaki, S.-i.; Siroma, Z.; Ioroi, T.; Senoh, H.; Yasuda, K., Nonenzymatic glucose fuel cells with an anion exchange membrane as an electrolyte. *Electrochemistry Communications* **2009,** *11* (2), 390-392,https://doi.org/10.1016/j.elecom.2008.11.031.

6. Park, S.; Boo, H.; Chung, T. D., Electrochemical non-enzymatic glucose sensors. *Analytica Chimica Acta* **2006,** *556* (1), 46-57,https://doi.org/10.1016/j.aca.2005.05.080.

7. Wang, P.. 2021, Polyviologen-modified anodes for carbohydrate biofuel cells. Doctoral Dissertation, *University of Oklahoma*, ShareOK.org

8. Zen, J.-M.; Lo, C.-W., A glucose sensor made of an enzymatic clay-modified electrode and methyl viologen mediator. *Analytical Chemistry* **1996,** *68* (15), 2635-2640,10.1021/ac960090j.

9. Liu, X.; Hao, M.; Feng, M.; Zhang, L.; Zhao, Y.; Du, X.; Wang, G., A one-compartment direct glucose alkaline fuel cell with methyl viologen as electron mediator. *Applied Energy* **2013,** *106*, 176-183,https://doi.org/10.1016/j.apenergy.2013.01.073.

10. Mock, W. L.; Shih, N. Y., Structure and selectivity in host-guest complexes of cucurbituril. *The Journal of organic chemistry* **1986,** *51* (23), 4440-4446,10.1021/jo00373a018.

11. Garrett, J. T., Host-guest complexation of benzyl and xylyl ammonium guests with cucurbit [7] uril for shuttle rotaxanes. **2017**,

12. Bird, C. L.; Kuhn, A. T., Electrochemistry of the viologens. *Chemical Society Reviews* **1981,** *10* (1), 49-82,10.1039/CS9811000049.

13. Farrington, J. A.; Ledwith, A.; Stam, M. F., Cation–radicals: Oxidation of methoxide ion with 1,1′-dimethyl-4,4′-bipyridylium dichloride (paraquat dichloride). *Journal of the Chemical Society D: Chemical Communications* **1969,** (6), 259-260,10.1039/C29690000259.

14. Iehl, J.; Frasconi, M.; de Rouville, H.-P. J.; Renaud, N.; Dyar, S. M.; Strutt, N. L.; Carmieli, R.; Wasielewski, M. R.; Ratner, M. A.; Nierengarten, J.-F., Π-dimerization of viologen subunits around the core of C_{60} from twelve to six directions. *Chemical Science* **2013,** *4* (4), 1462-1469

15. Kitamura, N.; Nambu, Y.; Endo, T., Preparation of a polymeric membrane crosslinked by the viologen structure from a cyanopyridinium salt polymer. *Journal of Polymer Science Part A: Polymer Chemistry* **1988,** *26* (4), 993-1001,https://doi.org/10.1002/pola.1988.080260404.

Chapter 6 Conclusions and Future Work

6.1 Conclusions

As part of an exploration of the fundamental processes in the functioning of ferrocene-modified LPEI bio-anodes, this work presented a study of the mechanism of iodide's mediation of GOx. The synthesis of our Fc-LPEI material made by the Glatzhofer group sometimes contained hard to remove iodide salt impurities. The iodide-containing materials produced anomalous results when used in the construction of GOx containing bio-anodes, slightly increasing the current produced by these anodes, even when oxygen was not present. Current literature suggests that iodide acts in conjunction with oxygen to mediate the oxidation of glucose. This work is the first to our knowledge to show the iodide can mediate the GOx without the presence of oxygen, making it a direct mediator, rather than an indirect mediator, changing the way iodide is perceived to interact with GOx.

New ferrocene- and carbon disulfide-ferrocene-substituted LPEI and BPEI were also synthesized and used to construct enzymatic glucose bio-anodes using the layer-by-layer (LBL) technique. The synthesis of novel ferrocene and carbon disulfide substituted LPEI and BPEI materials allowed their use as a base layer for the LBL construction of films on gold electrodes due to the strong affinity of sulfur for gold surfaces. The use of non-redox active CS_2-LPEI as the first layer in this LBL bio-anode allowed for a direct comparison of small-molecule vs polymer first layered systems, using soluble ferrocene derivatives as a probe. These studies showed that although the polymer inhibits diffusion near the electrode it allows for increased GOx deposition on the surface, roughly doubling the sensor's V_{Max} and making CS_2-LPEI first layers superior to using the tradition sulfur small-molecule cystamine for the first layer. We were also able to compare the CS_2-LPEI to the Fc-CS_2-LPEI, showing that the mediator in the first layer improves the sensor's V_{max} by a factor of ~5 in the 3-layer bio-anodes. In anodes with higher numbers of layers the initial Fc-CS_2-LPEI-layered electrodes gained V_{Max} with every layer up to 9 layers and a V_{Max} of ~1 mA/cm^2. While previous work with the cystamine first-layered annodes have achieved 1.6 mA/cm^2, this was not

until 32 layers (16 bilayers) had been deposited over the course of ~3 hours. The Fc-CS_2-LPEI allows for much faster electrode fabrication, as well as resulting in a more durable electrode as shown in this work's comparison of the two electrodes over 2 hours of continuous use. This work also presents the production of Fc-CS_2-BPEI first-layered glucose anodes with p-GOx and Fc-BPEI upper layers, analogous to the Fc-CS_2-LPEI electrodes. These electrodes built V_{Max} all the way up to 19-layers producing a V_{Max} of ~2 mA/cm^2. These Fc-CS_2-BPEI anodes were shown to retain more of their current after 2 hours of continuous use than either the Fc-CS_2-LPEI or the cystamine anodes, making them the clearly superior material for LBL bio-anodes.

While these LBL materials are clear advancements in the production of enzymatic glucose bio-sensor anodes, this work also presents studies of novel polyviologen materials for the fabrication of non-enzymatic glucose fuel cells. In Chapter 5 the formation of a polyviologen material was explored by electropolymerization on glassy carbon electrodes. Three different methods of depositing this material were used: cyclic voltammetry, pulsed voltages, and constant voltage. Electrodes constructed using 30 voltammetric cycles were found to produce the most current and power. This could be due to differing amounts of polyviologen material forming on the electrodes or different morphologies of the material based on the electrochemical method used. These electrodes produced ~20 μW/cm^2 at ~0.5 V when poised against a platinum air breathing cathode in a glucose bio-fuel cell at 1 M glucose . Cucurbituril (CB7) encapsulated monomers were used to produce the polyviologen material in order to protect the viologen from oxidation in the caustic environment of these fuel cells. The CB7 was shown to have a significant impact on the longevity of the life of the viologen material, improving the life of the fuel cell over a 2 hour test period in which the electrode retained ~90% of it's original current.

6.2 Future Work

While the mechanistic studies showing iodide can function as a mediator for GOx will certainly have an impact on how this system is understood in the scientific community, there is not much more work

to be done in this area. The crystallization of GOx with the iodine immobilized in it's active site might be accomplished so the interaction of these two species could be better understood. This knowledge could lead to a new or better use of iodide's mediation of GOx or other oxidoreductases, potentially allowing new technologies to be developed.

While this work presents an advancement in the production of LBL 2nd generation enzymatic glucose sensors using Fc-CS_2-LPEI and Fc-CS_2-BPEI, there is still a lot of work to be done to make this a viable technology that could compete with current CGMs on the market. While the sensors we have produced are more sensitive than the current CGMs, they are far less stable, falling to ~40% of their original current after 2 hours of use in 100 mM glucose (saturating conditions). While this demonstrates potential, it would be good to test these bioanodes at physiological glucose concentrations (~4-15 mM glucose) to really expolore their viability. Although they may perform better in these lower glucose concentrations it is still doubtful that they could last for the two week span that is the market standard today. These electrodes could also be improved by incorporating gold nanoparticles. This could be done by adding a dip into a nanoparticle solution into the production of these anodes or by coating the nanoparticles themselves using the Fc-CS_2-BPEI and GOx. While this could be an interesting area of study, the stability of the electrodes is the real problem with this technology that needs to be solved before these can be brought to the market. In the past it has been shown that the 3-carbon link to the LPEI was far more stable than the 1- or 6-carbon link. Other ways of attaching the ferrocene to the polymer backbone could also be explored, or another polymer backbone altogether (like polyvinylamine). Use of matrix stabilizing crosslinkers such as dipping these electrodes in di-epoxide or glutaraldehyde solution could also improve the longevity of these sensors.

This work has shown that CB7-encapsulation of polyviologens significantly improves the stability of the resulting non-enzymatic biofuel cells. This technology could be useful in areas where no grid is available, and electricity could be produced for very small electronics using simple sugars that are ubiquitous in most areas of the world. To improve this technology, finding a cheaper cathode (Pt cloth and Nafion are expensive) using a different biofuel or gas to complete the circuit would vastly increase it's viability as an off-grid power source. The caustic environment of the anode (these run better at a high pH)

could also present a danger and a limitation of what materials are viable to use in these fuel cells. If this high pH requirement were eliminated, this would be much more viable as a technology. This could be done by adding a basic polymer diffusion layer on top of the imidazole catalyst layer, forming a localized basic environment around the imidazole catalyst.

Appendix

^{1}H NMR spectra

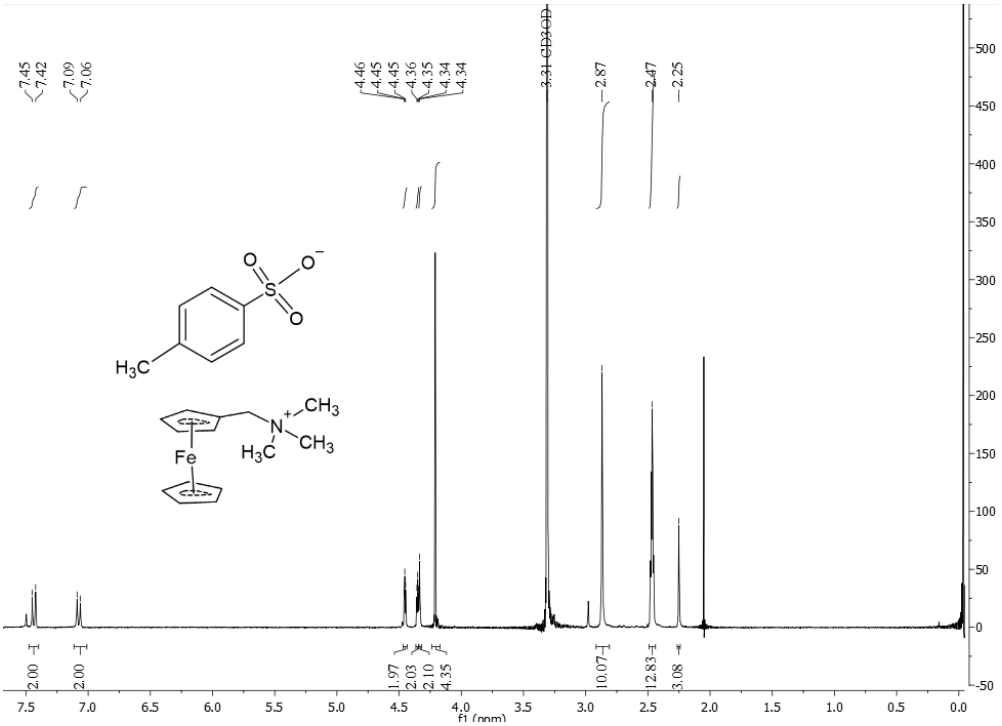

Figure A1 FcTMATos ^{1}H-NMR (CD_3COD) 300 MHz.

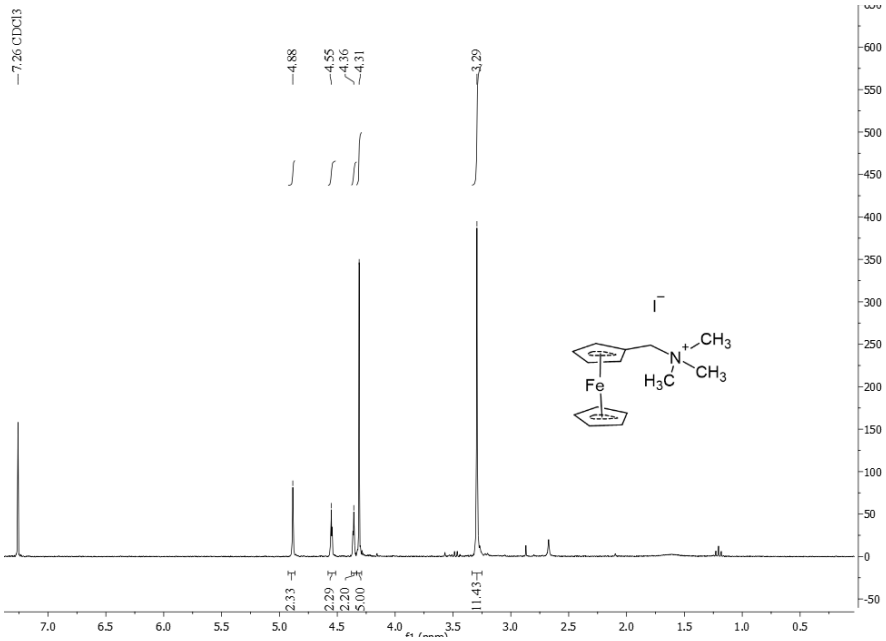

Figure A2 FcTMAI ^{1}H-NMR ($CDCl_3$) 300 MHz.

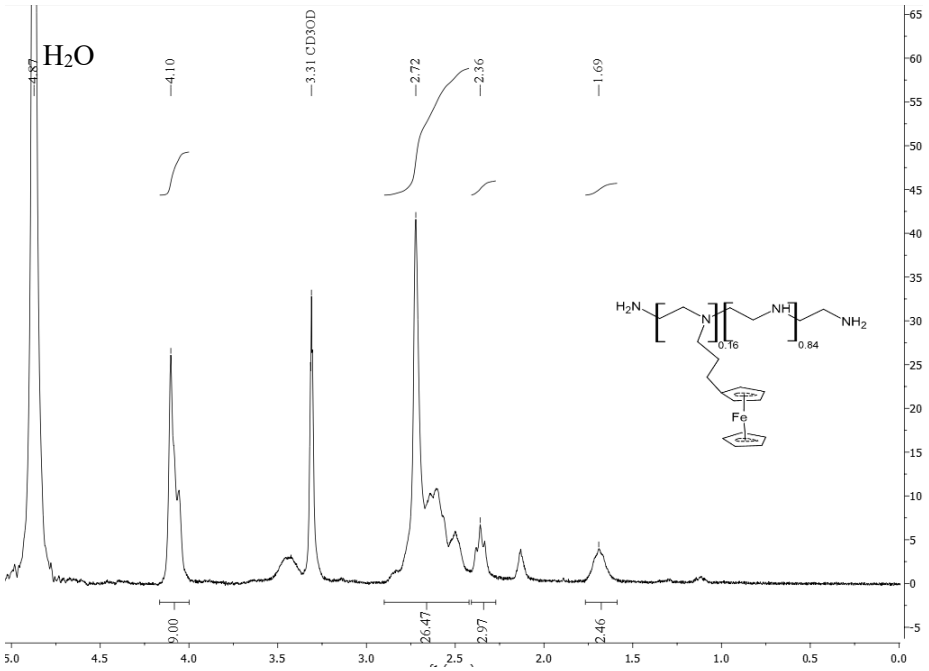

Figure A3 16 % Fc-LPEI ^{1}H-NMR (CD_3COD) 300 MHz.

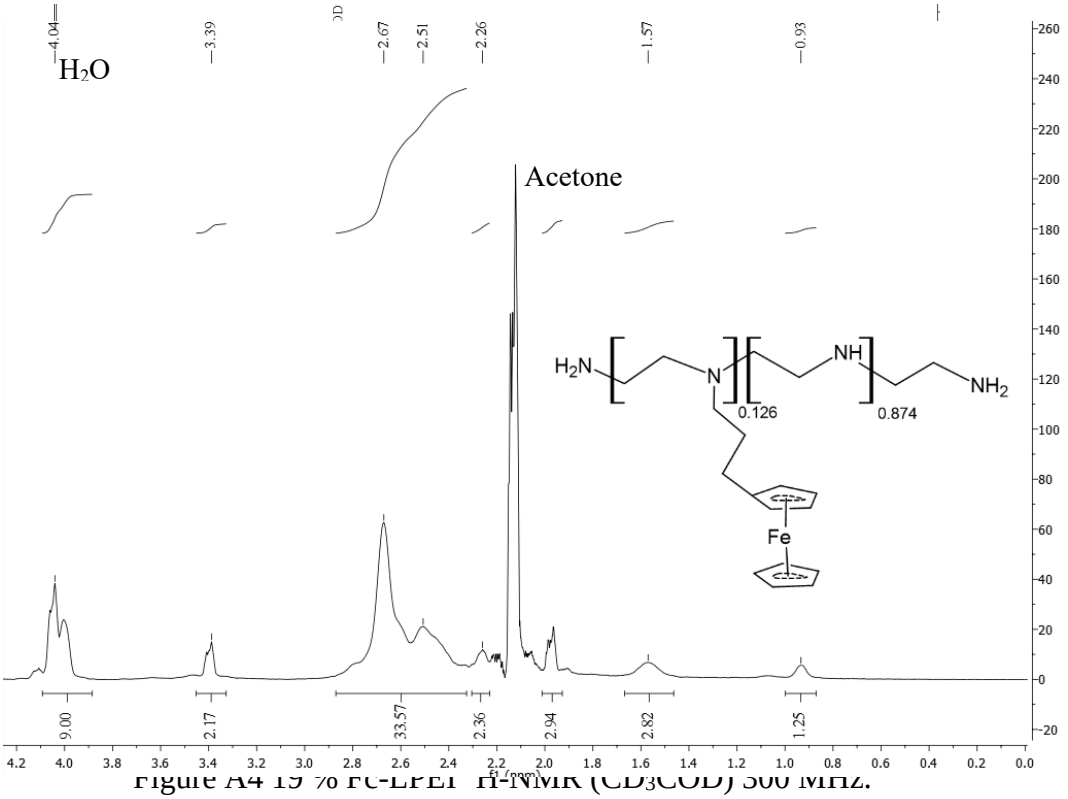

Figure A4 19 % Fc-LPEI ^{1}H-NMR (CD_3COD) 300 MHz.

Figure A5 12.6 % Fc-LPEI ^{1}H-NMR ($CDCl_3$) 300 MHz.